

Carboxylated Organic Matter Influences Magnesium Uptake in Three Low-Temperature Dolomite Models

By

Adam Yoerg

B.S. Geology, University of Kansas, 2016

© 2018

Submitted to the graduate degree program in Geology and the Graduate Faculty of the
University of Kansas in partial fulfillment of the requirements for the degree of Master of
Science.

Chair: Jennifer Roberts

Randy Stotler

Alison Olcott

Date Defended: 6/26/2018

The thesis committee for Adam Yoerg certifies that this is the approved version of the following thesis:

**Carboxylated Organic Matter Influences Magnesium Uptake in
Three Low-Temperature Dolomite Models**

Chair: Jennifer Roberts

Date Approved: 6/26/2018

Abstract

Numerous geochemical models explain the formation of dolomite at low temperature, a controversial mineral due to its abundance in geological deposits but paucity in modern environments. Several of these models are based on environments where dolomite either forms in the modern or is hypothesized to have formed in the past— mixing zones, sabkhas, and alkaline lakes. In the last twenty years, results of field and laboratory studies have found that microorganisms can promote the precipitation of dolomite at low temperature, either through active metabolism or by providing a reactive surface for mineral nucleation. The work summarized here utilizes bench-scale laboratory batch experiments to study simplified geochemical environments associated with low temperature dolomite formation both containing and excluding synthetic carboxylated organic matter in the form of functionalized polystyrene microspheres. These environments were characterized by their pH, alkalinity, and salinity to form geochemical end members. In effect, this combines longstanding geochemical models of dolomite formation with a mechanism known to overcome kinetic barriers to dolomite formation at low temperature.

Experiments did not demonstrate formation of significant amounts of dolomite, however, data suggest that while bulk precipitation products reflect the specific geochemical environments, the presence of carboxylated organic matter promotes the incorporation of magnesium into the precipitate across geochemical environments. The amount of magnesium in the precipitate on the microsphere surface appears to be a function of the Mg/Ca ratio of the bulk solution. Magnesium is observed both in precipitates forming on the microsphere surface and is more broadly distributed in the bulk precipitate when microspheres are present. These results

suggest that carboxylated organic matter can sequester magnesium into precipitates, which could have implications for magnesium availability during diagenesis.

Results from experiments studying the impact of carboxylated organic matter on dolomitization of calcium carbonate sediments in mixing, sabkha, and artificial fluids are inconclusive. These negative results potentially arise from short experimental time scales and scaling issues during analysis. Future low temperature dolomitization experiments should include advection in the experimental design to provide the mass transfer presumably necessary for significant dolomitization.

Acknowledgements

First and foremost, thank you to Jennifer Roberts for guidance, assistance, and encouragement. Jen has supported me from my first semester as a geology undergraduate to now and given me opportunities in this field I wouldn't have had otherwise. I would also like to acknowledge Randy Stotler, Alison Olcott, and Craig Marshall for their help and guidance in completing this project, navigating graduate school, and use of instruments.

Christopher Omelon was instrumental in giving me the skills necessary to complete my thesis. I would also like to thank Chris for always being available to answer questions, discuss science, and for putting in a lot of effort to help me complete this project.

The Kansas Interdisciplinary Carbonates Consortium (KICC) and the Society for Exploration Petrologists and Mineralogists (SEPM) have generously supported this research, and I would like to thank them. Finally, I would like to thank my parents, step-father, siblings, godparents, and extended family for supporting me, and my friends in Lawrence for making my time here memorable.

Table of Contents

Abstract	iii
Acknowledgements	v
Table of Contents	vi
List of Tables	viii
<i>Chapter 2</i>	<i>viii</i>
<i>Chapter 3</i>	<i>viii</i>
List of Figures	viii
<i>Chapter 2</i>	<i>viii</i>
<i>Chapter 3</i>	<i>viii</i>
Chapter 1: Introduction	1
References	3
Chapter 2: Primary Precipitation Batch Experiments	5
Introduction	5
Materials and Methods	9
<i>Research Approach</i>	9
<i>Batch Experiments</i>	10
<i>Geochemical Modeling</i>	11
<i>Fluid Chemistry</i>	12
<i>Electron Microscopy</i>	13
<i>X-ray Diffraction</i>	13
<i>Raman Spectroscopy</i>	14
Results	15
<i>Mixing Zone Environments</i>	15
<i>Sabkha Environments</i>	16
<i>Alkaline Lake Environments</i>	17
<i>Microsphere and Mineral Associations</i>	19
Discussion	20
<i>Mixing Zones</i>	20
<i>Sabkhas</i>	21
<i>Alkaline Lakes</i>	22
<i>Magnesium-bearing phases</i>	24
<i>Implications</i>	27
Conclusion.....	30
Tables	32
Figures.....	34
.....	46

References	47
Chapter 3: Dolomitization Experiments	55
Introduction	55
Materials & Methods	56
<i>Research Approach</i>	56
<i>Geochemical Modeling</i>	57
<i>Fluid Chemistry</i>	58
<i>Fluorescence Microscopy</i>	58
<i>Electron Microscopy</i>	59
<i>X-ray Diffraction</i>	59
Results	60
<i>Initial Ooid Characterization</i>	60
<i>Modified Zempolich & Baker Fluid</i>	60
<i>Mixing Zones</i>	61
<i>Sabkhas</i>	62
Discussion	63
Conclusion	65
Tables	66
Figures	67
References	78
Chapter 4: Conclusions	81
Appendix I: Primary Precipitation Geochemical Modeling	82
Appendix II: Dolomitization Geochemical Modeling	100
Appendix III: Primary Precipitation Aqueous Geochemistry	123
Appendix IV: Dolomitization Aqueous Geochemistry	124
Appendix V: Early Phase Experiments	125
Methodology	125
Results	125
Discussion	125
Appendix VI: Compiled SEM Images	128

List of Tables

Chapter 2

Table 1: Environmental parameters used to create geochemical end members during experimental design.

Table 2: Saturation indices of common carbonate minerals for each environment and treatment during experimentation.

Table 3: Magnitude of change for geochemical parameters for each set of experiments.

Chapter 3

Table 1: Geochemical parameters defining dolomitizing fluids.

List of Figures

Chapter 2

Figure 1: Normalized geochemical changes for Ca, Mg, and alkalinity for each set of experiments.

Figure 2: Diffractograms of precipitates from the mixing zone solution for each treatment.

Figure 3: SEM photomicrographs of precipitates from the mixing zone solution for each treatment.

Figure 4: Diffractograms of precipitates from the sabkha solution for each treatment.

Figure 5: SEM photomicrographs of precipitates from the sabkha solution for each treatment.

Figure 6: Diffractograms of precipitates from the alkaline lake solution for each treatment.

Figure 7: Raman spectra of precipitates from the alkaline lake solution after five days at 30°C.

Figure 8: Raman spectra of precipitates from the alkaline solution after five days at 40°C.

Figure 9: SEM photomicrographs of precipitates from the alkaline lake solution for each treatment.

Figure 10: EDS point spectra of precipitates from the alkaline lake solution showing chemical variation in the precipitate at the micron-scale.

Figure 11: TEM EDS data showing calcium and magnesium on the microsphere surfaces in the alkaline lake solution.

Figure 12: TEM/SEM photomicrographs showing morphologically similar precipitates co-occurring with microspheres across geochemical environments.

Figure 13: SEM EDS maps of precipitate from the alkaline solution after five days at 30°C showing microspheres impact the distribution of magnesium in the bulk precipitate.

Chapter 3

Figure 1: Notional diagram describing the geochemical environment created by the experiments.

Figure 2: Diffractogram of ooids prior to experimentation.

Figure 3: Fluorescence microscopy and SEM/EDS images of ooids prior to experimentation.

Figure 4: Geochemical changes (Mg, Ca, alkalinity, pH) for the Mg/Ca fluid over experiment duration with and without microspheres.

Figure 5: Fluorescence microscopy and SEM/EDS images of ooids after six weeks in the Mg/Ca fluid with and without microspheres.

Figure 6: Diffractogram of ooids with and without microspheres at each time step for each treatment.

Figure 7: Geochemical changes (Mg, Ca, alkalinity, pH) for the sabkha fluid over experiment duration with and without microspheres.

Figure 8: Fluorescence microscopy and SEM/EDS images of ooids after six weeks in the sabkha fluid with and without microspheres.

Figure 9: Geochemical changes (Mg, Ca, alkalinity, pH) for the mixing zone fluid over experiment duration with and without microspheres.

Figure 10: Fluorescence microscopy and SEM/EDS images of ooids after six weeks in the mixing zone fluid with and without microspheres.

Figure 11: Dolomite saturation indices at each time step for each environment with and without microspheres.

Chapter 1: Introduction

The carbonate mineral dolomite has been the subject of intense research for over one hundred years (van Tuyl 1916). Interest in dolomite stems from economic considerations – dolomite-rich rocks host natural resources including hydrocarbons, ores, and groundwater – and from scientific interest. Dolomite is abundant in the rock record but comparatively scarce in modern, low-temperature environments. Additionally, the mechanisms through which dolomite forms remain ambiguous, yet evidence suggests many dolomites in the rock record formed at low temperature (e.g. Ferry et al. 2011, Meister et al. 2013, Li et al. 2013). Combined, these issues form the dolomite problem and challenge assumptions regarding uniformitarianism.

Research on dolomite formation has progressed using both field studies and laboratory experiments to develop models of dolomite formation. Most natural dolomite results from replacement of calcium carbonate sediments. Field studies often focus on these secondary dolomites (e.g. Badiozamani 1973, Li et al. 2013). Nucleation is the critical first step to massive dolomitization. Many laboratory studies have focused on nucleation. In the past twenty-five years, microorganisms have been implicated in dolomite nucleation (e.g. Vasconcelos & McKenzie 1998, Roberts et al. 2004, Deng et al. 2011, Roberts et al. 2013), yet the literature has yet to bridge the gap between the formation of massive dolomite and microbial nucleation of minor amounts in nature and the laboratory.

Here, the dolomite problem is approached in two ways. Carboxylated organic matter has been shown to promote nucleation of dolomitic phases at low temperature in marine environments (Roberts et al. 2013). However, the impact of carboxylated organic matter in geochemical environments specific to dolomite models remains unexplored, as does the role of carboxylated organic matter on secondary dolomite formation (dolomitization). Laboratory-

scale batch experiments, representative of pore volumes at a single instant of time, were used to mimic dolomite-relevant geochemical environments for the purpose of evaluating the impact of carboxylated organic matter on dolomite nucleation and dolomitization.

References

- Badiozamani, K., 1973, The Dorag dolomitization model – application to the middle Ordovician of Wisconsin: *Journal of Sedimentary Petrology*, v. 43, p. 965-984.
- Deng, S., Dong, H., Lv, G., Jiang, H., Yu, B., Bishop, M.E., 2010, Microbial dolomite precipitation using sulfate reducing and halophilic bacteria: Results from Qinghai Lake, Tibetan Plateau, NW China: *Chemical Geology*, v. 278, p. 151-159.
- Ferry, J.M., Passey, B.H., Vasconcelos, C., Eiler, J.M., 2011, Formation of dolomite at 40-80C in the Latemar carbonate buildup, Dolomites, Italy, from clumped isotope thermometry: *Geology*, v. 39, p. 571-574.
- Li, Zhaoqi, Goldstein, R.H., Franseen, E.K., 2013, Ascending freshwater-mesohaline mixing: a new scenario for dolomitization: *Journal of Sedimentary Research*, v. 83, p. 277-283.
- Meister, P., McKenzie, J.A., Bernasconi, S.M., Brack, P., 2013, Dolomite formation in the shallow seas of the Alpine Triassic: *Sedimentology*, v. 60, p. 270-291.
- Roberts, J.A., Bennett, P.C., Gonzalez, L.A., Macpherson, G.L., Milliken, K.L., 2004, Microbial precipitation of dolomite in methanogenic groundwater: *Geology*, v. 32, p. 277-280.
- Roberts, J.A., Kenward, P.A., Fowle, D.A., Goldstein, R.H., Gonzalez, L.A., Moore, D.S. 2013, Surface chemistry allows for abiotic precipitation of dolomite at low temperature: *Proceedings of the National Academy of Sciences*, v. 110, p. 14540-14545.
- Van Tuyl, F.M., 1916, The present status of the dolomite problem: *Science*, v. 44, p. 688-690.
- Vasconcelos, C., McKenzie, J.A., 1997, Microbial mediation of modern dolomite precipitation and diagenesis under anoxic conditions (Lagoa Vermelha, Rio de Janeiro, Brazil): *Journal of Sedimentary Research*, v. 67, p. 378-390.
- Vasconcelos, C., McKenzie, J.A., 1997, Microbial mediation of modern dolomite precipitation

and diagenesis under anoxic conditions (Lagoa Vermelha, Rio de Janeiro, Brazil):
Journal of Sedimentary Research, v. 67, p. 378-390.

Chapter 2: Primary Precipitation Batch Experiments

Introduction

Dolomite [$\text{CaMg}(\text{CO}_3)_2$] is a rhombohedral carbonate mineral consisting of alternating layers of calcite and magnesite in the hexagonal crystal system. The mineral dolomite is a significant component of ancient carbonate rocks, and dolomite-rich carbonates host productive petroleum reservoirs (e.g. Cantrell et al. 2001), aquifers, and MVT-ore deposits (Anderson & Macqueen 1982). In addition to economic applications, dolomite is useful as a paleo-thermometer and a proxy for ancient seawater chemistry. Despite its economic and scientific significance, the formation mechanisms of dolomite deposits at low temperature ($< 80^\circ\text{C}$) remain poorly understood due to the difficulty of synthesizing anhydrous Mg-bearing carbonates at low temperature (e.g. Xu et al. 2013) and slow or impeded reaction kinetics at low temperature (e.g. Land 1998). Dolomite readily forms at high temperature, but isotopic and fluid inclusion evidence indicates that many ancient dolomites formed at Earth-surface temperatures (e.g. Ferry et al. 2011, Meister et al. 2013, Li et al. 2013). Dolomite is abundant in the rock record but forms only in minor, geographically limited amounts today, despite being significantly supersaturated in modern marine environments. The discrepancy in abundance between modern and ancient dolomites, combined with poorly understood formation mechanisms, forms the crux of the dolomite problem.

Dolomite can form via direct precipitation as a cement or via dolomitization of carbonate sediments (transformation of calcium carbonate to dolomite via reaction with Mg-bearing fluids). These are termed primary and secondary dolomite, respectively. Most massive dolomite deposits are secondary. Primary dolomite is observed in modern environments including sabkhas (e.g. Meister et al. 2013) and alkaline lakes (e.g. Rosen et al. 1989, De Deckker & Last

1988, Yoerg et al. 2016), and low temperature dolomite is observed in the ancient as well (e.g. Li et al. 2013). The study of ancient dolomites and the observation of modern, geographically-limited deposits has led to the development of numerous geochemical models of dolomite formation. The environments these models are based on are zones where distinct geochemical processes occur that are thought to promote dolomite formation. Examples include mixing zone, sabkha, and alkaline lake models of dolomite precipitation. These models function at low temperature, and other models, such as high temperature hydrothermal dolomite, will not be considered here.

Many researchers have hypothesized that the mixing of percolating, fresh groundwater and marine waters results in dissolution of aragonite and precipitation of dolomite (e.g. Badiozamani 1973). Dissolution/precipitation reactions and carbon dioxide exchange are common processes in mixing zones (e.g. Back et al. 1986). Geochemically, mixing zones fall in between two end members – fresh groundwater and marine seawater. For example, the mixing zone on the coast of the Yucatan Peninsula exhibits pH values between 7 and 8.2, with most closer to 7, which are bracketed by marine and phreatic water (Back et al. 1986). Salinity is higher than freshwater but lower than seawater. Carbonate minerals such as calcite and aragonite are typically supersaturated and near equilibrium, but at some points in space (and presumably time), these carbonate phases are undersaturated (Back et al. 1986). Despite the absence of pervasive dolomite, minor dolomite does occur in mixing zone environments. Dolomite precipitation in mixing zone environments such as the Yucatan Peninsula has been reported as fine-grained (3-15 μm), subhedral to anhedral, Ca-rich crystals that replace carbonate muds preferentially relative to larger grains. This Ca-rich dolomite is commonly found near vugs in limestones, suggesting that porosity influences mineral precipitation (Ward & Halley

1984). Dolomite precipitation occurs in these environments during or after dissolution of aragonite; however, the distribution of dolomite suggests it is controlled by aragonite dissolution and occurs in zones of high flow (Ward & Halley 1984).

Saline tidal flats, such as the Abu Dhabi sabkha, are prominent, modern dolomitic environments, with ancient deposits bearing significant similarities (Meister et al. 2013). The Abu Dhabi sabkha consists of -- in stratigraphic order -- Pleistocene sands, a gypsum layer, buried algal mats and lagoonal muds, and surficial gypsum and anhydrite evaporate layers and algal mats (e.g. Butler 1969). Air temperatures range from 16-44°C and precipitation is minimal (<1.5 inches/year), while temperatures at the sabkha ground surface can be as high as ~50°C. pH in sabkha fluids ranges from 6.0-8.3, depending on location within the sabkha. pH is lowest in zones of recharge and highest in lagoonal waters. Across the sabkha, Mg/Ca is variable, ranging from 1.5 to 35, depending on location; it is lowest in lagoonal areas and highest in the recharge zone, and the variation in the Mg/Ca ratio is attributed to dolomitization of muds and the precipitation of gypsum (Butler 1969). Within surficial and shallowly buried sabkha microbial mats, temperatures are more moderate (25-35°C), pH is neutral to slightly alkaline (7.0-7.5), alkalinity ranges from 2-3 mM HCO₃⁻, and Mg/Ca is moderate to high (3-30) (Bontognali et al. 2010). The most dolomite-relevant geochemical difference between the general sabkha environment and the microbial mat environment is elevated alkalinity (e.g. Bontognali et al. 2010).

Dolomite precipitation occurs in modern sabkhas. Dolomite precipitation typically co-occurs with microbial mats in modern sabkhas, even in the absence of active metabolism, suggesting microbial surfaces and locally elevated alkalinity play a role. Specifically, exopolymeric substances (EPS) have been identified as a surface that can bind cations and

promote mineral precipitation in sabkha environments (Bontognali et al. 2010). Bontognali et al. (2010) also report preferential binding of Mg^{2+} to EPS relative to Ca^{2+} , which may overcome kinetic barriers to dolomite precipitation. The association of sabkha dolomite with microbial mats suggests that microbes play a role in dolomite precipitation in these environments, and that geochemical factors alone are insufficient.

Dolomite precipitation occurs in the modern in evaporative, alkaline lakes such as the Coorong Lakes, coastal saline playas, and alkaline lakes in the Nebraska Sand Hills (Rosen et al. 1989, De Deckker & Last 1988, Yoerg et al. 2016). In coastal saline playas of western Australia, dolomite forms as nearly stoichiometric, disordered, fine-grained (0.1-3 μm) crystals in the absence of marine waters or gypsum precipitation. The waters enabling this precipitation are shallow, exhibit very high Mg/Ca (>25), high alkalinity, and seasonally variable salinity (De Deckker & Last 1988). In the Coorong Lakes of southern Australia, dolomite precipitates in two mineralogies: a Mg-rich disordered phase, and a Ca-rich disordered phase. These mineralogies reflect geochemical conditions in the precipitating brines; Ca-rich disordered dolomites are interpreted to result from slower precipitation out of less evaporitic brines relative to Mg-rich dolomites (Rosen et al. 1988).

These models of dolomite formation bracket a range of environmental parameters. Specifically, they represent salinity, alkalinity, and pH end members. In each environment, specific processes are thought to promote dolomite formation by producing a conducive geochemical environment. In addition to these geochemical mechanisms, numerous experimental studies have implicated microbes, indirectly and directly, with primary precipitation of dolomite (e.g. Vasconcelos & McKenzie 1998, Roberts et al. 2004, Deng et al. 2011). Microorganisms are thought to promote dolomite formation by actively altering the

geochemical environment to induce dolomite saturation or remove kinetic barriers (i.e. sulfate reduction) or passively, by providing a reactive surface on which nucleation and precipitation can occur. Past research has shown that salinity correlates with carboxyl group density on microbial surfaces, with microorganisms increasing the density of surface carboxyl groups at higher salinities to prevent cell lysis (Voegerl 2014, Edwards 2016). Highly carboxylated organic matter can dehydrate and preferentially bind complexed Mg^{2+} ions, facilitating the precipitation of ordered, stoichiometric dolomite in addition to other Mg-carbonate phases, from modern and Silurian seawater, in a series of energetically favorable steps (Kenward et al. 2013, Roberts et al. 2013). The binding of magnesium and carbonate to a functional group creates a hydrated magnesium carbonate, which is then free to bind other metal ions (Ca^{2+} , Mg^{2+} , etc.), creating a layer of carbonate mineral on the cell surface.

Past experimental results (Kenward et al. 2013, Roberts et al. 2013) suggest that only the presence of microbial surfaces is necessary to promote precipitation of dolomite and a specific metabolism may not be necessary. These data corroborate the field relationships observed by Bontognali et al. (2010) and the experimental results showing precipitation of dolomite in the presence of sulfate and halophilic bacteria (Deng et al. 2010). These previous results suggest a role for carboxylated organic matter in the formation of low temperature dolomite, but it is not clear if this mechanism is operative in all low temperature geochemical environments. This study evaluates whether carboxylated organic matter, similar to microbial surfaces, is a viable mechanism of dolomite precipitation in various chemical environments that represent accepted models for dolomite formation.

Materials and Methods

Research Approach

Small-scale, controlled, laboratory batch experiments were designed and conducted to investigate the impact of carboxylated microspheres on carbonate mineral precipitation in fluids representative of three different dolomite-related environments (mixing zones, sabkhas, and evaporative, alkaline lakes). Fluids were designed to mimic the salinity (often expressed in terms of parts per thousand by weight, described here using ionic strength in molar), pH, and alkalinity of each specific environment, while Ca and Mg concentrations were held constant for all environments (therefore, Mg/Ca was consistently high). Final solutions were combined with carboxylated polystyrene microspheres and shaken at 70 rpm at controlled temperature (30°C and 40°C, depending on the experiment).

Batch Experiments

Experimental fluids were designed using geochemical modeling, as described below, to mimic the major geochemical parameters that describe the environments of interest – pH, alkalinity, and salinity. Short term batch experiments investigated primary precipitation in three different environments and at two temperatures (30°C and 40°C). Previous experiments have reported dolomite in as few as twenty days (Roberts et al. 2013), and six weeks (Kenward et al. 2013) in marine environments. Here, experiments were limited to durations of five and ten days to evaluate the efficacy of carboxylated organic matter on facilitating dolomite precipitation in various environments (sabkhas, mixing zones, and alkaline lakes) over short periods of time. For each environment, cold-sterilized solutions were created using stock powders (NaCl, Na₂CO₃, CaCl₂•2H₂O, MgCl₂•6H₂O) to emulate environments typical of dolomite formation. The major variables describing these fluids are summarized in Table 1 and the saturation indices of common carbonate minerals are summarized in Table 2. These variables were determined from a literature search for each environment. Once the correct fluid composition was achieved, pH

was adjusted using CO₂(g) and the solutions were cold sterilized using a 0.45 μm vacuum filter. Once the pH was set, experimental vessels were seeded with carboxylated polystyrene microspheres (Bangs Laboratories, Inc., 0.82 μm with a carboxyl group density of 796 ueq g⁻¹) to a concentration of approximately 10¹² carboxyl groups per liter, to mimic the abundance of microorganisms in typical natural waters and set on shakers at 70rpm and the appropriate temperature for the duration of the experiment. After the duration of the run, experimental vessels were uncapped, pH was measured, alkalinity and cation samples were taken, and the solution was filtered using a Millipore 0.45μm white nylon filter to collect precipitates. Precipitates were then dried for further analyses, described below.

Geochemical Modeling

Geochemical modeling was conducted using batch version PHREEQC3 for MacOSX (Parkhurst & Appelo 2013) and the PHREEQC and Pitzer databases. Modeling was conducted to design fluids, determine environmental parameters, and predict thermodynamics of mineral phases of interest in primary and secondary precipitation experiments. The Pitzer database was chosen to accommodate the high ionic strengths of experimental fluids and to include a larger number of mineral species. Speciation models were used to determine saturation states during the experimental design for primary precipitation experiments. Input parameters included temperature, pH, ionic concentrations, and equilibrium phases. Other parameters, including p_e , water density, ionic strength, and saturation index (SI) were calculated by the software.

PHREEQC modeling results for all solutions are contained in Appendix I. These model results represent solutions as they were made in the lab, and closely match the parameters predicted during experimental design. Here, saturation index is defined as:

$$SI = \log \left[\frac{IAP}{K_{sp}} \right],$$

where IAP is the ion activity product for a given phase and K_{sp} is the solubility product for a given phase. Using this notation, a value of three for SI denotes 1000-fold supersaturation. A positive value denotes supersaturation and a negative value denotes under-saturation. A zero value represents equilibrium. All PHREEQC models used the Pitzer database to accommodate the elevated ionic strength of several of these solutions and to maintain consistency in modeling. Many PHREEQC databases draw on inconsistent thermodynamic data sources or draw from various literature sources. All models here draw on the same database. The Pitzer database is the most consistent database available, albeit for a limited set of species (Parkhurst & Appelo 2013). Additionally, the Pitzer equations are based on empirical data and are applicable at elevated ionic strength (>0.5), where equations such as the extended Debye-Hückel break down (Pitzer 1973). Pitzer equations use the ion-interaction virial coefficient approach to correct for activity in highly concentrated solutions (e.g. Parkhurst & Appelo 2013). Limitations of the Pitzer database, such as a limited number of species and the inability to handle redox reactions, are not problematic for this work. An additional limitation of activity modeling of brines, the scaling-dependence of activity, especially when models include measured pH, is discussed below (Plummer et al. 1988).

Fluid Chemistry

Fluid chemistry was tracked over experiment duration. pH was measured using an Accumet AB200 pH meter. Alkalinity titrations were conducted using 0.1N HCl and a handheld buret. Samples were titrated past the endpoint, then plotted to determine alkalinity using the inflection point method. For inductively coupled plasma optical emission spectroscopy (ICP-OES), samples were acidified, diluted on a mass-basis using an. ultrapure, trace metal grade 2% HNO_3 solution, if necessary, then analyzed using a Perkin Elmer ICP DV5300, and compared

against mass-based multi- and single-element standards. Raw ICP data was reduced and drift-corrected manually by placing a standard throughout the run and correcting all intensity values back to this standard using linear interpolation. Anions other than alkalinity were not analyzed due to the simple nature of experimental fluids, as the only anion other than carbonate was chlorine. Chlorine concentrations were determined from fluid construction based on relative amounts of stock powders and assumed to remain constant.

Electron Microscopy

Electron microscopy was conducted at the University of Kansas Microscopy and Analytical Imaging facility. For scanning electron microscopy (SEM), samples were collected by setting a carbon tape-covered stub on the filter containing the precipitate to collect the sample, gold coating the stub to 10 nm, and imaged on a FEI Versa DualBEAM SEM at a working distance of 10 mm and accelerating voltages of 2 KeV and 5 KeV. Elemental analysis was conducted using energy dispersive spectroscopy (EDS) at 10 KeV and analyzed using Aztec software (Oxford 11 Instruments). Because no actual organic matter was involved in these experiments, sequential dehydration using a graded ethanol series was unnecessary. For transmission electron microscopy, samples were collected on a lacy carbon grid and imaged using a FEI Tecnai F20 XT Field Emission Transmission Electron Microscope.

X-ray Diffraction

Bulk precipitate mineralogy was characterized using X-ray diffraction (XRD). XRD patterns were run at the KU Molecular Structures Laboratory following their protocol: room temperature x-ray powder patterns were obtained using monochromated CuK α radiation ($\alpha = 1.54178 \text{ \AA}$) on a Bruker Proteum Diffraction System equipped with Helios high-brilliance multilayer optics, a Platinum 135 CCD detector and a Bruker MicroStar microfocus rotating

anode x-ray source operating at 45kV and 60mA. The powders were mixed with a small amount of Paratone N oil to form a paste that was then placed in a small (< 0.5 mm.) nylon kryoloop and mounted on a goniometer head. The specimen was then positioned at the goniometer center-of-motion by translating it on the goniometer head. Two overlapping 1 minute 180° ϕ -scans were collected using the Bruker Apex2 V2010.3-0 software package with the detector at $2\theta = 35^\circ$ and 90° using a sample-to-detector distance of 50.0 mm. These overlapping scans were merged and converted to a .RAW file using the Pilot/XRD2 evaluation option that is part of the APEX2 software package. This .RAW file was then processed using the Bruker EVA powder diffraction software package. For the purposes of visualization, the .RAW file was converted to .UXD format, then again to .CSV format, and plotted using the R software package (R Core Team 2013) to allow rapid and interactive analysis of diffractograms, although peak picking was conducted using the Bruker database.

Raman Spectroscopy

For Raman analysis, bulk samples were homogenized and packed into a powder on a steel slide or analyzed directly on the filter paper. Backscattered Raman spectra were collected at room temperature with a Renishaw inVia Reflex Raman Microprobe (Renishaw plc, Wotton-under-Edge, UK). The Raman scattered light was dispersed by a diffraction grating with 1200 mm/line, and the signal was analyzed with a Peltier-cooled CCD camera (1024x256 pixels). Sample excitation was achieved with a Renishaw diode laser emitting at a wavelength of 785 nm. The laser was focused onto a 2 μm spot size through a 10x (NA = 0.25) microscope objective. The attached microscope is a Leica DMLM. The laser power impinging on the carbonate minerals were 0.5-5 mW in order to minimize laser-induced heating and to avoid structural modification of the sample. Multiple scans (three) were utilized to obtain the best

possible spectra; however, fluorescence, possibly caused by the presence of the polystyrene microspheres, was an issue for many samples. The Raman shift is calibrated by recording the Raman spectrum of the F_{1g} phonon of silicon for one accumulation and ten seconds. If necessary, an offset correction was performed to ensure that the position of the F_{1g} mode is at $520.50 \pm 0.10 \text{ cm}^{-1}$. No baseline correction or other spectral processing was undertaken.

Results

Mixing Zone Environments

The major environmental parameters (pH, alkalinity, ionic strength) and carbonate mineral saturation indices for each environment and treatment are summarized in Tables 1 and 2. The mixing zone solution, characterized by circumneutral pH, low alkalinity, and low salinity (ionic strength of 0.31-0.48 M), is supersaturated with respect to dolomite across all experimental treatments ($SI_{\text{dolomite}} = 0.95\text{-}1.26$). Saturation indices for other carbonate minerals are variable. Aragonite and calcite are near equilibrium. Aragonite is slightly undersaturated at 40°C for five days, but slightly oversaturated elsewhere. Calcite is slightly undersaturated at 30°C and slightly oversaturated at 40°C. The Mg-bearing carbonates, huntite ($\text{CaMg}_3(\text{CO}_3)_4$) and magnesite (MgCO_3), are always supersaturated. All other phases, such as the salts, are significantly undersaturated.

Over the duration of the experiments, changes in pH, Mg and Ca concentration, and alkalinity are slight and at or below the 5% resolution of the instrument (Table 3, Figure 1). Figure 1 shows the normalized changes in geochemistry, where the initial value is normalized to 1 and the end value is expressed as a proportion of the original value. All geochemical changes are similar in the presence and absence of microspheres. Normalizing the geochemical changes

across environments shows the relative geochemical change in mixing zone environments to be slight (Figure 1).

Characterization of the bulk mineral precipitate was conducted using X-ray diffraction. The dilute solution produces an inconclusive diffractogram under all experimental treatments (Figure 2). Scanning electron photomicrographs show very little precipitate is produced in the dilute solution, but that sub-spheroidal precipitates co-occur with the microspheres in this environment at both 30°C and 40°C after five days, and that micron-scale calcium carbonate crystals precipitated from the dilute solution with and without microspheres after ten days at 40°C (Figure 3).

Sabkha Environments

The sabkha solution, characterized by circumneutral pH, low to moderate alkalinity (modified during experimentation), and high salinity (ionic strength ~3M), is slightly oversaturated with respect to Ca-bearing carbonates such as calcite and aragonite, but significantly oversaturated with respect to Mg-bearing or Ca/Mg-bearing carbonate phases such as magnesite, huntite, and dolomite ($SI_{\text{dolomite}} = 1.40 - 3.48$). These values are more or less in agreement with models used to design fluids (see Table 1), where measured pH was not imparted on the speciation calculation.

The pH remains stable in the sabkha environment during the experiment durations. Changes in Ca and Mg concentration and drops in carbonate alkalinity are similar in the presence and absence of microspheres. Mg/Ca rises in all experiments, but the magnitude of the rise is higher in the absence of microspheres. When alkalinity is increased for the higher temperature experiments (to ~38 mmol), more precipitation occurs, and the geochemical changes are more pronounced. Relative to their initial values, concentrations of Ca, Mg, and alkalinity drop

significantly. At the lower alkalinity used for the initial 30°C experiment (~1 mmol), geochemical changes are subtle or at the limits of detection (Figure 1).

Diffractograms summarize the mineralogy of the sabkha solution precipitates (Figure 4). The sabkha solution produces primarily halite at 30°C (Figure 4A). At 40°C, after five and ten days, the sabkha solution produces aragonite in the presence and absence of carboxylated microspheres (Figure 4B, 4C; Note: alkalinity was increased for saline fluids after the 30°C experiments, see Tables 1 and 2). SEM photomicrographs of precipitate from the sabkha solutions are shown in Figure 4. Figure 5A shows carboxylated microspheres occurring on a mineral lath (potentially aragonite), and Figure 5B shows fine-grained precipitates on filter paper. Aragonite crystals from the sabkha solution occur both in the presence and absence of microspheres (Figures 5C, 5D). Calcium carbonate precipitated from the saline solution as large aragonite laths (Figure 5E) and as micron-scale precipitates (Figure 5F). Both habits were observed in the presence and absence of carboxylated microspheres. The carboxylated microspheres are observed on the surface of calcium carbonate mineral laths.

Alkaline Lake Environments

The alkaline lake solution, characterized by elevated pH (~9), alkalinity, and slightly elevated ionic strength (~1M), is significantly oversaturated for numerous Ca and Mg-bearing carbonates under all experimental treatments. Saturated phases include aragonite, artinite ($\text{Mg}_2\text{CO}_3(\text{OH})_2 \cdot 3\text{H}_2\text{O}$), calcite, dolomite, gaylussite ($\text{CaNa}_2(\text{CO}_3)_2 \cdot 5\text{H}_2\text{O}$), huntite, magnesite, nesquehonite ($\text{MgCO}_3 \cdot 3\text{H}_2\text{O}$), and pirssonite ($\text{Na}_2\text{Ca}(\text{CO}_3)_2 \cdot 2\text{H}_2\text{O}$).

The alkaline lake solution exhibited the most dramatic geochemical changes, with alkalinity dropping significantly for all treatments with and without carboxylated microspheres.

Both Mg and Ca decreased, with Ca decreasing more than Mg. Mg/Ca rose for all treatments (Figure 1, Table 3).

After five days at 30°C, the alkaline lake solution produces monohydrocalcite, hydromagnesite, and calcite (Figure 6A). At 40°C, after both five and ten days, the alkaline lake solution again produces hydromagnesite, monohydrocalcite, and precipitates with low crystallinity, indicated by the large shoulder at low two-theta (Figure 6B, 6C). After ten days, primarily hydromagnesite is observed (Figure 6B). Additional mineralogical analysis using Raman spectroscopy focused on the precipitates formed from alkaline lake solutions. Raman spectroscopy provides detailed mineralogical characterization of experimental precipitates and allows a measure of the degree of disorder in the bulk precipitate. Precipitates created in the alkaline solution at 30°C show broad, blended peaks at low Raman shift (Figure 7). The most significant phonon observable both in the presence and absence of microspheres occurs at 1069 cm^{-1} . Figure 8 shows spectra of precipitates created after five days at 40°C in the alkaline solution. The dominant peaks in both the presence and absence of carboxylated microspheres are A_{1g} phonons at Raman shifts of 1089 cm^{-1} and 1126 cm^{-1} . The E_g modes at lower Raman shift are broad and blend together.

Figure 9 shows photomicrographs of precipitates created in the alkaline solution. Figure 9A and 9B shows the precipitates from the alkaline solution after five days at 30°C. Hydromagnesite occurs as acicular crystals and appears to mantle calcium carbonate precipitates. Hydromagnesite from the alkaline solution occurs as acicular crystals, while calcium carbonate occurs as rounded and cubic crystals. The alkaline solution produces acicular hydromagnesite, similar to other treatments, in both the presence and absence of carboxylated microspheres. Carboxylated microspheres are observed on the mineral surface.

Analysis of experimental precipitates using SEM-EDS allows for determination of precipitate chemical distribution at a fine-scale. Elemental character can be analyzed using both point scans and maps. Point scans bridge the gap between XRD and SEM, and typically confirm mineral identification based on crystal habit. Point scans also reveal significant chemical heterogeneity in mineral precipitates from the alkaline solution (Figure 10). Within this sample, mixed Ca-Mg carbonates occur as spheroidal, micron scale precipitates (spectra 16, 17) on the surface of large hydromagnesite crystals (spectrum 15). Other precipitates are primarily Ca-rich (spectrum 14).

Microsphere and Mineral Associations

Across geochemical environments, microspheres appear to be coated in a thin layer of mineral, evidenced by their irregular surface, and sub-spheroidal precipitates occur near sphere surfaces. These precipitates are tens to hundreds of nanometers in diameter and observed exclusively in association with microspheres. Chemical characterization using TEM-EDS maps of microspheres from the alkaline solution show that both Ca and Mg occur on the microsphere surface in the alkaline solution, and that Mg is enriched on the surface relative to Ca by a factor of approximately ten based on EDS data (Figure 11). Detailed microscopic analysis of the microsphere surfaces reveals that morphologically similar precipitates co-occur in association with the sphere surface across geochemical environments (Figure 12).

Beyond the microsphere surface, EDS mapping reveals trends in chemical distribution related to the presence and absence of carboxylated microspheres. Figure 13 shows SEM images of precipitates from the alkaline solution (30°C, five days) and associated EDS maps. The EDS maps reveal that Mg and Ca occur in discrete phases in the absence of microspheres. Precipitate occurs as a Ca-rich core mantled by Mg-rich material. In contrast, in the presence of

microspheres, Mg and Ca are more evenly distributed throughout the bulk precipitate, although Ca still composes the core of the precipitates.

Discussion

The geochemical environments studied here are important locations of carbonate mineral precipitation and diagenesis, and have specific relevance to the formation of dolomite at low temperature. Here, the products of each experiment are put into environmental context, and the set of experiments is then discussed in context of low-temperature dolomite.

Mixing Zones

Mixing zones are zones in which percolating fresh groundwater mixes with marine water. Despite a thermodynamic foundation, mixing zone dolomite formation lacks the support of field evidence (e.g. Smart et al. 1988, Luczaj 2006). Most modern mixing zone dolomites are restricted in size, and do not explain the massive dolomite platforms seen in the rock record (e.g. Ward & Halley 1984). Additionally, the geochemical window in which dolomitization may occur in such a setting is very restrictive when the impacts of cation ordering on equilibrium constants are considered (Hardie 1987). Overall, mixing of fresh and marine waters appears to promote dissolution, not dolomitization, but may increase porosity and enable movement of a dolomitizing fluid (Hardie 1987). This characterization is consistent with the results produced here. Geochemical changes were slight and very little precipitate formed in the mixing zone solutions, although nanoscale precipitate does appear on microsphere surfaces. Because these experiments were conducted in batch, the results are best understood as representative of geochemical processes occurring in one pore volume over a short period of time. The total amount of precipitate for solutions here is dictated by its carbonate alkalinity. For a solution like the mixing zone, with low carbonate alkalinity, the volume of precipitate able to be produced is

slight. Advective flux could potentially promote sustained precipitation and should be the subject of future research (e.g. Hardie 1987), as it could also promote extensive dissolution. Modifications of the mixing zone model, such as the ascending freshwater-mesohaline mixing model (Li et al. 2013), should also be the subject of experimental work.

Sabkhas

The Abu Dhabi sabkha is one of the most notable environments forming dolomite today, and refluxing brines have been suggested to form massively dolomitized carbonate platforms observed in the rock record. Here, the sabkha environment was emulated with high ionic strength, low to moderate alkalinity, circumneutral pH, and elevated Mg/Ca solutions. Secular variations in seawater Mg/Ca control the calcium carbonate polymorph that precipitates (e.g. Wilkinson & Given 1986). Elevated concentrations of magnesium poison calcite crystal growth and promote precipitation of aragonite (Folk 1974). In general, a Mg/Ca >2 represents aragonite seas, while a Mg/Ca <2 represents seas likely to form calcite. Experimental study has suggested that Mg/Ca is not the only factor controlling aragonite vs. calcite seas: alkalinity pCO₂ also control the polymorph precipitated. Depending on the combination of Mg/Ca, alkalinity, and pCO₂, either calcite or aragonite is the primary component, and in the Mg/Ca range, differences in these parameters produce significantly different results (Lee & Morse 2010).

The sabkha solution studied here had a Mg/Ca of 10, which places it in the realm of aragonite seas. This is consistent with the XRD and SEM observations, which showed aragonite as the predominant precipitate (Figure 4, 5). Raman spectra of experimental precipitates confirm XRD results, and can provide insight into the degree of order/disorder in the precipitate. Due to limited alkalinity, no other carbonate phases formed in the sabkha environment. This is likely due to the rapid precipitation kinetics of calcium carbonate consuming the available alkalinity.

Additionally, without elevated alkalinity, very little carbonate precipitate was produced and only halite was observed. The halite produced here likely results from the solution drying on the filter and is therefore an artifact of sample collection – solutions were not supersaturated with respect to halite. In natural environments, Bontognali et al. (2014) observe dolomite in buried microbial mats with slightly elevated alkalinity within the Abu Dhabi sabkha. As mentioned above, these experiments failed to account for advective flux. Reflux dolomitization requires long-term advective flux of saline fluids driven by a density differential (Adams & Rhodes 1960), and dolomitization has significant mass transfer requirements (Hardie 1987). Future work should focus on emulating this in a laboratory setting.

Alkaline Lakes

Solutions modeled after alkaline lakes produced the most carbonate mineral precipitate due to excessively high alkalinity. Examining the measured geochemical changes in the batch experiments, most of the data reflect mineral precipitation as thermodynamically predicted (by PHREEQC or from published thermodynamic data), and the impact of the carboxylated microspheres is not apparent in the bulk solution chemistry (Table 1). Relative geochemical changes are also the most significant in alkaline lake environments, evidenced by the large drops in Ca, Mg, and alkalinity (Figure 1).

The minerals produced reflect what was predicted using geochemical modeling and the temperature and chemical conditions of the experiments. XRD reveals hydromagnesite and monohydrocalcite are common components of the precipitate (Figure 6). Hydromagnesite formed in alkaline solutions at warmer temperatures (40°C) is morphologically similar to hydromagnesite found in natural environments (e.g. Canaveras et al. 1999), as shown under SEM (Figure 8). The $\log(K_{sp})$ for hydromagnesite ranges from -37.08 to -38.90 at 25°C and 50°C

(Gautier et al. 2014). This is substantially less soluble than dolomite ($\log(K_{sp}) = -17.4$), calcite ($\log(K_{sp}) = -8.35$), and aragonite ($\log(K_{sp}) = -8.22$), which explains why it is the dominant precipitate observed in the alkaline solutions studied here. Sequestration of magnesium into carbonate minerals could have relevance as a future source of magnesium for dolomitization of sediments; however, because dolomite is metastable relative to hydromagnesite, it is unlikely that hydromagnesite could act as a source for future dolomitization in the geochemical environment of the experiment. Environments that produce abundant hydromagnesite are geochemically unique (pH >9 and wide range of Mg/Ca; Braithwaite & Zedef 1996) and may not be applicable to other depositional and diagenetic settings.

Additionally, monohydrocalcite is a common component of precipitate produced from the alkaline solution. Like hydromagnesite, this phase was not predicted in the geochemical modeling but is thermodynamically reasonable. The $\log(K_{sp})$ for monohydrocalcite has been determined to be -7.6 (Hull & Turnbull 1973) and -7.05 (Kralj & Brecevic 1995), making it metastable relative to the other carbonate phases produced here. Monohydrocalcite ($\text{CaCO}_3 \cdot \text{H}_2\text{O}$) has been synthesized in the lab and observed in nature (e.g. Neumann & Epple 2007). It is the product of unique geochemical environments in which carbonate alkalinity exceeds calcium concentration and magnesium is present in solution, and co-precipitates with hydrous magnesium carbonates (Nishiyama et al. 2013). It has been found in nature in marine, cave, and lacustrine settings (Dahl & Buchardt 2006, Fischbeck & Müller 1972, Stoffers & Fischbeck 1974). Monohydrocalcite has been experimentally shown to transform into aragonite with time (Munemoto & Fukushi 2008). Its occurrence in these experiments may be a product of short experimental duration and unique geochemistry.

The Raman shifts observed on samples from the alkaline solution at 40°C (Figure 8) detect both hydromagnesite (A_{1g} at 1126 cm^{-1}) and calcium carbonate with incorporated magnesium (A_{1g} at 1089 cm^{-1}). At 30°C, the spectra are consistent with monohydrocalcite (Coleyshaw et al. 2003). In these samples, the phonon modes observed at lower Raman shift are generally broad and blend together. This suggests a large degree of disorder in the crystal structure, which is hypothesized to be a result of rapid precipitation rates facilitated by elevated alkalinity.

Magnesium-bearing phases

The purpose of these experiments was to evaluate the hypothesis that carboxylated organic matter can promote dolomite precipitation at low temperature in chemical environments modeled after three classic dolomite models: mixing zone, sabkha, and alkaline lake (e.g. Badiozamani 1973, Adams & Rhodes 1960, and De Deccker & Last 1988). In effect, this combines longstanding models of dolomite precipitation with more recently recognized kinetic factors. This was accomplished using batch experiments conducted at 30°C and 40°C for five and ten days. Dolomite has yet to be clearly shown in the data summarized here, but various interpretations regarding carbonate mineral precipitation can still be drawn. Previous studies have required TEM selected area electron diffraction (SAED) data to show nanometer-scale dolomite (Roberts et al. 2013), which is currently unavailable for this work. Due to this scale issue, the data shown here may not preclude dolomite on the microsphere surface.

In general, Mg-bearing phases such as hydromagnesite occur in the bulk precipitate only in solutions with abundant alkalinity and elevated pH. When alkalinity is lower, either calcium carbonate or halite precipitate (Figures 2, 4, 6). This suggests that elevated alkalinity facilitates magnesium removal from solution. One potential reason for this is reaction kinetics. Calcium

carbonate precipitates rapidly, and if alkalinity in solution is low, precipitation will cease once the alkalinity is consumed. If alkalinity is high enough to sustain carbonate precipitation, Mg-bearing phases will occur after fast-precipitating calcium carbonates have formed. This is supported by the microscopy data, which shows Mg-bearing phases mantling Ca-bearing phases (Figure 13).

While differences in the nature of the bulk precipitate across geochemical environments are obvious, examining the microsphere-related precipitate is more challenging and ambiguous. To determine the role of carboxylated microspheres in low-temperature carbonate mineral precipitation, it is essential to use techniques with high enough resolution that this nanometer-scale interface can be targeted. Several of the techniques as they were applied in this work, such as XRD and Raman spectroscopy, are bulk measurements and do not provide explicit data regarding the microspheres. The results obtained using XRD show that the phases produced in batch experiments largely reflect the phases predicted by geochemical modeling (with the addition of some phases not in the model database, but thermodynamically realistic). Because the solutions studied were significantly supersaturated, a large amount of precipitate was produced. This poses two problems for XRD analysis: dilution and a scaling issue. The microspheres, with an average diameter of 0.82 μm , likely produced a mineralogical signal that is too small relative to the macroscale, bulk precipitate. This makes detailed microscopy essential. Very small particles produce broad XRD peaks. This is described using the Scherrer equation:

$$L = \frac{K\lambda}{\beta \cos\theta};$$

where L is crystallite size, K is a shape constant, λ is the X-ray wavelength, and β is the peak width at half maximum (e.g. Monshi et al. 2012). The equation shows that peak width and

crystallite size are inversely proportional, therefore, analysis of the nanoscale precipitates on the microsphere surface using XRD would be problematic even without the dilution problem. In light of these considerations, the best use of XRD for this work is to characterize the mineralogy of the bulk precipitate.

Despite not finding ordered, stoichiometric dolomite in the bulk analysis of these experiments, the data presented here suggest that carboxylated organic matter does influence the chemistry of precipitates. TEM EDS data show that magnesium is more abundant than calcium by a factor of approximately ten (Figure 11). The stability constants for the Mg-carboxyl and Ca-carboxyl complexes are similar, both near one. This suggests that the Mg/Ca ratio on the sphere surface is controlled by the Mg/Ca ratio of solution and the process controlling the abundance on the sphere could be competitive sorption/complexation. The co-occurrence of Mg and Ca on the sphere surface is significant because it precludes the precipitation of a pure phase on the microsphere. Whatever carbonate phase forms, it will be somewhere in the calcite-dolomite-magnesite solid solution. The phase that forms must be a carbonate, because carbonate is the only anion available for precipitation in the solutions considered here (halite is an artifact of filter drying and not representative of solution chemistry during experimentation). The stoichiometry of the precipitate may be controlled by solution Mg/Ca, and also could be problematic for producing ordered, stoichiometric dolomite. This hypothesis would explain the results of Roberts et al. (2013), who produced stoichiometric dolomite at low Mg/Ca on carboxylated microspheres, and explains the results produced here. In both sets of experiments, the stoichiometry on the microsphere surface reflects the Mg/Ca of solution. The production of a precipitate in the calcite-dolomite-magnesite solid solution is to be expected due to the similar ionic radii of calcium and magnesium. This is unique to the Ca-Mg-carbonate system because

substitution is allowed. In systems with large differences in ionic radii, such as the Pb-Mg-carbonate system, substitution does not occur and precipitation of a stoichiometric, ordered, mixed phase is more easily accomplished (Lindner & Jordan 2018).

In addition to mixed Mg/Ca-carbonates detected on microsphere surfaces, small spheroidal precipitates and layers of precipitate are observed near and on the microspheres in all chemical environments – dilute, saline, and alkaline (Figure 12). Because all solutions were oversaturated with respect to dolomite and usually other carbonates, and all solutions had similar Mg/Ca, the phase that precipitates presumably is a mixed Mg/Ca carbonate based on the evidence mentioned above. This is significant because it shows that regardless of the bulk solution chemistry (i.e. alkalinity, salinity, and pH), a mixed Mg/Ca carbonate is being produced at the nanoscale by this reactive surface, provided carbonate phases are thermodynamically favorable.

Electron microscopy reveals that in the absence of microspheres, calcium and magnesium occur in discrete phases in the alkaline lake solution (Figure 13). This is interpreted to reflect precipitation kinetics, as mentioned above, and elevated alkalinity promoting precipitation of Mg-bearing phases. This is in contrast to the precipitates created in the presence of the microspheres, where magnesium is more evenly distributed throughout the bulk precipitate. It is possible that templating on the sphere surface enables further precipitation of a mixed Mg/Ca precipitate in chemically favorable environments (e.g. the alkaline lake solution). Carboxylated organic molecules have been shown to enrich precipitates with magnesium (Wang et al. 2009). On the basis of microscopy data, it is possible the microspheres used here may be functioning in a similar way, despite similar mineralogical signals in the bulk precipitate.

Implications

The experiments summarized here were optimized for low temperature dolomite precipitation by increasing carbonate alkalinity, increasing temperature, increasing or decreasing salinity, using a high Mg/Ca (10), excluding any known inhibitors (e.g. sulfate), and including a catalyst (carboxylated microspheres) known to promote dolomite precipitation at lower Mg/Ca from marine water (Roberts et al. 2013). Elevated alkalinity is an important component to the organogenic model of dolomite precipitation (e.g. Bontognali et al. 2010, Baker & Kastner 1981). Additionally, low salinity and high Mg/Ca promote dolomite precipitation (Folk & Land 1975). Field examples (the Abu Dhabi sabkha) and laboratory experiments involving microorganisms implicate high salinity in promoting dolomite formation (e.g. Qiu et al. 2017, Baker & Kastner 1981). Experimental work previously identified sulfate as an inhibitor of dolomite precipitation at low temperature (Baker & Kastner 1981), although subsequent experiments have cast doubt on this idea (Sanchez-Roman 2009). The complexation of Mg ions by sulfate and/or water has been considered the rate limiting step for low temperature dolomite precipitation, and recently, microbial surface processes have been suggested to assist in overcoming this barrier (Roberts et al. 2013, Deng et al. 2010). The fact that ordered, stoichiometric dolomite has yet to be found in the precipitate, combined with numerous reports of dolomite precipitation under different chemical conditions, may draw some of the assumptions about the chemical factors leading to dolomite precipitation into question. For example, dilute solutions, with low Mg/Ca, have produced dolomite in the presence of methanogens (Roberts et al. 2004) and dolomite has been produced from seawater with low Mg/Ca (Roberts et al. 2013).

The Mg/Ca ratio is a parameter used to describe both secular variations in seawater, and to describe the possibility of dolomite precipitation. The origin of Mg/Ca as a dolomite-relevant

parameter is unclear. It could come either from the observation of high Mg/Ca in dolomitizing brines following gypsum precipitation (i.e. Adams & Rhodes 1960), or as a reduction of the law of mass action of the dolomitization reaction:



Taking the law of mass action and assuming the activity of a solid equals one, the dolomitization reaction above reduces to Ca/Mg. A low Ca/Mg (high Mg/Ca) would be indicative of a thermodynamic driver of the forward reaction. Experiments studying low temperature dolomite precipitation on carboxylated microspheres have found that dolomite is favored in calcite seas, where Mg/Ca is less than two (Roberts et al. 2013). This is in stark contrast to much of the literature, which suggests that elevated Mg/Ca is necessary for dolomite precipitation (e.g. Kenward et al 2013, Hardie 1987). The results summarized here, while not corroborating this idea, do not support a high Mg/Ca, or extreme distance from equilibrium, alone facilitating low temperature precipitation of dolomite.

The experiments run in this study were, for the most part, far from equilibrium, especially for those that produced Mg-bearing phases. This is largely due to excessive alkalinity in the alkaline lake solutions. The distance from equilibrium translates to rapid precipitation kinetics and a disordered precipitate. It is possible that slower kinetics and longer reaction times are necessary to produce the ordering structure of dolomite at low temperature. There is abundant evidence that dolomite precipitation and dolomitization occur rapidly at high temperature (e.g. Zempolich & Baker 1993, Kaczmarek & Sibley 2011, Kaczmarek & Sibley 2014). To produce a kinetically slow environment, the system should either be only slightly elevated above equilibrium or have limited diffusion of species.

Additionally, dolomite is observed in modern environments in microbial mats in both sabkhas and alkaline lakes (e.g. Bontognali et al. 2010, Wright 1999). In these environments, dolomite is thermodynamically favored due to elevated alkalinity, Mg/Ca, salinity, and kinetically favored due to the presence of catalysts. However, diffusion is the process that will govern the transport of solutes throughout a microbial mat. Because diffusion is the controlling factor for continued precipitation, these environments might be kinetically slow, despite oversaturation, allowing time for cation ordering of the precipitate. The experiments discussed here were thermodynamically favorable for dolomite (and other carbonates), but not diffusion or advection limited, and therefore enabled rapid precipitation of non-dolomite phases. These batch experiments can be best understood as representative of a pore at a moment in time. Future experimentation should focus on kinetically slow, diffusion-limited environments just above equilibrium, and should be designed to account for diffusive and advective flux to allow for more accurate representation of geological environments.

Conclusion

Batch experiments were conducted that mimicked the geochemical environments of three environments related to the precipitation of dolomite at low temperature: mixing zones, sabkhas, and alkaline lakes. These experiments included synthetic carboxylated organic matter to evaluate the impact of reactive surfaces on carbonate mineral precipitation. Batch experiments lack diffusive or advective flux, and are therefore best understood as representative of a pore space at a moment in time. The results summarized show that the environments associated with these models may not rapidly form dolomite, and that carboxylated organic matter can promote the precipitation of both a more Mg-rich phase and a mixed Mg/Ca carbonate that occurs in the calcite-dolomite-magnesite solid solution regardless of the nature of the bulk solution chemistry.

Its place in the solid solution appears to be governed by the Mg/Ca of solution. Future experiments studying low temperature dolomite should consider advective and diffusive flux to more accurately emulate natural environments and consider the relationship between precipitation rate and cation order.

Tables

Environment	pH	Salinity (M)	Mg/Ca	Alkalinity (HCO ₃ ⁻)
Sabkha	7	~ 6*	10	1 mmol**
Alkaline Lake	9	~1, variable	10	213 mmol
Mixing Zone	7	0.4	10	5 mmol

Table 1: Major environmental parameters used to design experimental fluids for primary dolomite precipitation. Dolomitization fluids were similar (detailed below). *Initial experiments used this ionic strength, but it later had to be lowered due to solubility constraints. **Initial experiments used this alkalinity value, but it was later increased (to ~38 mmol) to emulate microbial mats in sabkhas and promote carbonate mineral precipitation.

	30°C			40°C		
	Dilute	Saline	Alkaline	Dilute	Saline*	Alkaline
SI _{dolomite}	0.95	1.40	6.74	1.26	3.48	6.93
SI _{aragonite}	-0.38	-0.19	2.60	-0.26	0.84	2.67
SI _{calcite}	-0.08	0.11	2.90	0.06	1.16	3.00
SI _{huntite}	0.02	0.99	11.41	0.95	5.44	12.11
SI _{magnesite}	0.24	0.50	3.04	0.32	1.45	3.06

Table 2: Saturation indices of some carbonate phases in batch experiments for both treatment temperatures. Dolomite is significantly supersaturated in all solutions. Huntite and magnesite are near equilibrium to supersaturated in all solutions. Aragonite and calcite are sub-saturated in low alkalinity environments and oversaturated with increased alkalinity. *To facilitate carbonate precipitation, the alkalinity of the saline solution was increased after the first run. This is reflected in the resulting saturation indices. Phases not included in the Pitzer database are not included here.

	30°C 5 days						40°C 5 days						40°C 10 days					
	Alkaline		Saline		Dilute		Alkaline		Saline		Dilute		Alkaline		Saline		Dilute	
	<i>S</i>	<i>NS</i>	<i>S</i>	<i>NS</i>	<i>S</i>	<i>NS</i>	<i>S</i>	<i>NS</i>	<i>S</i>	<i>NS</i>	<i>S</i>	<i>NS</i>	<i>S</i>	<i>NS</i>	<i>S</i>	<i>NS</i>	<i>S</i>	<i>NS</i>
ΔpH	-0.10	-0.03	-0.2	-0.3	-0.09	-0.10	-0.14	-0.18	0.25	0.05	0.13	0.12	-0.41	-0.33	-0.40	-0.41	0.1	-0.14
ΔMg					-4.45	-6.24	-24.53	-24.09	6.67*	-0.43	2.86	-1.22	-31.13	-32.42	-0.02	-0.48	-4.02	-2.08
ΔCa					-0.09	-0.12	-1.34	-1.32	-1.79	-2.81	0.25	-0.09	-4.23	-4.25	-3.27	-3.34	-1.06	-2.13
$\Delta\text{Mg:Ca}$	227	216	0	0.7	-0.72	-1.02	38.13	34.25	13.09	29.38	1.43	0.53	266	475	142	186	1.90	7.94
ΔCO_3	-31.4	-23.48	-0.07	-0.04	-0.40	-0.20	-48.9	-40	-4.86	-6.24	-0.5	-0.1	-88.2	-88.6	-6.96	-9.24	-2.38	-4.77

Table 3: Magnitude of change for each parameter after experimental runs for seeded (S) and control (NS) experimental vessels. *A positive value is indicative of a rise, which is physically unlikely. This value is likely within error. Data for blank cells is currently unavailable.

Figures

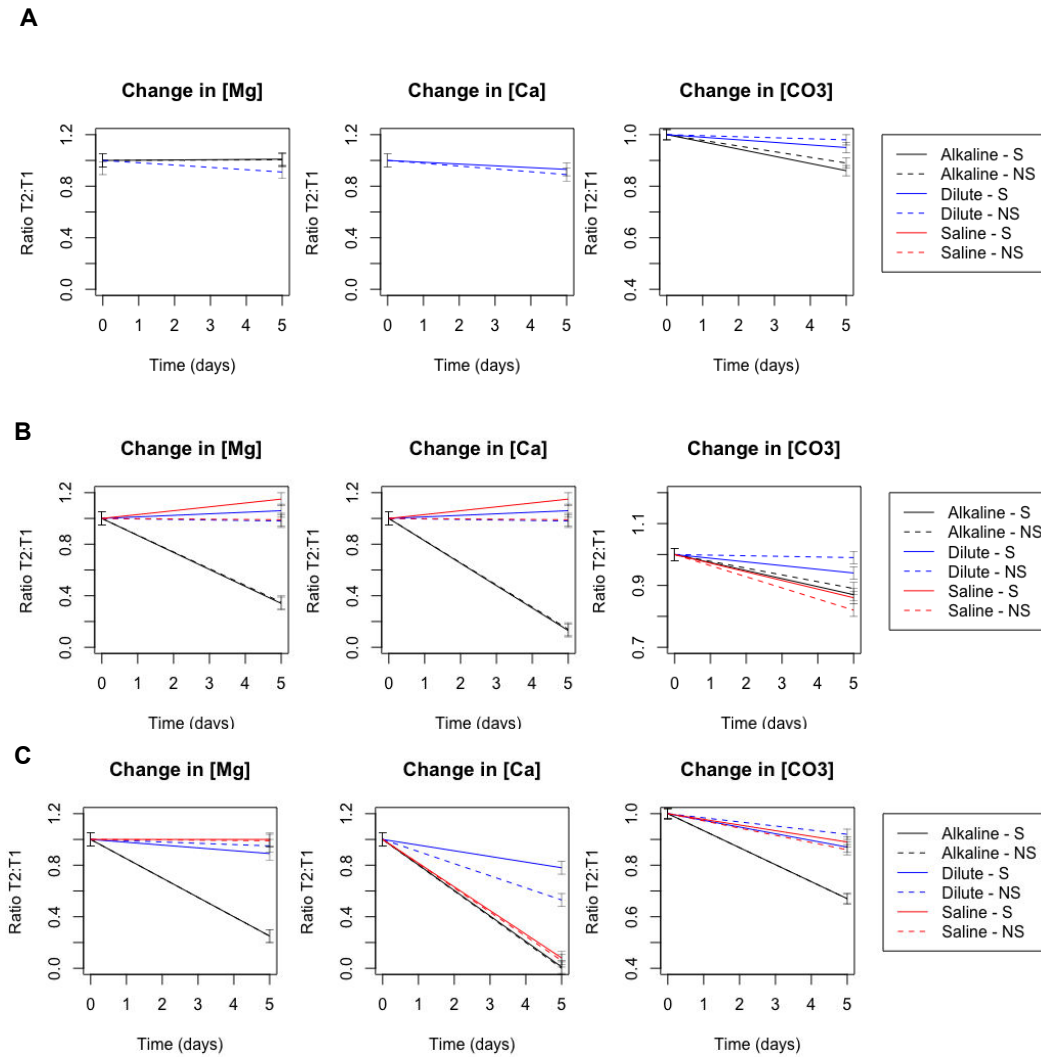


Figure 1: Normalized geochemical changes for all environments for each different treatment. A: 30°C for five days; B: 40°C for five days; C: 40°C for ten days. Note that data for the 30°C experiments is incomplete. The starting value is fixed to 1, and the change is represented as a proportion relative to the starting value.

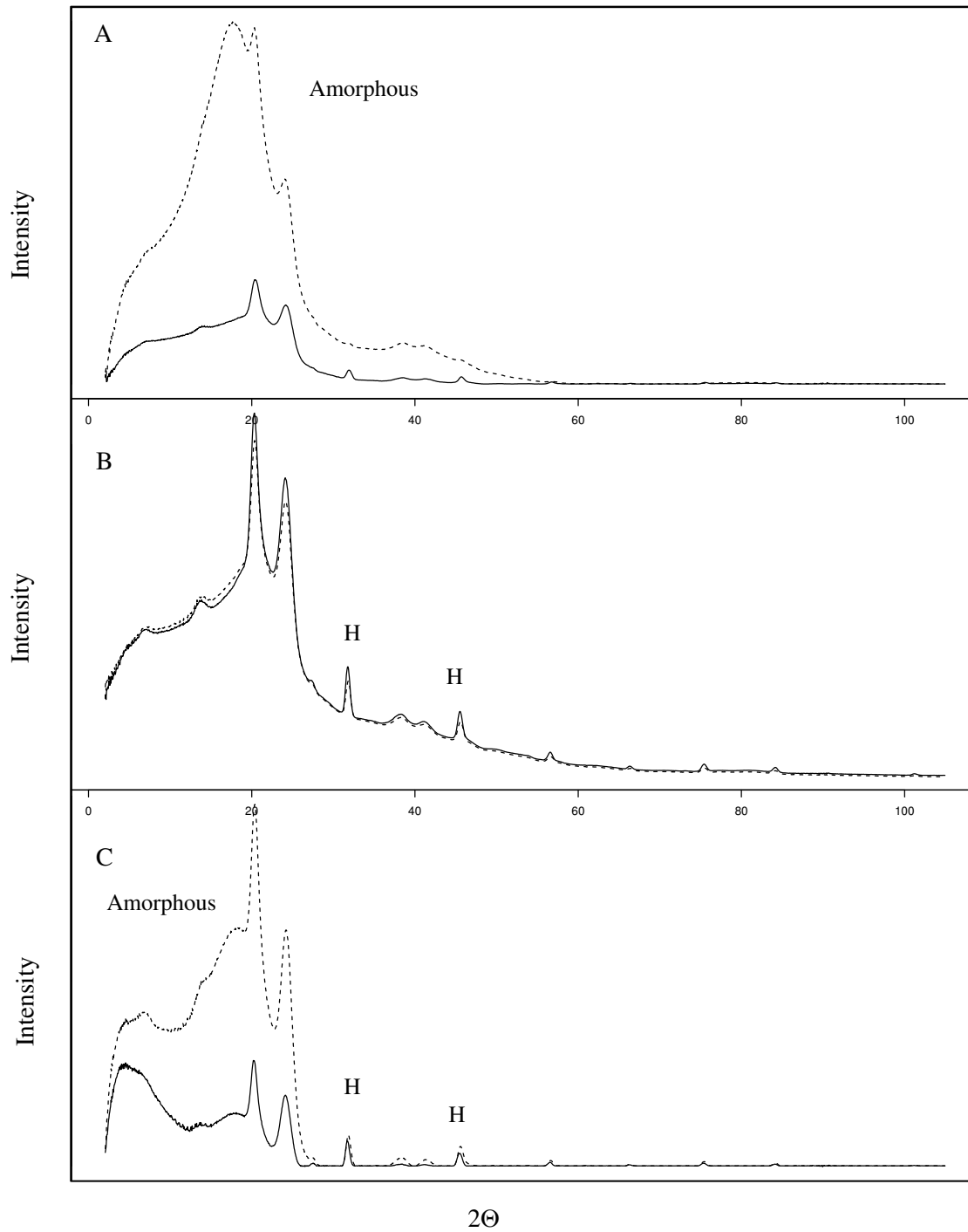


Figure 2: X-ray diffractograms of precipitates produced from mixing zone solutions after (A) 5 days at 30°C, (B) 5 days at 40°C and (C) 10 days at 40°C. Solid line = spheres; dashed line = control. H = halite.

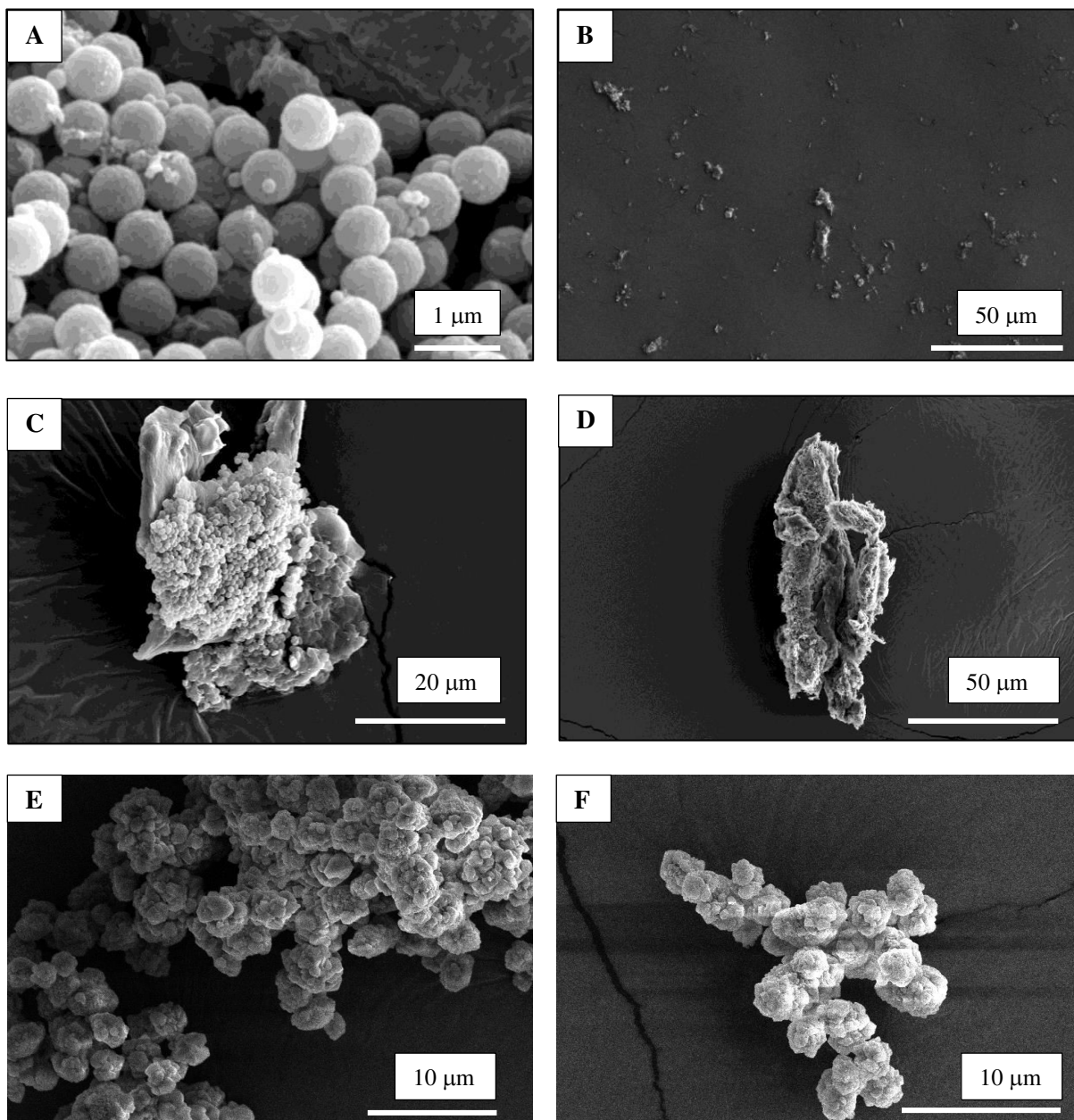


Figure 3: SEM photomicrographs of precipitates produced from the mixing zone solution after (A) 5 days at 30°C with spheres (A) and without (B), 5 days at 40°C with spheres (C) and without (D); and 10 days at 40°C with spheres (E) and without (F).

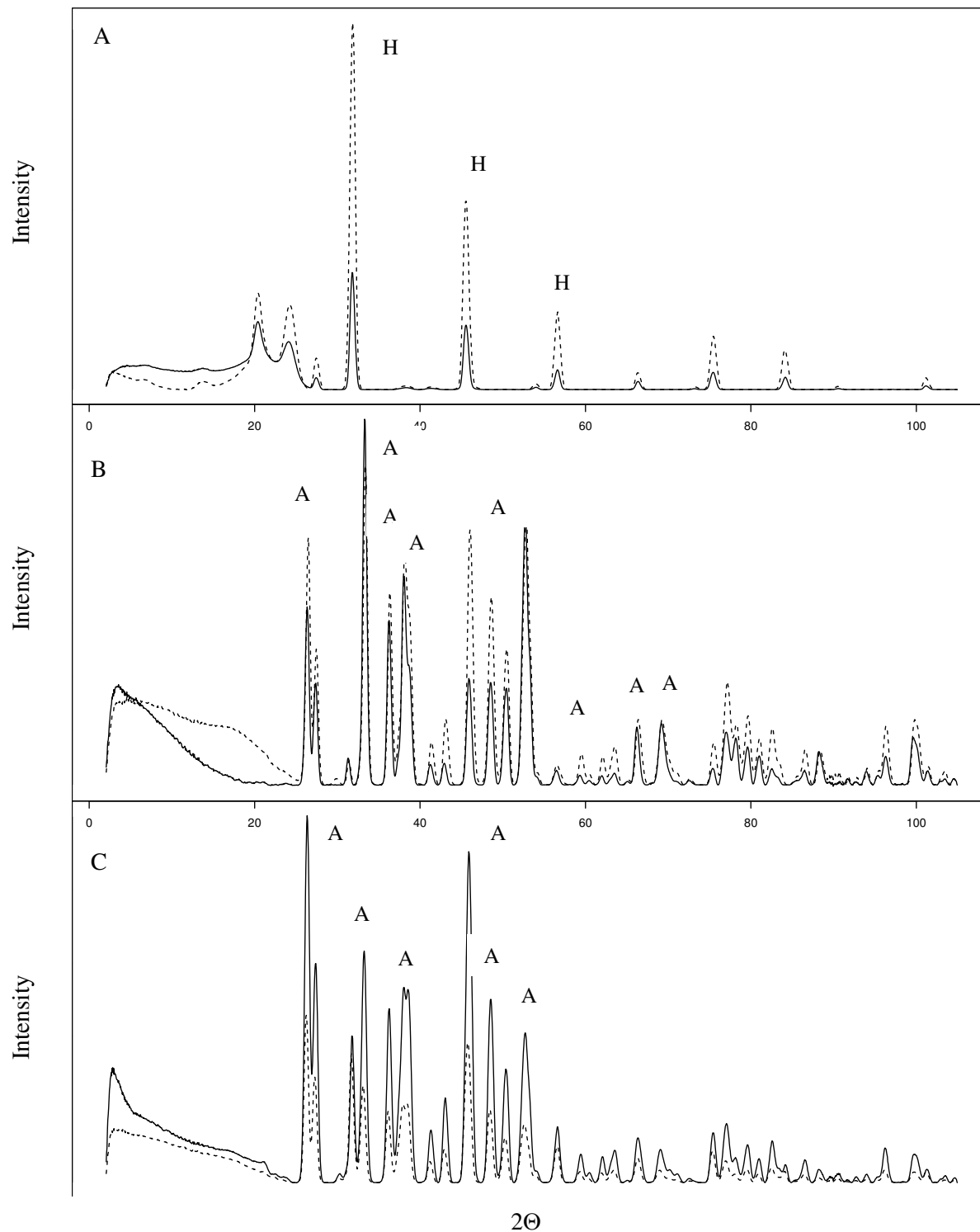


Figure 4: X-ray diffractograms of precipitates produced from sabkha solutions after (A) 5 days at 30°C, (B) 5 days at 40°C and (C) 10 days at 40°C. Solid line = spheres; dashed line = control. A = aragonite.

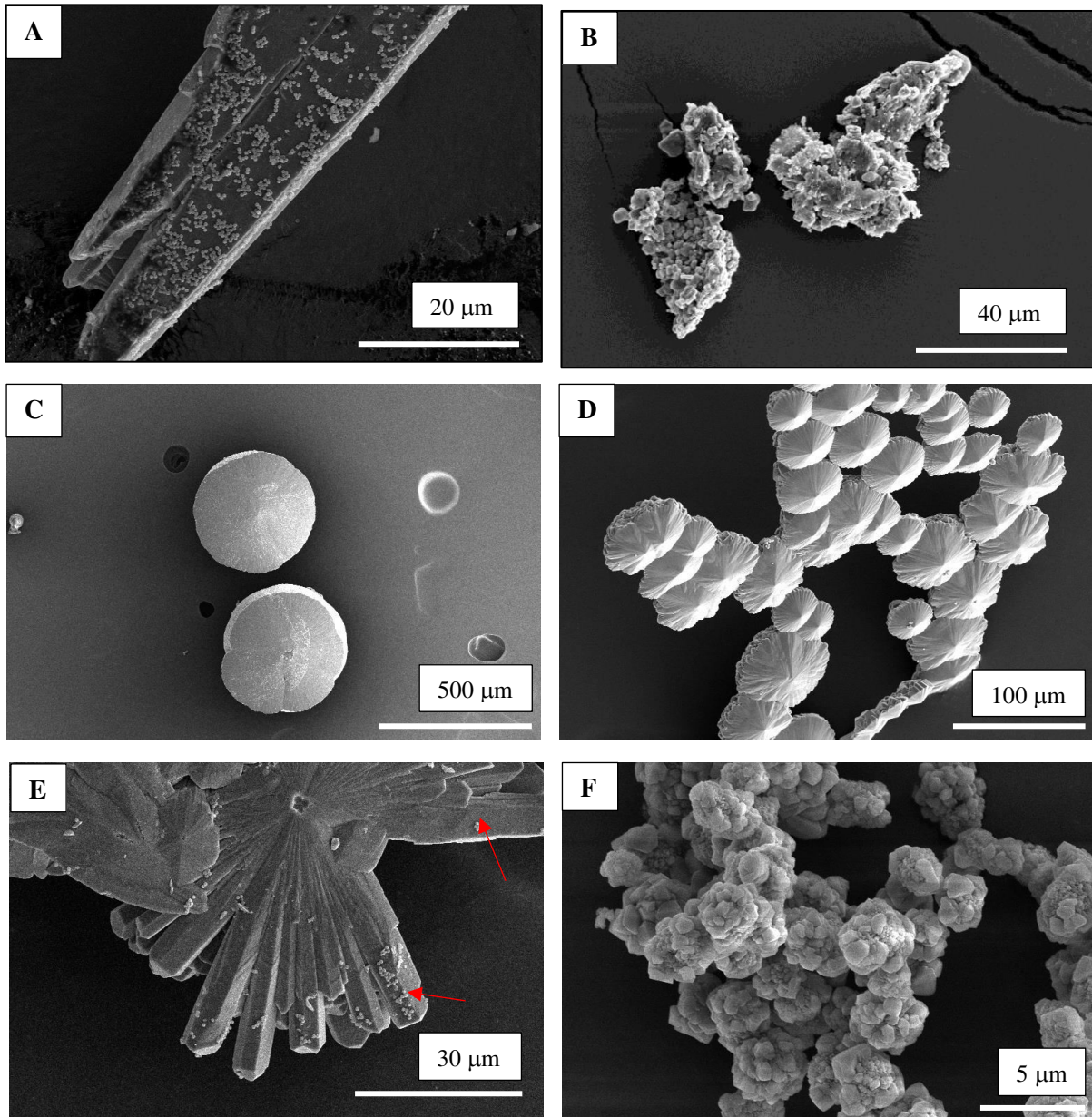


Figure 5: SEM photomicrographs of precipitates produced from the sabkha solution. after (A) 5 days at 30°C with spheres (A) and without (B), 5 days at 40°C with spheres (C) and without (D); and 10 days at 40°C with spheres (red arrows) (E) and without (F).

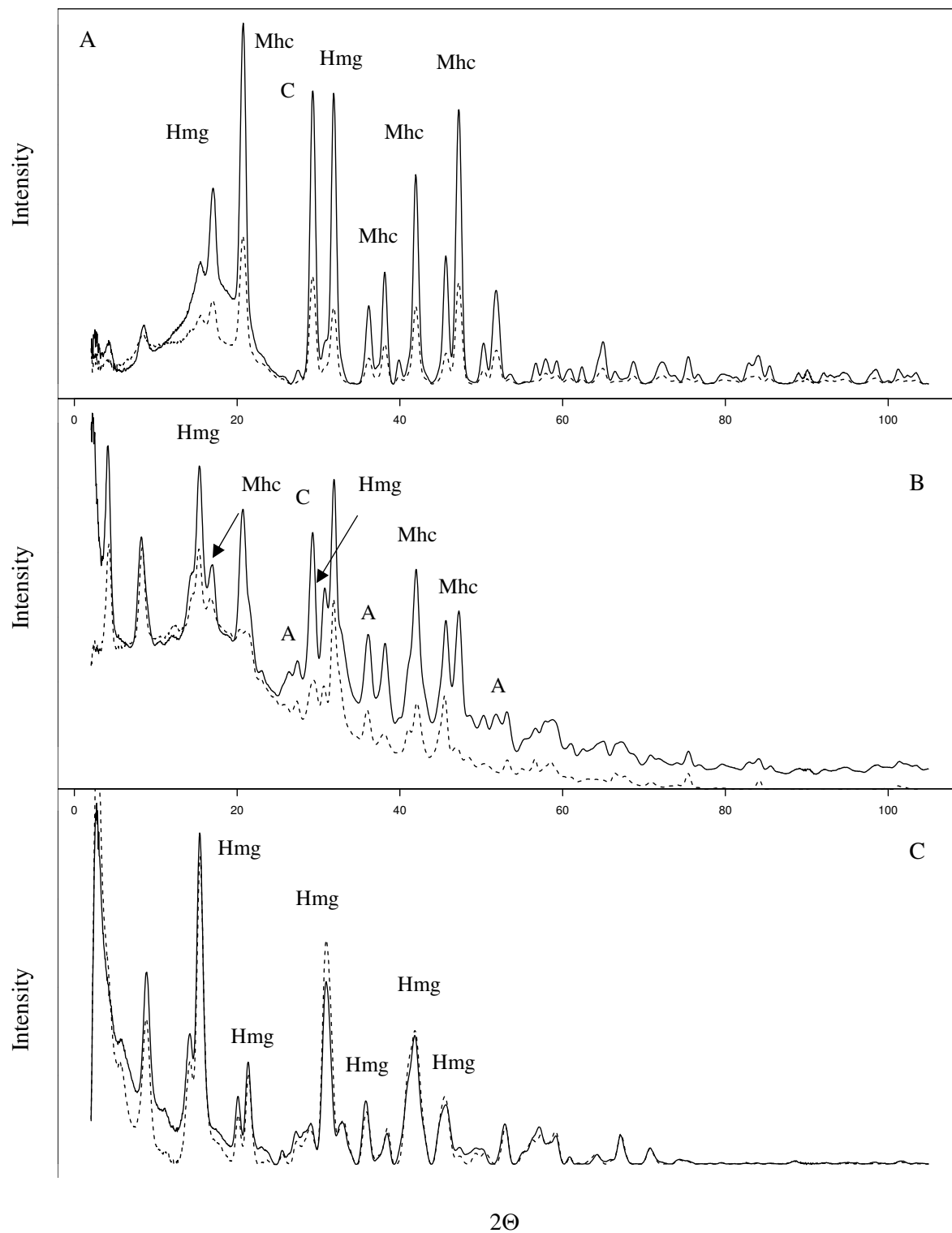


Figure 6: X-ray diffractograms from the alkaline solution after after (A) 5 days at 30°C, (B) 5 days at 40°C and (C) 10 days at 40°C. Solid line = spheres; dashed line = control. A = aragonite; C = calcite; Hmg = hydromagnesite; Mhc = monohydrocalcite.

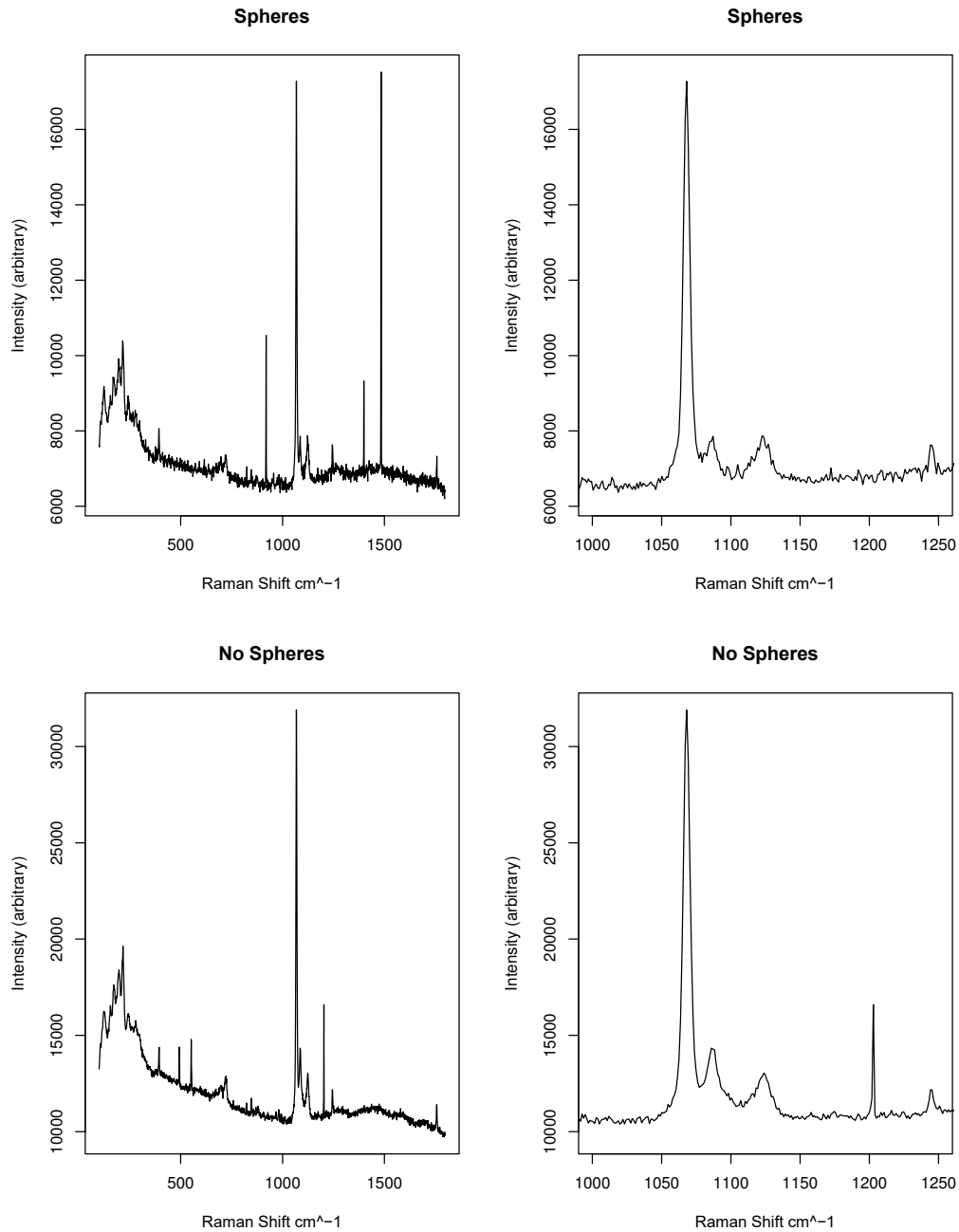


Figure 7: Raman spectra of precipitates created after five days at 30°C in the alkaline solution with and without microspheres. The plots on the right focus on the A_{1g} phonon at 1069 cm^{-1} , indicative of monohydrocalcite. The sample containing spheres exhibited cosmic rays at $\sim 1500\text{ cm}^{-1}$ and at $\sim 900\text{ cm}^{-1}$.

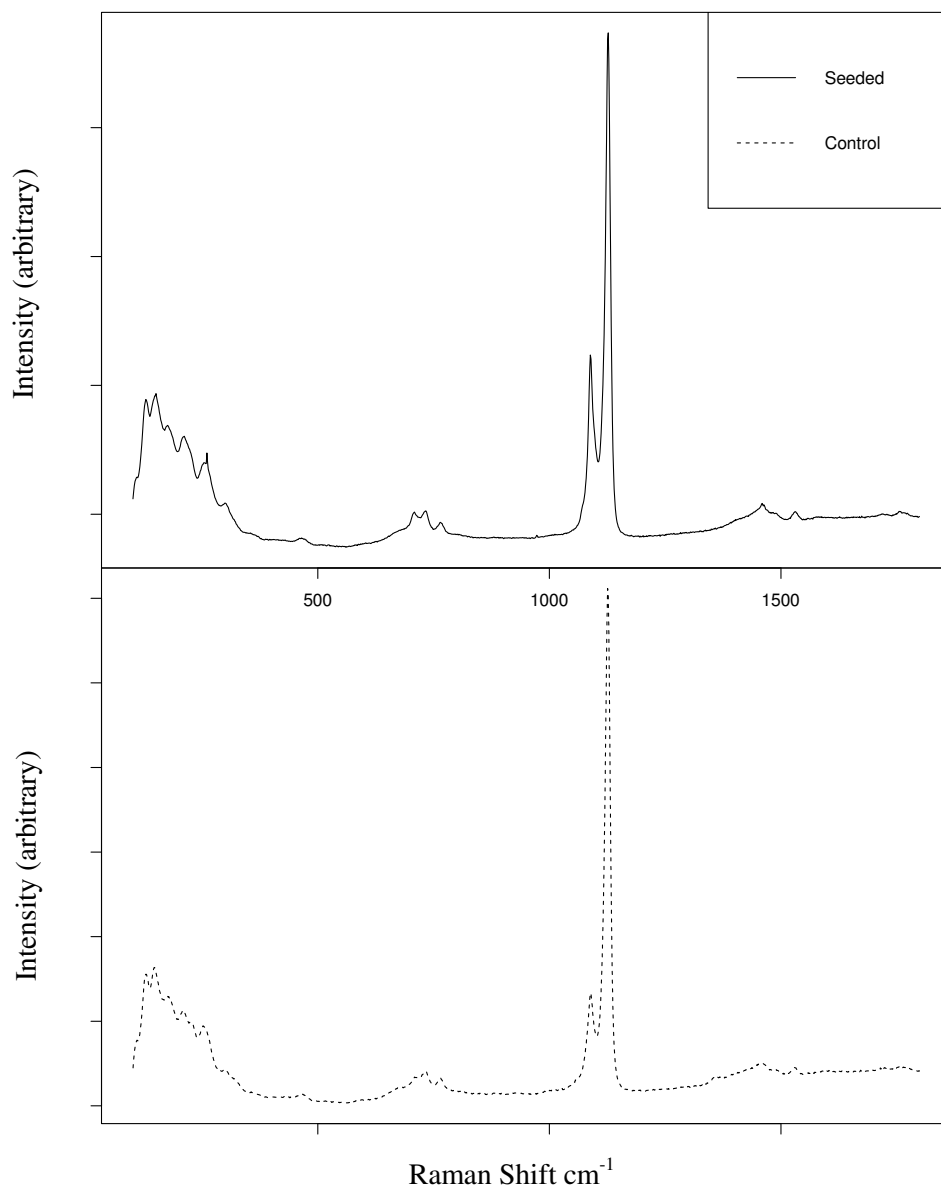


Figure 8: Raman spectra of precipitates from the alkaline solution after five days at 40°C. Peaks are consistent with monohydrocalcite and hydromagnesite.

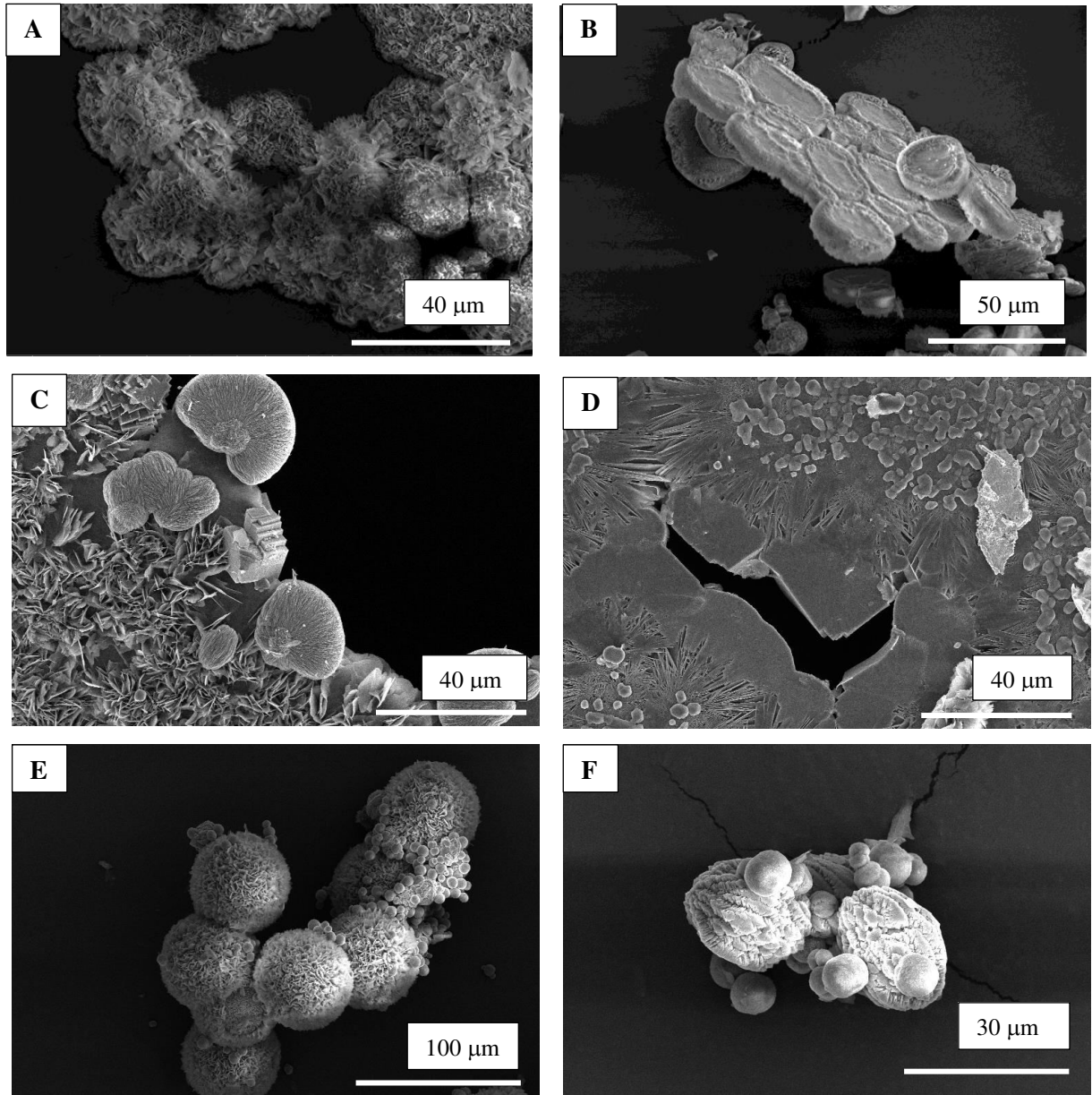


Figure 9: SEM photomicrographs of precipitates produced from the alkaline lake solution. after (A) 5 days at 30°C with spheres (A) and without (B), 5 days at 40°C with spheres (C) and without (D); and 10 days at 40°C with spheres (E) and without (F).

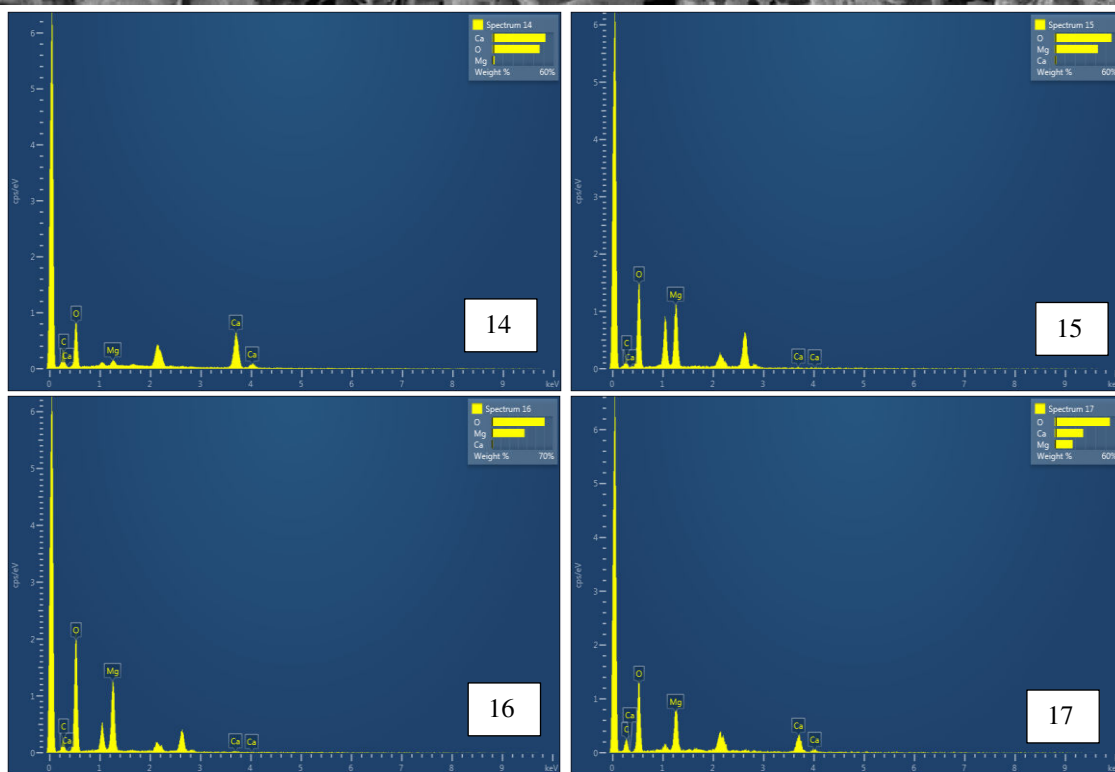
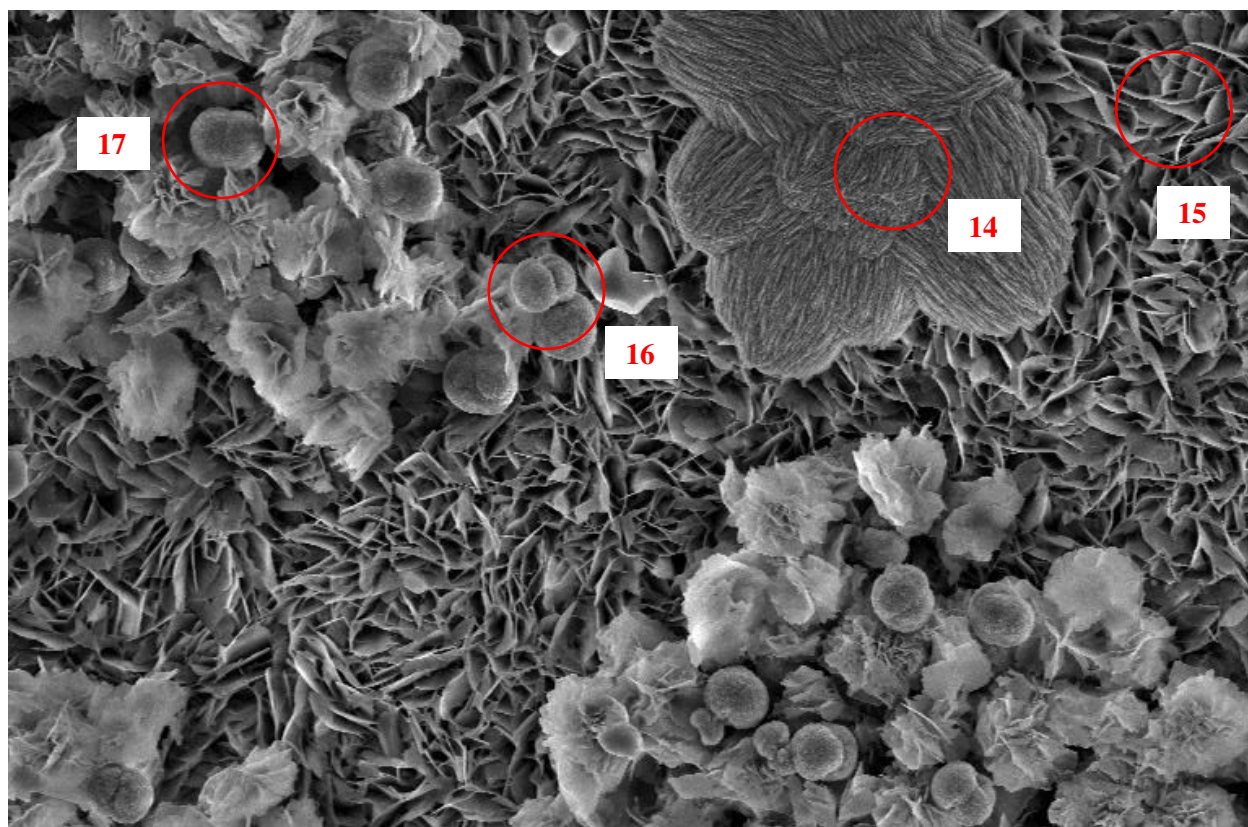


Figure 10: SEM photomicrograph of precipitate from the alkaline solution after ten days at 40C. EDS point scans display chemical heterogeneity in the sample. Spheroidal and dumbbell shaped micron-scale precipitates contain mixtures of Mg and Ca (spectrum 16, 17), while other morphologies are Ca-rich (spectrum 14) or Mg-rich (spectrum 15, presumably a large hydromagnesite crystal).

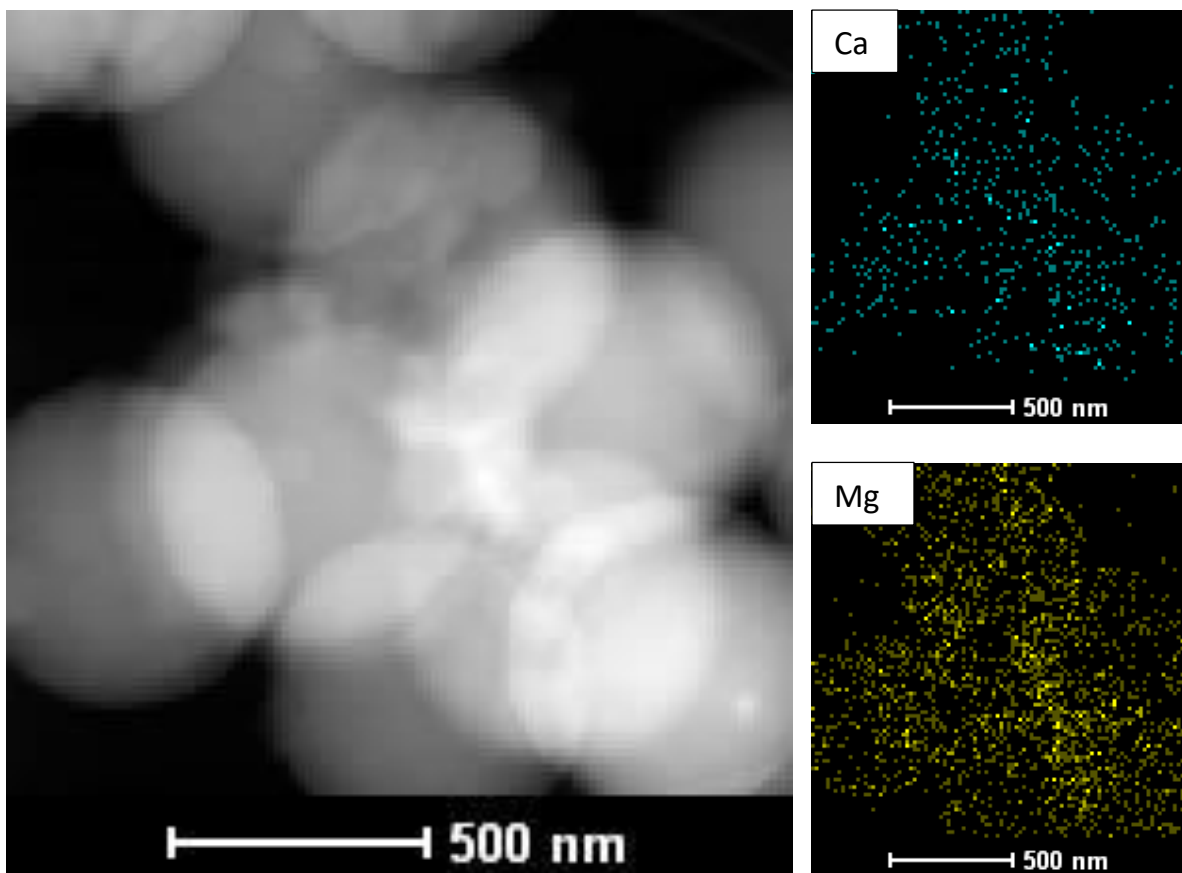


Figure 11: TEM EDS maps of microspheres from alkaline solution showing distribution of both Ca and Mg on the microsphere surface.

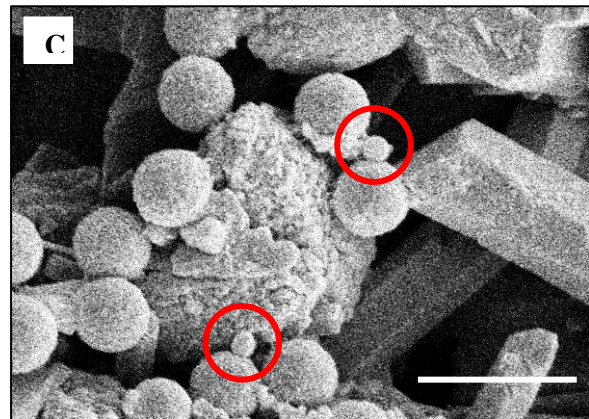
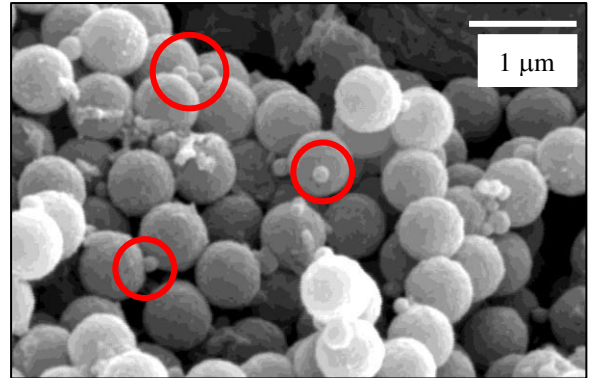
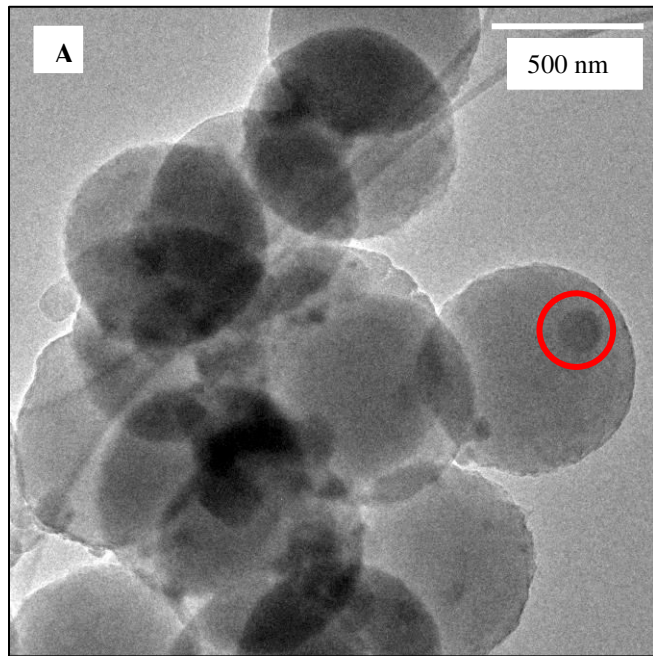


Figure 12: TEM/SEM photomicrographs show sub-stoichiometric, nanoscale precipitates (red circles) co-occurring with carboxylated microspheres across geochemical environments. A: alkaline; B: dilute; C: saline.

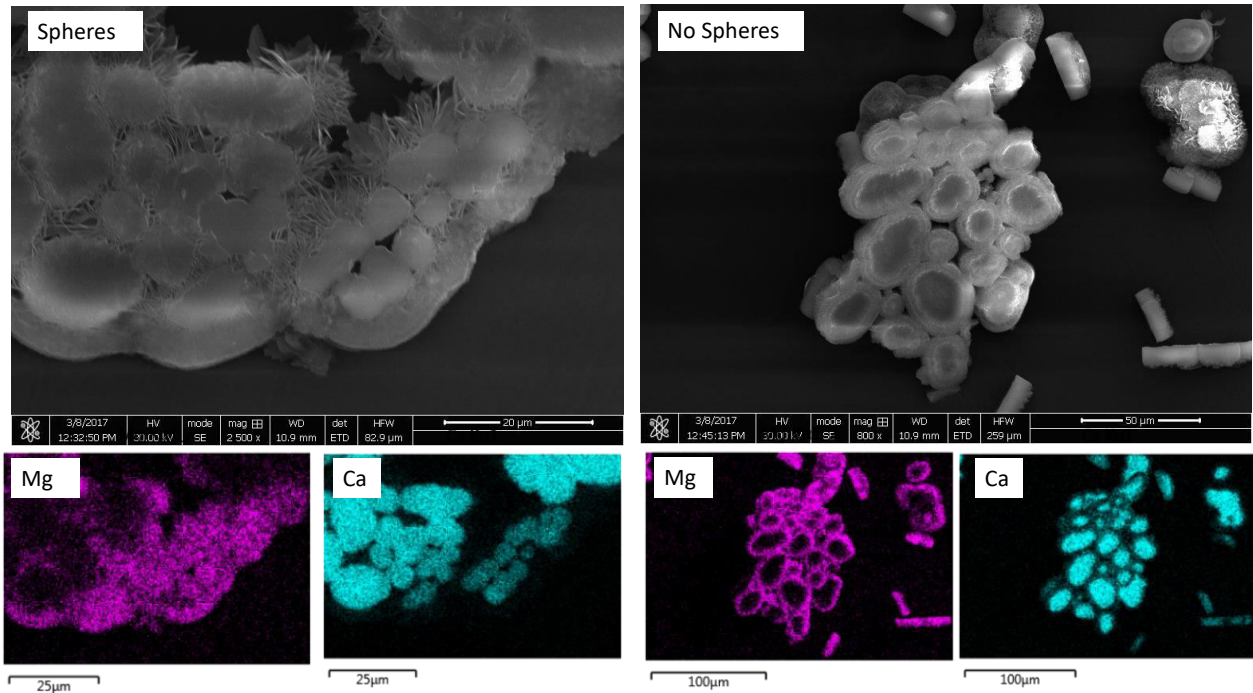


Figure 13: SEM photomicrographs and EDS maps of precipitate from the alkaline lake solution (5 days, 30C). Precipitates consist of spheroidal to sub-spheroidal cores rimmed by acicular crystals. EDS maps show that in the presence of microspheres, Mg is distributed throughout the precipitate. In the absence of microspheres, Mg and Ca occur in discrete phases.

References

- Adams, J.E., Rhodes, M.L., 1960, Dolomitization by seepage refluxion: AAPG Bulletin, v. 44, p. 1912-1920.
- Anderson, G.M., Macqueen, R.W., 1982, Ore Deposit Models – 6. Mississippi Valley-Type Lead-Zinc Deposits: Geoscience Canada, v. 9, p. 108-117.
- Badiozamani, K., 1973, The Dorag dolomitization model – application to the middle Ordovician of Wisconsin: Journal of Sedimentary Petrology, v. 43, p. 965-984.
- Back, W., Hanshaw, B.B., Herman, J.S., Van Driel, J.N., 1986, Differential dissolution of a Pleistocene reef in the ground-water mixing zone of coastal Yucatan, Mexico: Geology, v. 14, p. 137-140.
- Baker, P.A., Kastner, M., 1981, Constraints on the formation of sedimentary dolomite: Science, v. 213, p. 214-216.
- Bontognali, T.R.R., Vasconcelos, C., Warthmann, R.J., Bernasconi, S.M., Dupraz, C., Strohmenger, C.J., McKenzie, J.A., 2010, Dolomite formation within microbial mats in the coastal sabkha of Abu Dhabi (United Arab Emirates): Sedimentology, v. 57, p. 824-844.
- Braithwaite, C.J.R., Zedef, V., 1996, Hydromagnesite stromatolites and sediments in an alkaline lake, Salda Gölü, Turkey: Journal of Sedimentary Research, v. 66, p. 991-1002.
- Butler, G.P., 1969, Modern Evaporite Deposition and Geochemistry of Coexisting Brines, the Sabkha, Trucial Coast, Arabian Gulf: Journal of Sedimentary Petrology, v. 39, p. 70-89.
- Canaveras, J.C., Hoyos, M., Sanchez-Moral, S., Sanz-Rubio, E., Bedoya, J., Soler, V., Groth, I., Schumann, P., Laiz, L., Gonzalez, I., Saiz-Jimenez, C., 1999, Hydromagnesite and

- needle-fiber aragonite deposits in a karstic cave (Altamira, Northern Spain):
Geomicrobiology Journal, v. 16, p. 9-25.
- Cantrell, D.L., Swart, P.K., Handford, R.C., Kendall, C.G., Westphal, H., 2001, Geology and Production Significance of Dolomite Arab-D Reservoir, Ghawar Field, Saudi Arabia: GeoArabia, v. 6, p. 45-60.
- Coleyshaw, E.E., Crump, G., Griffith, W.P., 2003, Vibrational spectra of the hydrated carbonate minerals ikaite, monohydrocalcite, lansfordite, and nesquehonite: Spectrochimica Acta, v. 59, p. 2231-2239.
- Dahl, K., Buchardt, B., 2006, Monohydrocalcite in the Arctic Ikka Fjord, SW Greenland: First Reported Marine Occurrence: Journal of Sedimentary Research, v. 76, p. 460-471.
- De Deckker, P., Last, W.M., 1988, Modern dolomite deposition in continental, saline lakes, western Victoria, Australia: Geology, v. 16, p. 29-32.
- Deng, S., Dong, H., Lv, G., Jiang, H., Yu, B., Bishop, M.E., 2010, Microbial dolomite precipitation using sulfate reducing and halophilic bacteria: Results from Qinghai Lake, Tibetan Plateau, NW China: Chemical Geology, v. 278, p. 151-159.
- Edwards, M., 2016, The Magnitude and Rate of Change of Cell Surface Functional Groups as a Function of Salinity: Implications for Environments of Microbially Facilitated Carbonate Formation: MS Thesis, University of Kansas.
- Ferry, J.M., Passey, B.H., Vasconcelos, C., Eiler, J.M., 2011, Formation of dolomite at 40-80C in the Latemar carbonate buildup, Dolomites, Italy, from clumped isotope thermometry: Geology, v. 39, p. 571-574.
- Fischbeck, R., Müller, G., 1971, Monohydrocalcite, hydromagnesite, nesquehonite, dolomite, aragonite, and calcite in speleothems of the Fränkische Schweiz, Western Germany:

- Contributions to Mineralogy and Petrology, v. 33, p. 87-92.
- Folk, R.L., 1974, The natural history of crystalline calcium carbonate: effect of magnesium Content and salinity: *Journal of Sedimentary Petrology*, v. 44, p. 40-53.
- Folk, R.L., Land, L.S., 1975, Mg/Ca Ratio and Salinity: Two Controls over Crystallization of Dolomite: *AAPG Bulletin*, v. 59, p. 60-68.
- Gautier, Q., Benezeth, P., Mavromatis, V., Schott, J., 2014, Hydromagnesite solubility product and growth kinetics in aqueous solution from 25 to 75 °C: *Geochimica et Cosmochimica Acta*, v. 138, p. 1-20.
- Gregg, J.M., Bish, D.L., Kaczmarek, S.E., Machel, H.G., 2015, Mineralogy, nucleation and Growth of dolomite in the laboratory and sedimentary environment: A review: *Sedimentology*, v. 62, p. 1749-1769.
- Hardie, L.A., 1987, Dolomitization: A Critical View of Some Current Views: *Journal of Sedimentary Petrology*, v. 57, p. 166-183.
- Hull, H., Turnbull, A.G., 1973, A thermochemical study of monohydrocalcite: *Geochimica et Cosmochimica Acta*, v. 37, p. 685-694.
- Kaczmarek, S.E., Sibley, D.F., 2007, A comparison of nanometer-scale growth and dissolution features on natural and synthetic dolomite crystals: implications for the origins of dolomite: *Journal of Sedimentary Research*, v. 77, p. 424-432.
- Kaczmarek, S.E., Sibley, D.F., 2011, On the evolution of dolomite stoichiometry and cation order during high-temperature synthesis experiments: An alternative model for the geochemical evolution of natural dolomites: *Sedimentary Geology*, v. 240, p. 30-40.
- Kaczmarek, S.E., Sibley, D.F., 2014, Direct physical evidence of dolomite recrystallization: *Sedimentary Geology*, v. 61, p. 1862-1882.

- Kelleher, I.J., Redfern, S.A.T., 2002, Hydrous Calcium Magnesium Carbonate, A Possible Precursor to the Formation of Sedimentary Dolomite: Molecular Simulation, v. 28, p. 557-572.
- Kenward, P.A., Fowle, D.A., Goldstein, R.H., Ueshima, M., Gonzaléz, L.A., Roberts, J.A., 2013, Ordered low-temperature dolomite mediated by carboxyl-group density of microbial cell walls: AAPG Bulletin, v. 97, p. 2113-2125.
- Konhauser, K., 2007, Introduction to Geomicrobiology: Blackwell Publishing, Malden, MA, USA.
- Kralj, D., Brecevic, L., 1995, Dissolution kinetics and solubility of calcium carbonate monohydrate: Colloids and Surfaces: Physicochemical and Engineering Aspects, v. 96, p. 287-293.
- Lane, J., Morse, J.W., 2010, Influences of alkalinity and $p\text{CO}_2$ on CaCO_3 nucleation from estimated Cretaceous composition seawater representative of “calcite seas”: Geology, v. 38, p. 115-118.
- Li, Zhaoqi, Goldstein, R.H., Franseen, E.K., 2013, Ascending freshwater-mesohaline mixing: a new scenario for dolomitization: Journal of Sedimentary Research, v. 83, p. 277-283.
- Lindner, M., Jordan, G., 2018, On the growth of witherite and its replacement by the Mg-bearing double carbonate norsethite: Implications for the dolomite problem: American Mineralogist, v. 103, p. 252-259.
- Luczaj, J.A., 2006, Evidence against the Dorag (mixing-zone) model for dolomitization along the Wisconsin arch – A case for hydrothermal diagenesis: AAPG Bulletin, v. 90, p. 1719-1738.
- Machel, H.G., 2004, Concepts and models of dolomitization: a critical reappraisal. FROM:

- Braithwaite, C.J.R., Rizzi, G., Darke, G. (eds) 2004: The Geometry and Petrogenesis Of Dolomite Hydrocarbon Reservoirs. Geological Society, London, Special Publications. v. 235, p. 7-63.
- McKenzie, J.A., 1991, The Dolomite Problem: An Outstanding Controversy. *In* Muller, D.W., McKenzie, J.A., Weissert, H., Controversies in Modern Geology: Evolution of Geological Theories in Sedimentology, Earth History, and Tectonics. Academic Press, Harcourt Brace Jovanovich, Publishers. New York.
- Meister, P., McKenzie, J.A., Bernasconi, S.M., Brack, P., 2013, Dolomite formation in the shallow seas of the Alpine Triassic: *Sedimentology*, v. 60, p. 270-291.
- Monshi, A., Foroughi, M.R., Monshi, M.R., 2012, Modified Scherrer Equation to estimate more accurately nano-crystallite size using XRD: *World Journal of Nano Science and Engineering*, v. 2, p. 154-160.
- Munemoto, T., Fukushi, K., 2008, Transformation kinetics of monohydrocalcite to aragonite in aqueous solutions: *Journal of Mineralogical and Petrological Sciences*, v. 103, p. 345-349.
- Neumann, M., Epple, M., 2007, Monohydrocalcite and its relationship to hydrated amorphous calcium carbonate in biominerals: *European Journal of Inorganic Chemistry*, p. 1953 – 1957.
- Nishiyama, R., Munemoto, T., Fukushi, K., 2013, Formation condition of monohydrocalcite from $\text{CaCl}_2\text{-MgCl}_2\text{-Na}_2\text{CO}_3$ solutions: *Geochimica et Cosmochimica Acta*, v. 100, p. 217-231.
- Parkhurst, D.L., Appelo, C.A.J., 2013, Description of input and examples for PHREEQC Version 3 – a computer program for speciation, batch-reaction, one-dimensional

- transport, and inverse geochemical calculations: U.S. Geological Survey Techniques and Methods, book 6, chap. A43, p. 497. <https://pubs.usgs.gov/tm/06/a43/>.
- Plummer, L.N., Parkhurst, D.L., Fleming, G.W., Dunkle, S.A., 1988, A computer program Incorporating Pitzer's equations for calculations of geochemical reactions in brines: U.S Geological Survey Water-Resources Investigations Report 88-4153.
- Qiu, X., Wang, H., Yao, Y., Duan, Y., 2017, High salinity facilitates dolomite precipitation mediated by *Haloferox volcanii* DS52: Earth and Planetary Science Letters, v. 472, p. 197-205.
- Roberts, J.A., Bennett, P.C., Gonzalez, L.A., Macpherson, G.L., Milliken, K.L., 2004, Microbial precipitation of dolomite in methanogenic groundwater: Geology, v. 32, p. 277-280.
- Roberts, J.A., Kenward, P.A., Fowle, D.A., Goldstein, R.H., Gonzalez, L.A., Moore, D.S. 2013, Surface chemistry allows for abiotic precipitation of dolomite at low temperature: Proceedings of the National Academy of Sciences, v. 110, p. 14540-14545.
- Rodriguez-Blanco, J.D., Shaw, S., Benning, L.G., 2015, A route for the direct crystallization of dolomite: American Mineralogist, v. 100, p. 1172-1181.
- Rosen, M.R., Miser, D.E., Starcher, M.A., Warren, J.K., 1989, Formation of dolomite in the Coorong region, South Australia: Geochimica et Cosmochimica Acta, v. 53, p. 661-669.
- Sanchez-Roman, M., McKenzie, J.A., de Luca Rebellow Wagener, A., Rivadeneyra, M.A., Vasconcelos, C., 2009, Presence of sulfate does not inhibit low-temperature dolomite precipitation: Earth and Planetary Science Letters, v. 285, p. 131-139.
- Slaughter, M., Hill, R.J., 1991, The influence of organic matter in organogenic dolomitization: Journal of Sedimentary Petrology, v. 61, p. 296-303.
- Smart, P.L., Dawans, J.M., Whitaker, F., 1988, Carbonate dissolution in a modern mixing zone:

- Nature, v. 335, p. 811-813.
- Stoffers, P., Fischbeck, R., 1974, Monohydrocalcite in sediments of Lake Kivu (East Africa):
Sedimentology, v. 21, p. 163-170.
- Van Tuyl, F.M., 1916, The present status of the dolomite problem: Science, v. 44, p. 688-690.
- Vasconcelos, C., McKenzie, J.A., 1997, Microbial mediation of modern dolomite
precipitation and diagenesis under anoxic conditions (Lagoa Vermelha, Rio de Janeiro,
Brazil): Journal of Sedimentary Research, v. 67, p. 378-390.
- Voegerl, R.S., 2014, Quantifying the Carboxyl Group Density of Microbial Cell Surfaces as a
Function of Salinity: Insights into Microbial Precipitation of Low-Temperature Dolomite:
MS Thesis, University of Kansas.
- Wang, D., Wallace, A.F., De Yoreo, J.J., Dove, P.M., 2009, Carboxylated molecules regulate
magnesium content of amorphous calcium carbonates during calcification: PNAS, v. 106,
p. 21511-21516.
- Ward, W.C., Halley, R.B., 1984, Dolomitization in a Mixing Zone of Near-Seawater
composition, late Pleistocene, Northeastern Yucatan Peninsula: Journal of Sedimentary
Petrology, v. 55, p. 407-420.
- Warthmann, R., van Lith, Y., Vasconcelos, C., McKenzie, J.A., Karpoff, A.M., 2000, Bacterially
induced dolomite precipitation in anoxic culture experiments: Geology, v. 28, p. 1091-
1094.
- Wilkinson, B.H., Given, R.K., 1986, Secular variation in abiotic marine carbonates: Constraints
on Phanerozoic atmospheric carbon dioxide contents and oceanic Mg/Ca ratios: The
Journal of Geology, v. 94, p. 321-333.
- Wright, D.T., 1999, The role of sulphate-reducing bacteria and cyanobacteria in dolomite

- formation in distal ephemeral lakes of the Coorong region, South Australia: *Sedimentary Geology*, v. 126, p. 147-157.
- Xiaoxian, L., Jun, P., Du, L., Yan, J., Hou, Z., 2017, Characterization of the microbial dolomite of the Upper Sinian Dengying Formation in the Hanyuan Area of Sichuan Province, China: *Acta Geologica Sinica (English Edition)*, v. 91, p. 806-821.
- Xu, J., Yan, C., Zhang, F., Konishi, H., Xu, H., Teng, H.H., 2013, Testing the cation-hydration effect on the crystallization of Ca-Mg-CO₃ systems: *Proceedings of the National Academy*, v. 110, p. 17750-17755.
- Yoerg, A., Roberts, J.A., Omelon, C.R., Stotler, R., Fowle, D., 2016, Geochemical controls on sediment mineralogy and morphology in alkaline lakes: Nebraska Sand Hills, USA. KICC Annual Meeting, Lawrence, KS. Poster.
- Zempolich, W.G., Baker, P.A., 1993, Experimental and natural mimetic dolomitization of aragonite ooids: *Journal of Sedimentary Petrology*, v. 63, p. 596-606.
- Zhang, F., Xu, H., Konishi, H., Shelobolina, E.S., Roden, E.E., 2012, Polysaccharide-catalyzed nucleation and growth of disordered dolomite: A potential precursor of sedimentary dolomite: *American Mineralogist*, v. 97, p. 556-567

Chapter 3: Dolomitization Experiments

Introduction

Dolomite [$\text{CaMg}(\text{CO}_3)_2$] is a significant constituent of many carbonate rocks that host hydrocarbon deposits, ore minerals, and groundwater aquifers. Dolomite is abundant in the rock record but is not found forming in large amounts in modern environments, and despite its economic importance, the formation mechanisms of dolomite at low temperature remain unclear. This is generally called the dolomite problem. Additionally, most dolomite-rich carbonate rocks formed from preexisting limestone via a process called dolomitization and are considered secondary deposits. The majority of dolomite in the rock record is secondary.

The transformation from calcium carbonate to dolomite is kinetically slow, explaining the paucity of dolomite in modern environments, and requiring most experimental work on dolomitization to be conducted at high temperature. Results of high temperature experiments show that dolomitization rate is strongly temperature dependent and proceeds through intermediate Mg-bearing phases which recrystallize to dolomite over the course of the experiment (Kaczmarek & Thornton 2017). Kinetically, the precipitation rate of these intermediate phases controls the rate at which dolomitization proceeds (Kaczmarek & Thornton 2017). At lower temperatures, a longer induction period is observed where no mineralogical changes occur. Insights from reactive transport modeling suggest that dolomitization rate is also controlled by flow rate, temperature, surface area, and salinity (Jones & Xiao 2005).

Nucleation of dolomite is a critical first step in dolomitization of calcium carbonate sediments. Recent studies of low temperature dolomite have shown that microbial surfaces, specifically carboxylated organic matter, can act as catalysts to dolomite nucleation by binding magnesium and making it available for precipitation (Roberts et al. 2013). This is in contrast to

studies that have suggested active microbial metabolism produces a chemical environment conducive to dolomite precipitation (i.e. Vasconcelos & Mckenzie 1998). Because the rate of dolomitization is controlled by the kinetics of the intermediate phases, the binding of magnesium by carboxylated organic matter could potentially enhance the rate of dolomitization.

The experiments discussed here simplified the aqueous geochemistry of environments associated with dolomitization (mixing zones and sabkhas) and modified fluids previously used to dolomitize at high temperature (i.e. Zempolich & Baker 1993) and combined these simplified fluids with a carboxylated polystyrene microspheres, a known catalyst to dolomite precipitation. These fluids optimized geochemically for dolomite by exhibiting high Mg/Ca and either low or high salinity. The goal of these experiments was to determine if carboxylated organic could promote dolomitization of calcium carbonate cements at low temperature over a short time period. Parameters such as temperature and reactive surface area were the same across experiments, so that each environment was tested with and without carboxylated microspheres.

Materials & Methods

Research Approach

Batch experiments investigating dolomitization were conducted by combining stock powders with deionized water to emulate the major parameters of the environment associated with dolomitization (sabkhas and mixing zones, Table 1). An additional fluid, mimicking the geochemistry of high temperature dolomitization experiments (Zempolich & Baker 1993) was also used. Solutions were cold sterilized and adjusted to the proper pH using CO₂. Carboxylated polystyrene microspheres (Bangs Laboratories, Inc., 0.82 μm with a carboxyl group density of 796 ueq g⁻¹) were added to a concentration of approximately 10¹² carboxyl groups per liter. This concentration mimics the abundance of microorganisms in typical natural waters. Experiments

were then set on shakers at 70 rpm. Natural ooids (not sieved, heterogeneous, medium to very coarse), collected from various parts of the Bahamas were air dried, disinfected using 70% ethanol, and dried again. XRD data identified aragonite as the dominant mineral in the ooids. Approximately 3 grams (~0.1 mole aragonite) of disinfected ooids were added to each experimental vessel, bringing the volumetric water: rock ratio to approximately 100:1. Experimental vessels were set on shakers for the duration of the experiment (6 weeks total for dolomitization experiments) at 40°C. Following the experiment, vessels were uncapped and all water chemistry analyses were completed. The precipitate was collected using a Millipore 0.45µm white nylon filter and air dried for further analyses. For two series of dolomitization experiments, initial fluid alkalinity was set at zero to induce aragonite dissolution and supply alkalinity for dolomite precipitation (see Figure 1).

Figure 1 is a conceptual diagram describing how these experiments attempted to induce dolomitization. The dissolution of ooids in the presence of aggressive weathering fluids drives the system to dolomite saturation. Provided the environment is kinetically favorable (i.e. microspheres are present), it was hypothesized that dolomite precipitation would occur. PHREEQC modeling shows that at equilibrium with aragonite, dolomite is supersaturated in the system (Appendix II).

Geochemical Modeling

The batch version of PHREEQC3 for MacOSX (Parkhurst & Appelo 2013) and the PHREEQC and Pitzer databases was used for geochemical modeling. Modeling was conducted to design fluids, determine environmental parameters, and predict thermodynamics of mineral phases of experiments. Because the solutions here exhibit high salinity, the Pitzer database was chosen (Pitzer 1973). Speciation and equilibrium models were used to determine saturation state

and equilibrium conditions during the experimental design for dolomitization experiments. Input parameters included temperature, pH, ionic concentrations, and equilibrium phases, and the remaining parameters were calculated by the software. For the purposes of modeling, the ooids were assumed to be pure aragonite.

PHREEQC modeling results for all dolomitization experiments are contained in Appendix II. Here, saturation index (SI) is defined as:

$$SI = \log \left[\frac{IAP}{K_{sp}} \right],$$

where IAP is the ion activity product for a given phase and K_{sp} is the solubility product for a given phase. Therefore, equilibrium would be represented by a value of zero. The Pitzer database is the most consistent database available, despite containing a limited set of species (Parkhurst & Appelo 2013), so it was used for all models generated here.

Fluid Chemistry

Fluid chemistry was tracked over experiment duration to elucidate geochemical processes occurring in batch. pH was measured using an Accumet AB200 pH meter. Alkalinity titrations were conducted with a handheld buret and 0.1 N HCl using the inflection point method. For inductively coupled plasma optical emission spectroscopy (ICP-OES), samples were acidified with trace metal grade HNO₃, diluted on a mass-basis using 2% HNO₃ solution, if necessary, then analyzed using a Perkin Elmer ICP DV5300. To determine concentrations, samples were compared against mass-based multi- and single-element standards. Manual drift correction on raw ICP data was conducted using linear interpolation. Anions other than alkalinity were not analyzed because experiments were simple and anions other than carbonate (chloride) were assumed to be conservative. Chloride concentrations were calculated based on solution recipes.

Fluorescence Microscopy

Fluorescence microscopy (FM) was conducted using an Olympus BX51 Petrographic Scope with a mercury vapor-arc-discharge lamp, and two exciter filters designed to transmit in the UV (330-385 nm wavelength) and violet blue (400-440 nm wavelength) region.

Micrographs were described qualitatively.

Electron Microscopy

For scanning electron microscopy (SEM), samples were embedded and mounted on glass thin sections by National Petrographic Service (Rosenberg, Texas). Thin sections were gold coated to 10 nm and imaged on a FEI Versa DualBEAM SEM. This work used a working distance of 10 mm and accelerating voltages of 2 KeV and 5 KeV. Elemental analysis was conducted using energy dispersive spectroscopy (EDS) at 10 KeV and analyzed using Aztec software (Oxford 11 Instruments).

X-ray Diffraction

Prior to XRD analysis, samples were air dried and ground to a fine powder in a mortar and pestle. XRD patterns were run at the KU Molecular Structures Laboratory following their protocol: room temperature x-ray powder patterns were obtained using monochromated CuK α radiation ($\alpha = 1.54178 \text{ \AA}$) on a Bruker Proteum Diffraction System equipped with Helios high-brilliance multilayer optics, a Platinum 135 CCD detector, and a Bruker MicroStar microfocus rotating anode x-ray source operating at 45kV and 60mA. The powders were mixed with a small amount of Paratone N oil to form a paste that was then placed in a small (< 0.5 mm.) nylon kryoloop and mounted on a goniometer head. The specimen was then positioned at the goniometer center-of-motion by translating it on the goniometer head. Two overlapping 1-minute 180° ϕ -scans were collected using the Bruker Apex2 V2010.3-0 software package with the detector at $2\theta = 35^\circ$ and 90° using a sample-to-detector distance of 50.0 mm. These overlapping

scans were merged and converted to a .RAW file using the Pilot/XRD2 evaluation option that is part of the APEX2 software package. This .RAW file was then processed using the Bruker EVA powder diffraction software package. For the purposes of visualization, the .RAW file was converted to. UXD format, then again to .CSV format, and plotted in R to allow rapid and interactive analysis of diffractograms.

Results

Initial Ooid Characterization

Prior to experimentation, ooids were characterized using XRD and microscopy on embedded thin sections. XRD shows that aragonite is the primary mineral present (Figure 2). Fluorescence microscopy (FM) reveals that ooids are sub-spheroidal to sub-angular, tens to hundreds of microns in diameter, sometimes concentrically laminated, and often show dissolution features in their natural state (Figure 3). These ooids exhibit a large degree of natural heterogeneity. Observation under SEM confirms FM findings, and EDS mapping shows that while the primary cation present in the ooids is calcium, there are natural zones of magnesium enrichment in the unreacted ooids (Figure 3).

Modified Zempolich & Baker Fluid

To evaluate the feasibility of this experimental design, equilibrium modeling was conducted using PHREEQC. Full PHREEQC outputs are found in Appendix II, but are briefly summarized here. The Mg/Ca fluid, based on the fluid used by Zempolich & Baker (1993), is initially an aggressive weathering fluid characterized by low pH, complete undersaturation, and high ionic strength (1.25 M). Modeling results indicate that after equilibrating with aragonite ooids, pH increases to ~8, a small amount of ooids dissolve, and alkalinity increases in solution.

The Mg/Ca-rich fluid is modeled to dissolve 0.00007 moles aragonite. The resulting solution is supersaturated with respect to calcite, dolomite, huntite, and magnesite.

At each time step of the experiment, the solutions were analyzed to track processes occurring in the vessels. pH, initially slightly acidic, rapidly rises to slightly under 8 and stabilizes. Alkalinity rapidly rises to ~0.3 mmol then slowly increases to higher concentrations, more in the absence of spheres. Magnesium concentrations initially drop, especially in the presence of spheres, and then slowly rise. Calcium concentrations remain mostly stable, within error (Figure 4).

After six weeks in the Mg/Ca fluid, the general character of the ooids observed under FM remain largely the same relative to the unreacted ooids. SEM EDS maps show that the composition of the ooids remain predominantly Ca-rich, but that there are some localized zones of magnesium enrichment on the basis of EDS spectra intensity (Figure 5). Diffraction data indicate the dominant mineralogy of the ooids was not changed by experimentation (Figure 6A).

Mixing Zones

The mixing zone dolomitization fluid is supersaturated with respect to aragonite, calcite, dolomite, huntite, and magnesite, prior to reaction with aragonite ooids. Following equilibration, no ooids dissolve, but saturation indices of carbonate minerals decrease. The dilute fluid is modeled to precipitate 0.0001 moles of aragonite.

In contrast to the other fluids used here, the mixing zone solution had non-zero initial alkalinity. The geochemical changes for the dilute fluid are shown in Figure 7. pH increases slightly while alkalinity decreases slightly, similarly in the presence and absence of microspheres. Magnesium concentrations drop similarly, and calcium concentrations are stable, within error.

After six weeks in the mixing zone fluid, again the ooids appear to be unchanged relative to unreacted ooids under SEM and FM (Figure 8). XRD shows that after experimentation, aragonite remains the primary mineralogical component in all environments, and that there is no significant difference (detected by XRD) between ooids exposed to the fluid and the spheres, and ooids exposed only to the fluids (i.e. experimental and control vessels, Figure 6C).

Sabkhas

The sabkha dolomitization fluid is initially undersaturated with respect to all minerals due to a lack of carbonate alkalinity. After equilibrating with ~0.1 mole of aragonite ooids, pH increases to 8.7 and alkalinity increases in solution, while a small amount of ooids are predicted to dissolve. For the sabkha fluid, 0.0002 moles of aragonite dissolution are expected. The resulting solution, modeled at equilibrium with aragonite, is significantly supersaturated with respect to dolomite and huntite, and slightly oversaturated with respect to artinite, calcite, and magnesite.

For the sabkha fluid, pH and alkalinity both rise over the course of the experiment. Alkalinity starts to plateau around 0.8 millimoles. Magnesium concentrations are highly variable in the absence of spheres but increase overall in both the presence and absence of spheres. Calcium increases slightly, both with and without spheres, over the course of the run (Figure 9).

After six weeks of reaction in the sabkha fluid, the ooids appear largely unchanged under FM and SEM, although some enrichment of magnesium may be occurring in the presence of microspheres, again on the basis of EDS spectra intensity (Figure 10). Diffraction data again shows that the ooids remain predominantly aragonite (Figure 6B).

Dolomite saturation index was calculated for both initial fluids and fluids at each time step (Figure 11). The sabkha and Mg/Ca fluids are initially undersaturated with respect to

dolomite, but reach dolomite saturation in less than one to two weeks, and remain supersaturated for the remainder of the experiment. The mixing zone fluid is initially supersaturated with respect to dolomite ($SI \approx 1.6$), with SI increasing over the course of the experiment.

Discussion

In their experiments, Zempolich & Baker (1993) observed non-fabric destructive dolomitization of ooids after one week in high temperature (200°C) brines. No evidence of dolomite precipitation or dolomitization of aragonite was observed in the experiments described here. There are numerous reasons that could help explain this observation, including: inhibited dissolution, lack of a mechanism to remove calcium, and sample dilution. Additionally, slow reaction rates may require advection and longer timescales to produce noticeable changes in mineralogy.

Typically, dissolution rate is considered to be linearly proportional to surface area (e.g. Fischer et al. 2012). More recently, dissolution rates have been suggested to be variable and best modeled in a probabilistic way (Fischer et al. 2012). The ooids here are fairly coarse (millimeters, in general) and therefore have relatively low reactive surface area, which should inhibit dissolution rate. Dissolved magnesium has been shown to inhibit calcite dissolution even at low concentrations (millimoles) (Arvidson et al. 2006). In these experiments, magnesium concentrations were on the molar scale, thus significant inhibition might be likely. Additionally, dissolution rates are hard to predict and variable across even short distances. Surface area normalization obscures variation in dissolution rate and may lead to inaccurate predictions (Fischer et al. 2012). Carbonate minerals also exhibit retrograde solubility. Therefore, they are less soluble at warmer temperatures. These experiments were run at 40°C , and this warmer

temperature could have slowed dissolution. Despite these considerations, dissolution of several millimoles of ooids was measured in these experiments, and dolomite saturation was achieved.

The dolomitization reaction consumes magnesium and releases calcium. Dolomite is more insoluble than calcite, but if calcium is not removed from the system, calcite saturation will eventually be reached, and the kinetics of calcite precipitation will likely outpace dolomitization. This poses problems for studying kinetically slow (i.e. low temperature) dolomitization reactions in batch. While the scale of dissolution here precludes detection of any increases in calcium during experimentation (millimole changes are below the resolution of ICP-OES) (Figures 5,7,9), it is possible that calcite saturation is reached during equilibration with aragonite. To overcome this problem, flow-through cells that can remove dissolution-released calcium may be effective. Utilizing flow through cells would also allow examination of mass transfer and longer timescales as controls on dolomitization (e.g. Hardie 1987). Without advection, these experiments are best understood as examining processes within a pore in one instant in time. Since dolomitization occurs over longer timescales, batch experiments at low temperature may be poor analogues.

Thermodynamically, and presumably kinetically, dolomite should have precipitated on the microspheres surfaces. It was hypothesized this would also promote dolomitization of the ooids. As discussed above, the small size of the microspheres complicates analysis, especially when they are intermixed with larger material. Any mineral precipitate on the micron surface occurs in a total amount less than a millimole, which would likely not be detected among moles of ooids. Because the microspheres are small (average diameter of 0.82 μm), any mineralogical signal they produce is likely too small relative to the ooids. Additionally, the small size of the microspheres would likely produce broad XRD peaks based on the Scherrer equation:

$$L = \frac{K\lambda}{\beta \cos\theta};$$

where L is crystallite size, K is a shape constant, λ is the X-ray wavelength, and β is the peak width at half maximum (e.g. Monshi et al. 2012). Because of these two factors, here XRD is useful to characterize the mineralogy of the bulk precipitate. Future advection experiments with sustained supersaturation could potentially grow the material on the microsphere surface to detectable sizes under XRD or SEM.

Conclusion

Here, experiments were conducted to investigate if carboxylated organic matter could promote dolomitization of calcium carbonate sediments at low temperature in batch experiments over short time periods (six weeks). Experiments were conducted using fluids representative of dolomite-producing environments (mixing zones, sabkhas) and fluids modified from successful high temperature synthesis experiments. The data demonstrate no significant changes in the bulk mineralogy of the sediments over the experiment duration, both with and without carboxylated microspheres. Measured geochemical changes, however, suggest that microspheres may be influencing mineral precipitation/dissolution kinetics, but these changes are either not reflected or undetectable in the bulk mineralogy. Future experiments should account for advection and mass transfer to more accurately represent a dolomitizing environment and should run for longer periods of time to promote significant mineralogical changes.

Tables

Fluid	Initial pH	Equilibrium pH	Ionic Strength (M)	Initial Alkalinity (mmol)	Equilibrium Dolomite SI
Mg/Ca	5.2	8.31	1.25	0	1.16
Mixing Zone	7.5	7.31	0.31	0.005	2.20
Sabkha	7.5	8.7	3.24	0	1.80

Table 1: Parameters describing dolomitizing fluids. Two fluids (sabkha, Mg/Ca) are characterized as aggressive weathering fluids, while the mixing zone fluid represents an already supersaturated fluid.

Figures

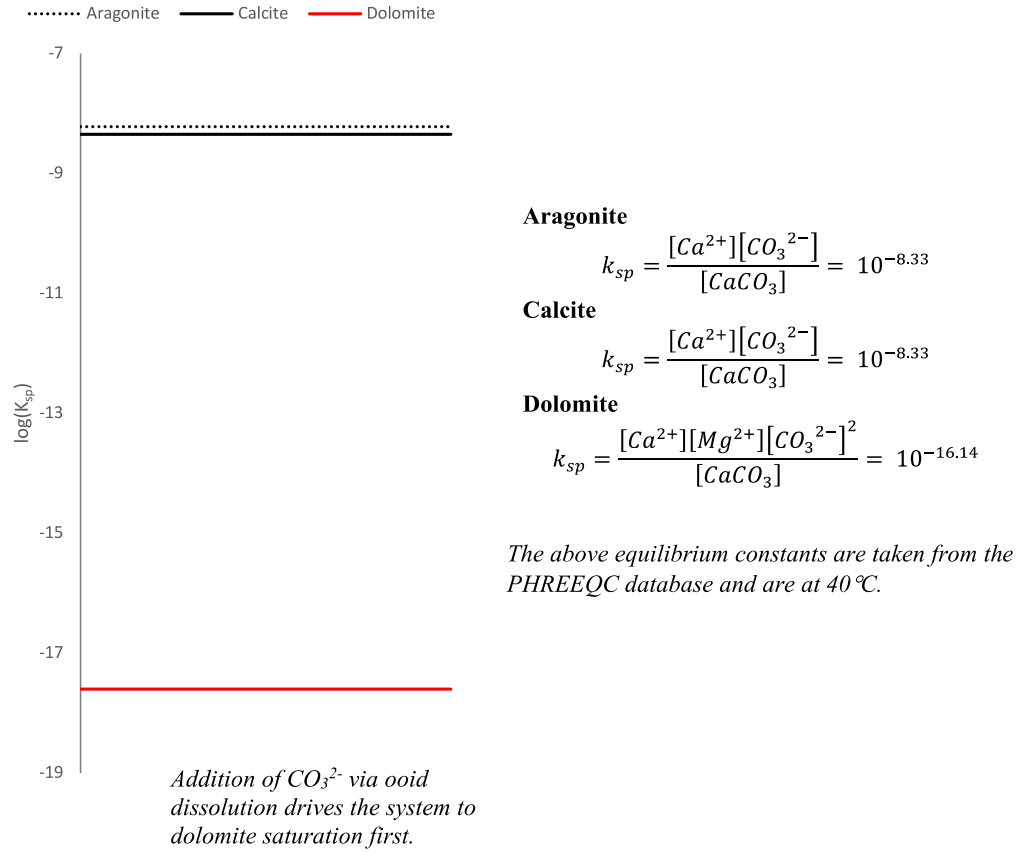


Figure 1: Notional diagram describing the experimental setup for ooid dolomitization experiments. The combination of limiting alkalinity and the microspheres was intended to isolate dolomite as the only thermodynamically favored phase in a kinetically favorable environment. Note, however, that given the temperature and chemical concentrations, the thermodynamics of all the carbonates are fairly similar.

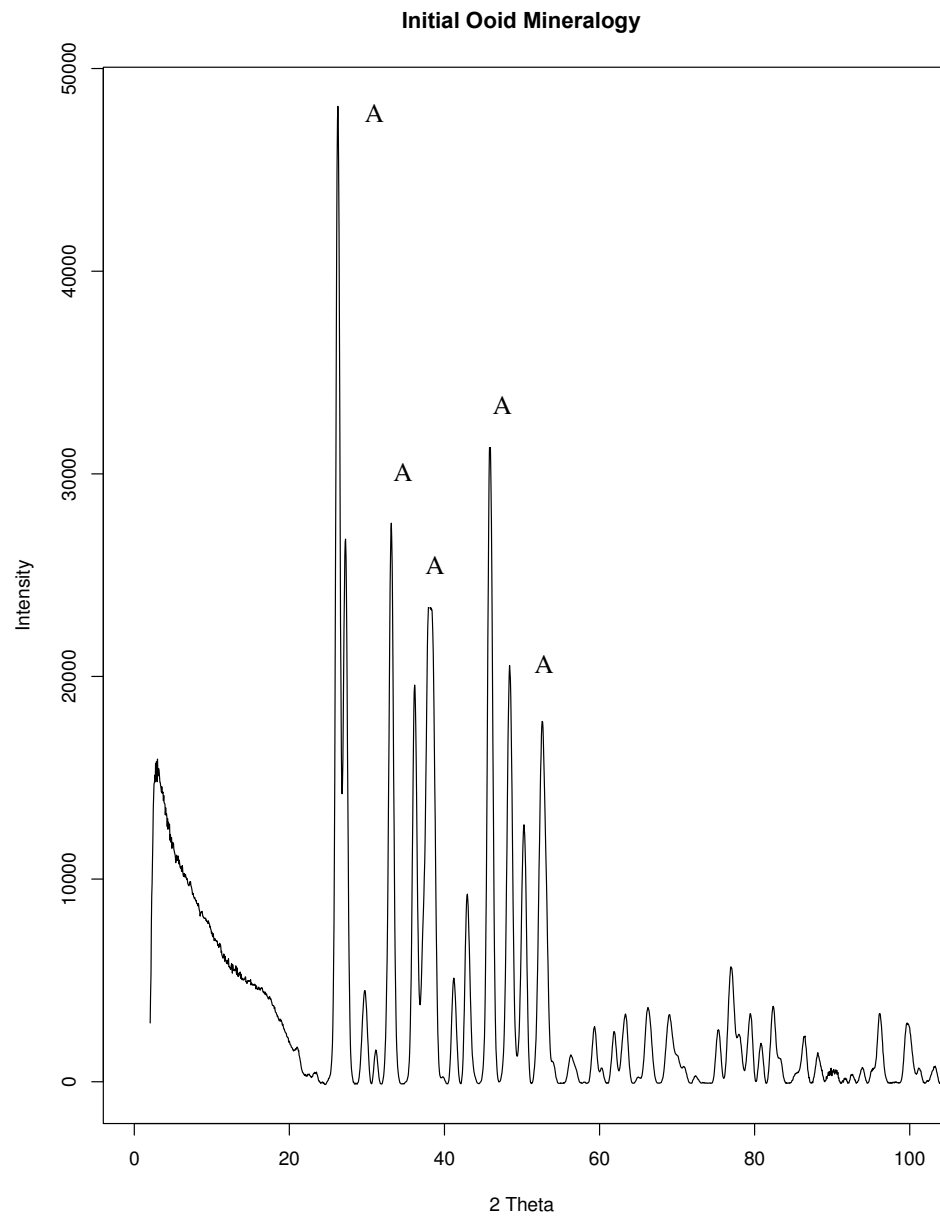


Figure 2: X-ray diffractogram of raw, unreacted ooids shows they are predominantly aragonite.

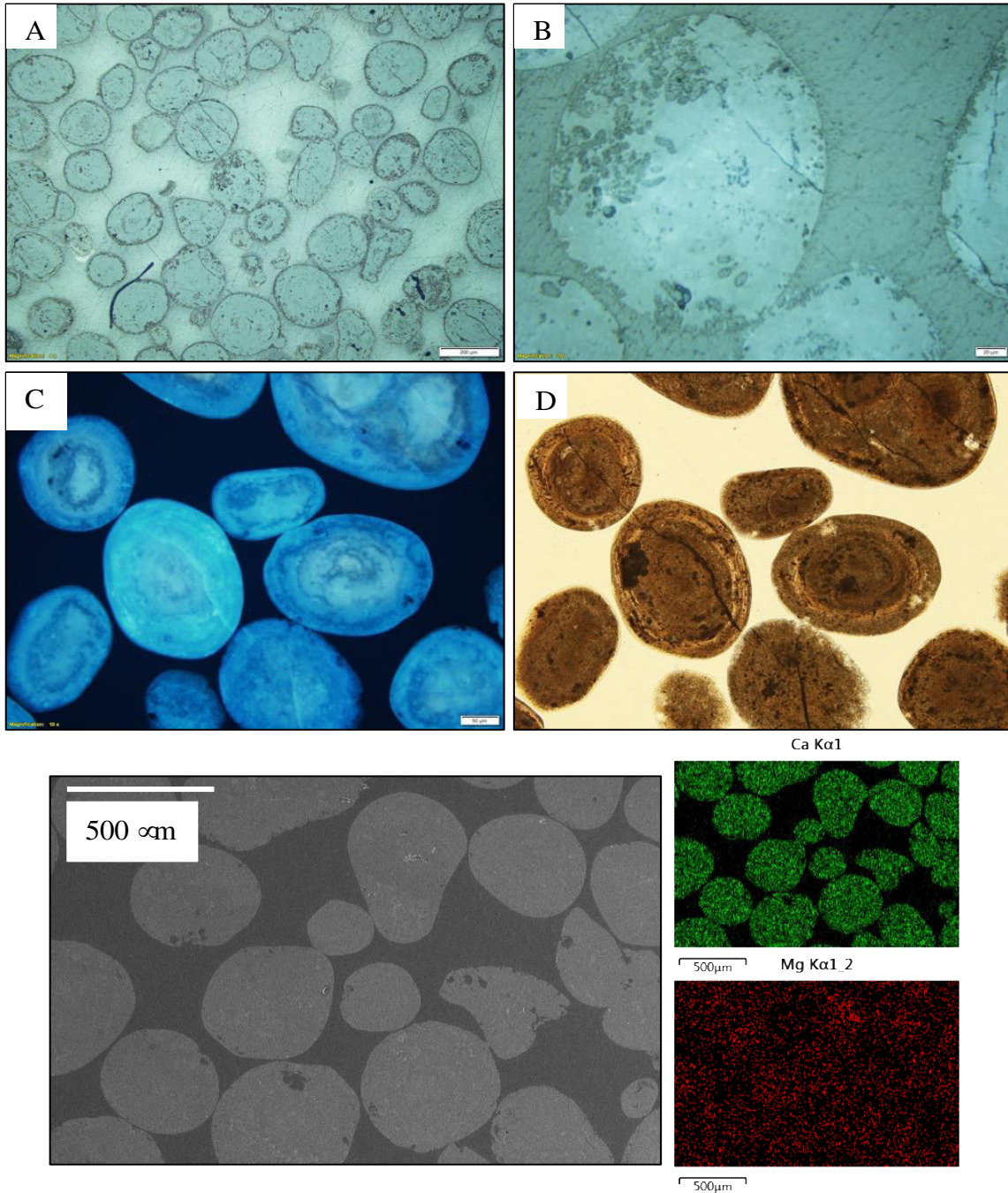


Figure 3: Fluorescence microscopic (FM) images of ooids prior to experimentation. A: brightfield illumination, 10x. B: brightfield, 20x. C: Ultraviolet, 10x. D: Transmitted light, 10x. These images reveal ooids are sub-spheroidal to sub-angular, occasionally concentrically laminated precipitates showing irregular fractures and dissolution features. These features are all observed prior to experimentation. Embedded thin sections under SEM reveal that the ooids are primarily Ca-bearing, although some zones of Mg enrichment occur (EDS maps).

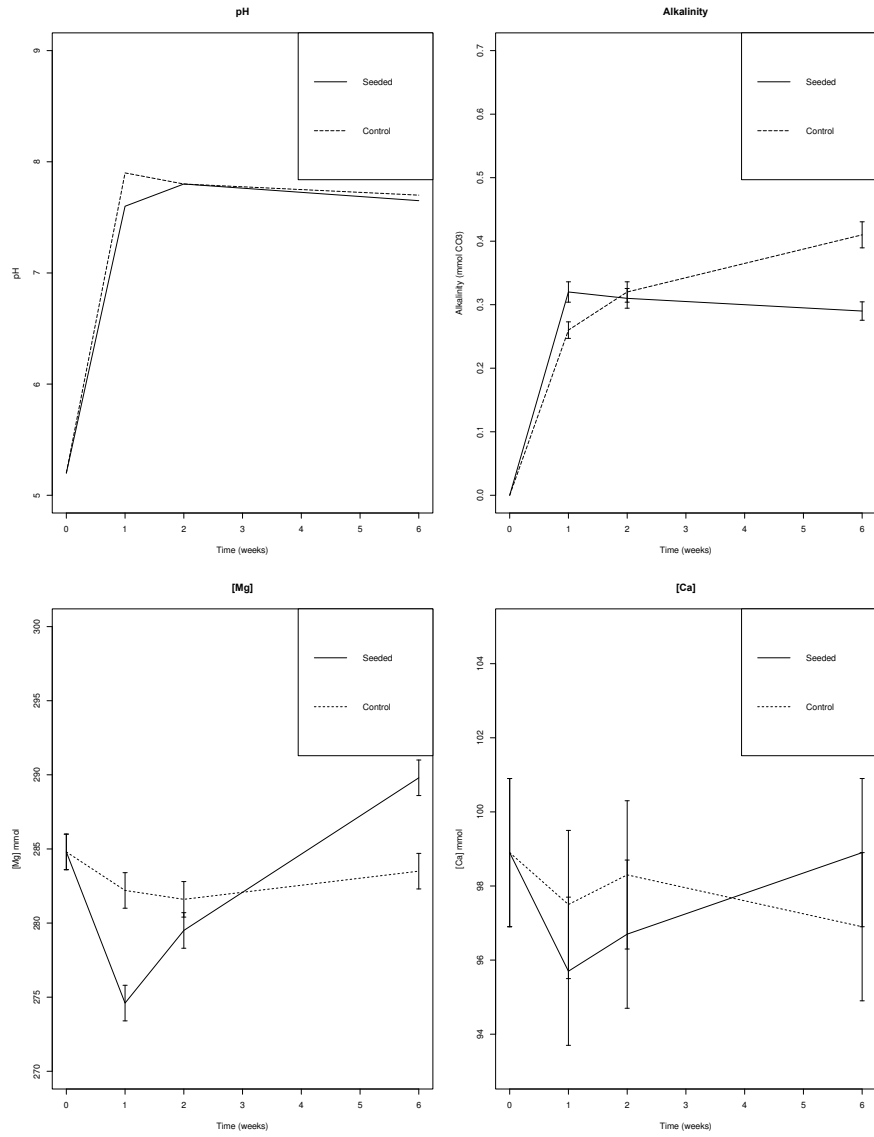


Figure 4: Geochemical changes during the six week experimental duration for dolomitization using a fluid modeled after Zempolich & Baker 1993. pH and alkalinity both increase, while cation concentrations are more variable.

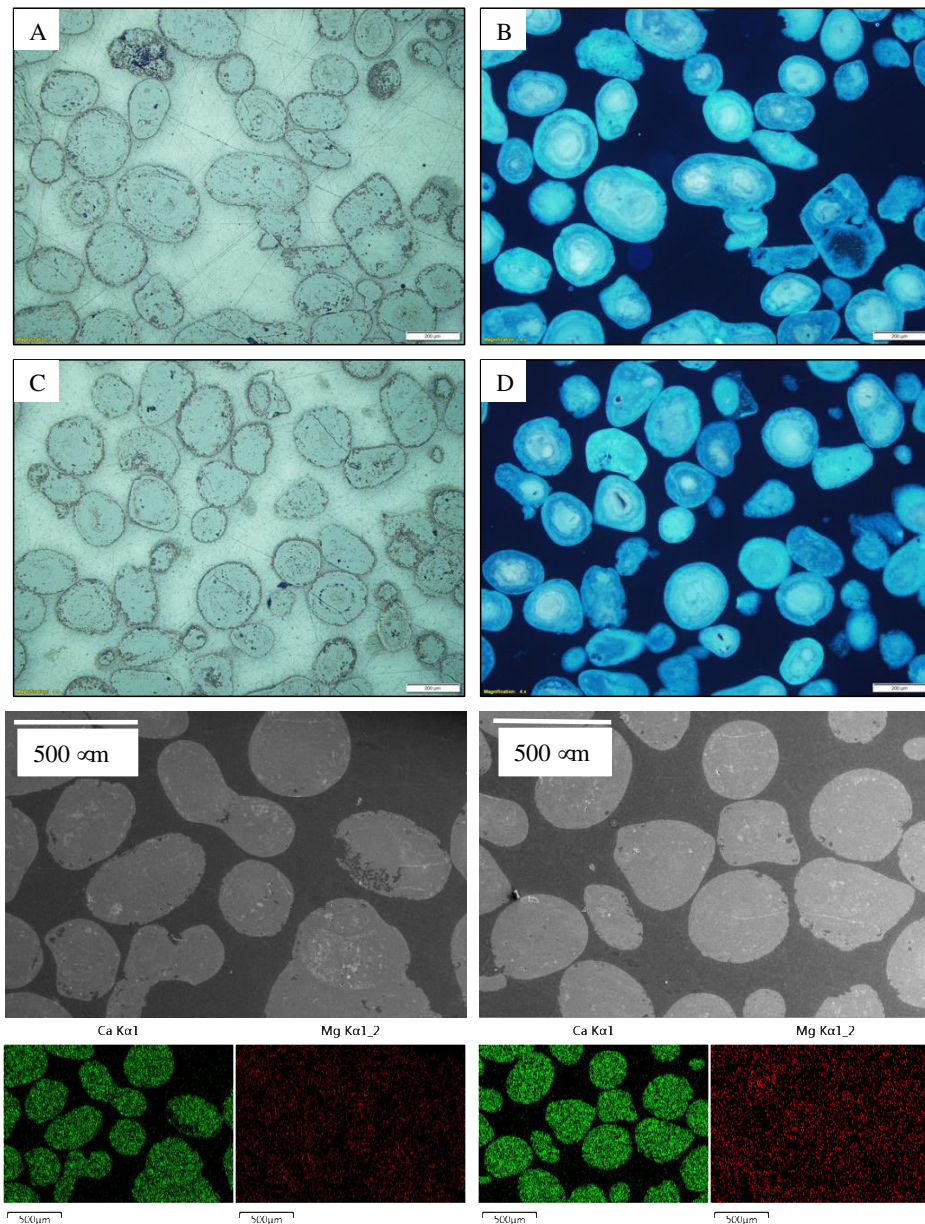


Figure 5: Ooids after six weeks in the Mg/Ca fluid (after Zempolich & Baker 1993). A, B are from control vessels (H). C, D were included with carboxylated microspheres (G). A, C are brightfield images at 10x. B, D are UV images at 10x. The general character of the ooids, observed at this scale, remains largely unchanged from their original, unreacted state. SEM EDS maps show Mg/Ca fluid ooids for control H (left) and with spheres G (right) after six weeks. that Ca remains the primary cation, but that there are some localized areas of Mg enrichment.

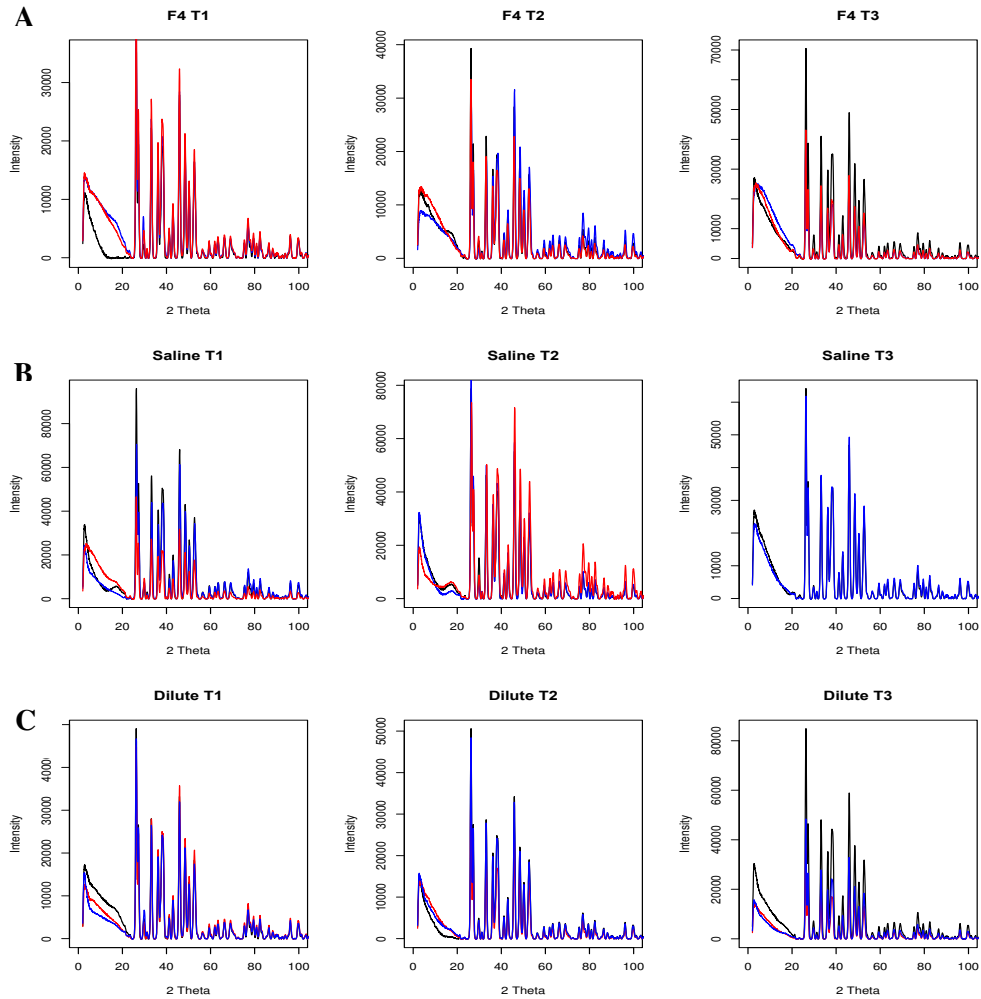


Figure 6: Diffractograms for each time step from dolomitization experiments. Black lines denote diffractograms from controls, while red and blue lines are diffractograms from replicate experiments containing carboxylated microspheres. A -- Zempolich & Baker fluid; B -- Sabkha Fluid; C – Mixing Zone Fluid.

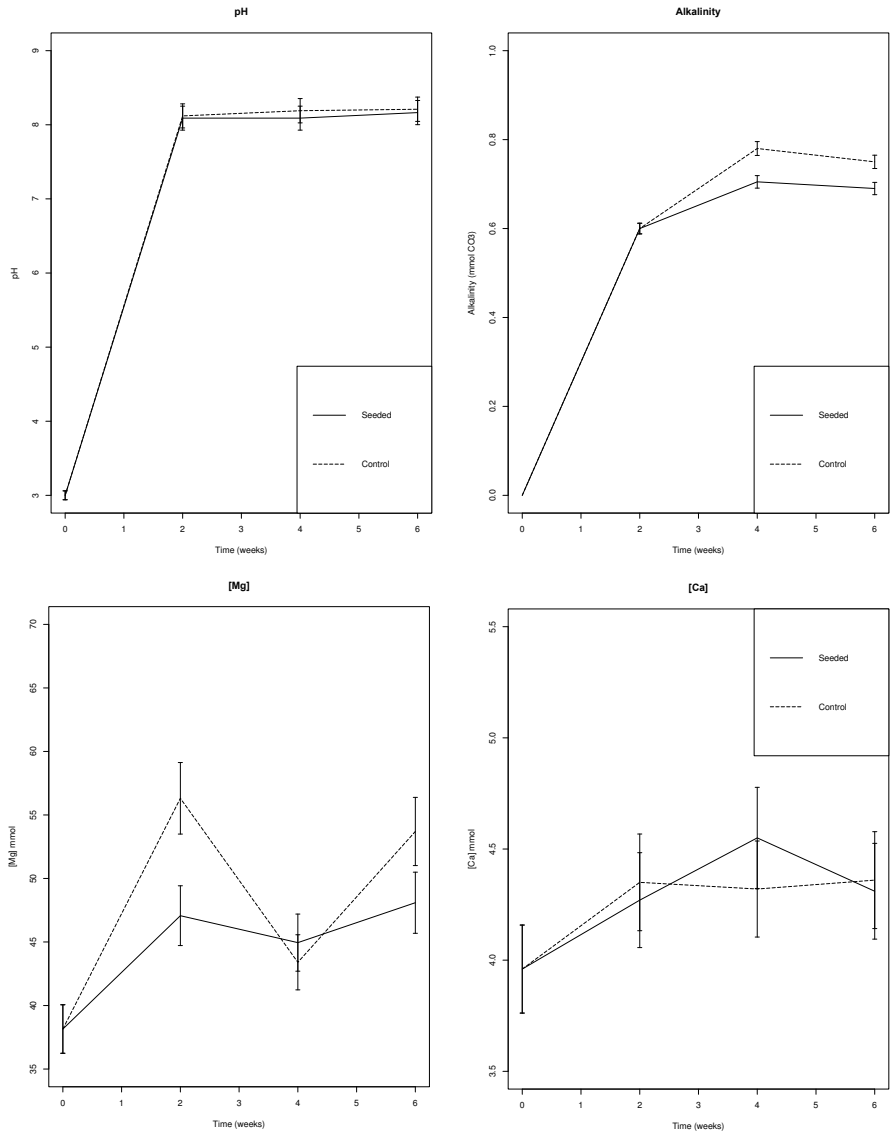


Figure 7: Geochemical changes during the six-week experimental duration for dolomitization using the sabkha fluid. pH and alkalinity both increase, while cation concentrations are more variable.

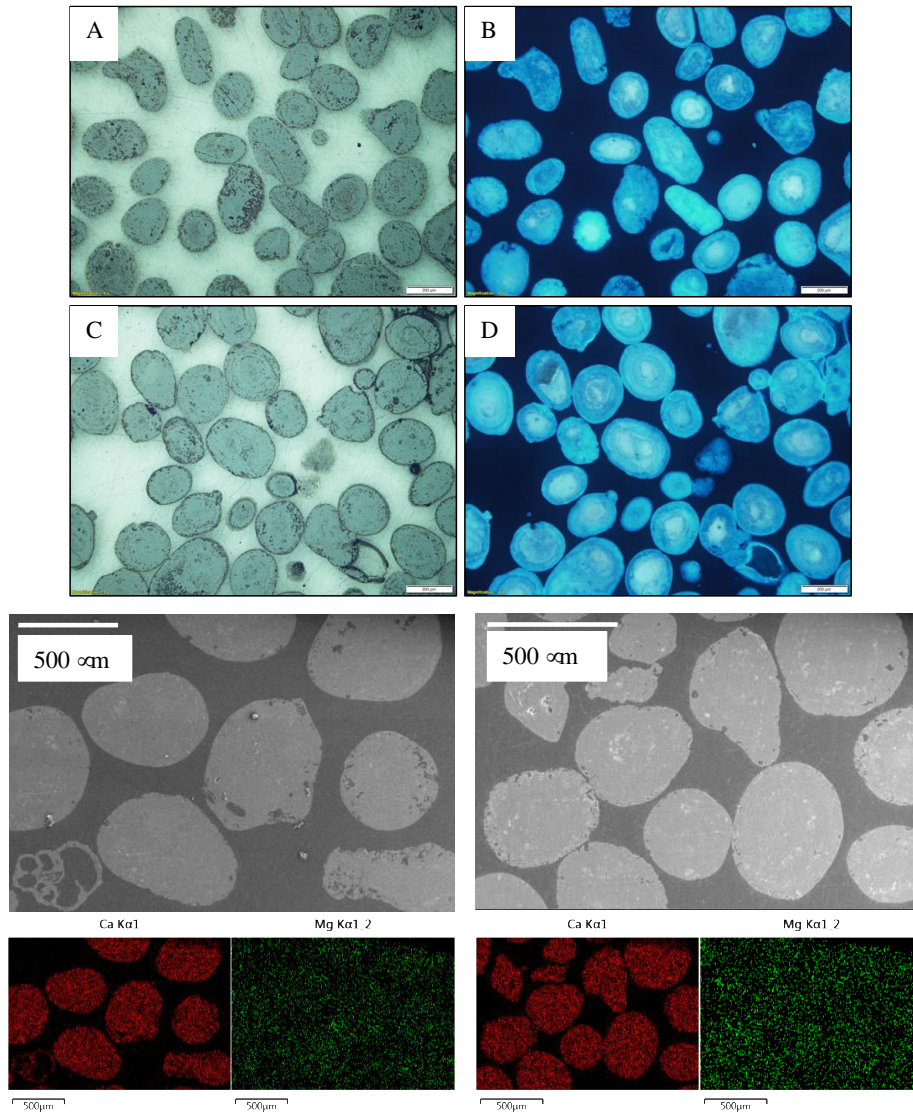


Figure 8: Ooids after six weeks in a sabkha fluid. A, B are from control vessels (SD7). C, D were included with carboxylated microspheres (SD9). A, C are bright field images at 10x. B, D are ultraviolet images at 10x. In general, the bulk character of the ooids remains unchanged relative to their initial state. Dissolution features are observed in both samples, and no visible overgrowths or compositional changes are immediately obvious. Control SD7 (left) and with spheres SD9 (right) after six weeks.

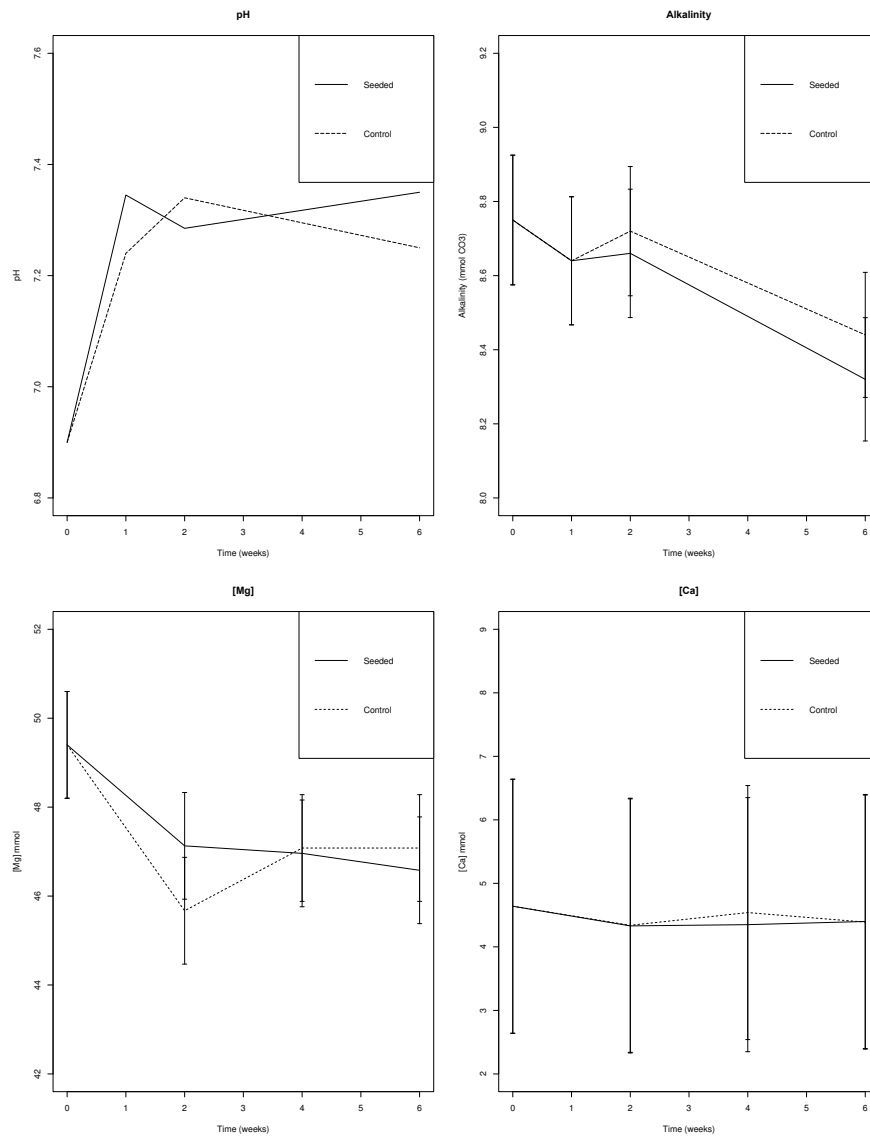


Figure 9: Geochemical changes during the six-week experimental duration for dolomitization using the mixing zone fluid. pH increases slightly, alkalinity decreases slightly, magnesium decreases slightly, and calcium is stable within error.

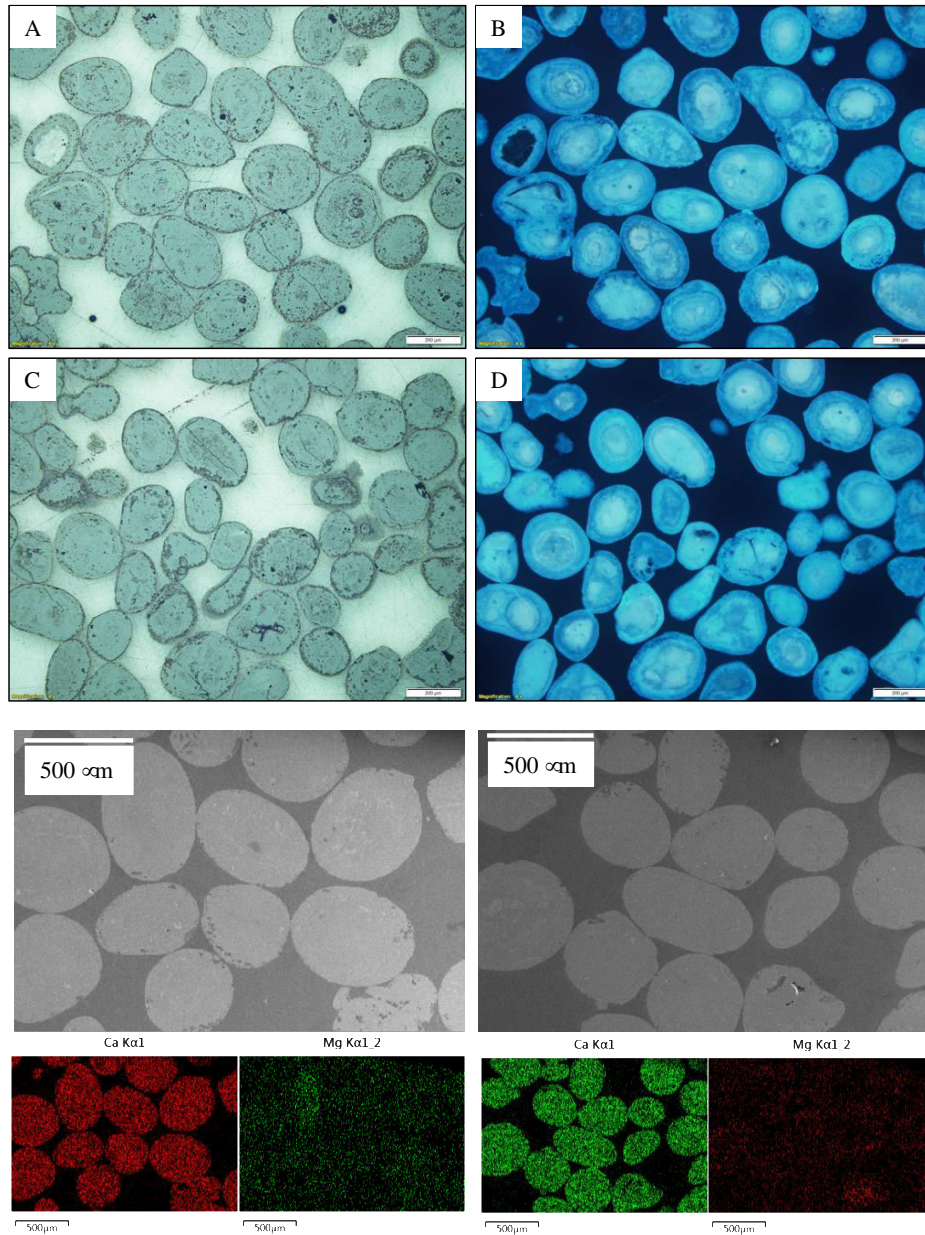


Figure 10: Ooids after six weeks in mixing zone fluid. A, B are from control vessels (AF). C, D were included with carboxylated microspheres (AC). A, C are bright field images at 10x. B, D are ultraviolet images at 10x. In general, the bulk character of the ooids remains unchanged relative to their initial state. Dissolution features are observed in both samples, and no visible overgrowths or compositional changes are immediately obvious. Control AF (left) and with spheres AC (right) after six weeks.

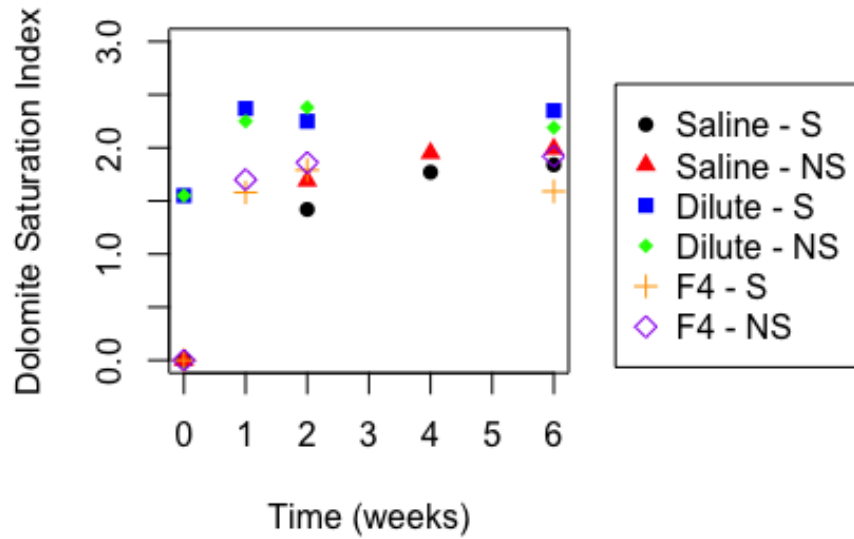


Figure 11: Calculated dolomite saturation indices for all time steps in dolomitization experiments. All experiments, with and without spheres, are supersaturated with respect to dolomite after the time zero. The dilute experiments are initially supersaturated with respect to dolomite. The saline and Mg/Ca fluids are not but reach saturation within one to two weeks.

References

- Adams, J.E., Rhodes, M.L., 1960, Dolomitization by seepage refluxion: AAPG Bulletin, v. 44, p. 1912-1920.
- Anderson, G.M., Macqueen, R.W., 1982, Ore Deposit Models – 6. Mississippi Valley-Type Lead-Zinc Deposits: Geoscience Canada, v. 9, p. 108-117.
- Arvidson, R.S., Collier, M., Davis, K.J., Vinson, M.D., Amonette, J.E., Luttge, A., 2006, Magnesium inhibition of calcite dissolution kinetics: Geochimica et Cosmochimica Acta, v. 70, p. 583-594.
- Badiozamani, K., 1973, The Dorag dolomitization model – application to the middle Ordovician of Wisconsin: Journal of Sedimentary Petrology, v. 43, p. 965-984.
- Back, W., Hanshaw, B.B., Herman, J.S., Van Driel, J.N., 1986, Differential dissolution of a Pleistocene reef in the ground-water mixing zone of coastal Yucatan, Mexico: Geology, v. 14, p. 137-140.
- Bontognali, T.R.R., Vasconcelos, C., Warthmann, R.J., Bernasconi, S.M., Dupraz, C., Strohmenger, C.J., McKenzie, J.A., 2010, Dolomite formation within microbial mats in the coastal sabkha of Abu Dhabi (United Arab Emirates): Sedimentology, v. 57, p. 824-844.
- Butler, G.P., 1969, Modern Evaporite Deposition and Geochemistry of Coexisting Brines, the Sabkha, Trucial Coast, Arabian Gulf: Journal of Sedimentary Petrology, v. 39, p. 70-89.
- Cantrell, D.L., Swart, P.K., Handford, R.C., Kendall, C.G., Westphal, H., 2001, Geology and Production Significance of Dolomite Arab-D Reservoir, Ghawar Field, Saudi Arabia: GeoArabia, v. 6, p. 45-60.
- Ferry, J.M., Passey, B.H., Vasconcelos, C., Eiler, J.M., 2011, Formation of dolomite at 40-80C

- in the Latemar carbonate buildup, Dolomites, Italy, from clumped isotope thermometry: *Geology*, v. 39, p. 571-574.
- Fischer, C., Arvidson, R.S., Lüttge, A., 2012, How predictable are dissolution rates of crystalline material?: *Geochimica et Cosmochimica Acta*, v. 98, p. 177-185.
- Hardie, L.A., 1987, Dolomitization: A Critical View of Some Current Views: *Journal of Sedimentary Petrology*, v. 57, p. 166-183.
- Jones, G.D., Xiao, Y., 2005, Dolomitization, anhydrite cementation, and porosity evolution in a reflux system: Insights from reactive transport models: *AAPG Bulletin*, v. 89, p. 577-601.
- Land, L.S., 1998, Failure to precipitate dolomite at 25°C from dilute solution despite 1000-fold oversaturation after 32 years: *Aquatic Geochemistry*, v. 4, p. 361-368.
- Li, Zhaoqi, Goldstein, R.H., Franseen, E.K., 2013, Ascending freshwater-mesohaline mixing: a new scenario for dolomitization: *Journal of Sedimentary Research*, v. 83, p. 277-283.
- Lindner, M., Jordan, G., 2018, On the growth of witherite and its replacement by the Mg-bearing double carbonate norsethite: Implications for the dolomite problem: *American Mineralogist*, v. 103, p. 252-259.
- Meister, P., McKenzie, J.A., Bernasconi, S.M., Brack, P., 2013, Dolomite formation in the shallow seas of the Alpine Triassic: *Sedimentology*, v. 60, p. 270-291.
- Monshi, A., Foroughi, M.R., Monshi, M.R., 2012, Modified Scherrer Equation to estimate more accurately nano-crystallite size using XRD: *World Journal of Nano Science and Engineering*, v. 2, p. 154-160.
- Parkhurst, D.L., Appelo, C.A.J., 2013, Description of input and examples for PHREEQC Version 3 – a computer program for speciation, batch-reaction, one-dimensional transport, and inverse geochemical calculations: U.S. Geological Survey Techniques

- and Methods, book 6, chap. A43, p. 497. <https://pubs.usgs.gov/tm/06/a43/>.
- Pitzer, K.S., 1973, Thermodynamics of electrolytes. I. Theoretical basis and general equations: The Journal of Physical Chemistry, v. 77, p. 268-277.
- Roberts, J.A., Kenward, P.A., Fowle, D.A., Goldstein, R.H., Gonzalez, L.A., Moore, D.S. 2013, Surface chemistry allows for abiotic precipitation of dolomite at low temperature: Proceedings of the National Academy of Sciences, v. 110, p. 14540-14545.
- Vasconcelos, C., McKenzie, J.A., 1997, Microbial mediation of modern dolomite precipitation and diagenesis under anoxic conditions (Lagoa Vermelha, Rio de Janeiro, Brazil): Journal of Sedimentary Research, v. 67, p. 378-390.
- Ward, W.C., Halley, R.B., 1984, Dolomitization in a Mixing Zone of Near-Seawater composition, late Pleistocene, Northeastern Yucatan Peninsula: Journal of Sedimentary Petrology, v. 55, p. 407-420.
- Xu, J., Yan, C., Zhang, F., Konishi, H., Xu, H., Teng, H.H., 2013, Testing the cation-hydration effect on the crystallization of Ca-Mg-CO₃ systems: Proceedings of the National Academy, v. 110, p. 17750-17755.
- Zempolich, W.G., Baker, P.A., 1993, Experimental and natural mimetic dolomitization of aragonite ooids: Journal of Sedimentary Petrology, v. 63, p. 596-606.

Chapter 4: Conclusions

Results from primary precipitation batch experiments show that dolomite did not form in significant amounts in either the control experiments or in those seeded with carboxylated organic matter. Carboxylated organic matter was shown to promote the precipitation of a mixed mineralogy phase in which the Mg/Ca of the precipitate reflected the Mg/Ca of solution, and Mg is more evenly distributed throughout the precipitate in the presence of carboxylated organic matter. In dolomitization experiments, no evidence of replacement of calcium carbonate sediments was observed, but geochemical data suggests that precipitation/dissolution reactions involving magnesium may be occurring.

The nucleation of dolomite is a critical first step for primary precipitation of dolomite and for dolomitization of calcium carbonate sediments. The presence of millimeter-scale material in experiments complicates examination of micron-scale processes and features. A potential avenue to overcome this issue is advective or diffusive transport. Devising experimental methods that provide a steady supply of Mg while removing Ca may enable the nucleation and subsequent growth of magnesium-bearing phases on synthetic organic matter to sizes that are more easily analyzed. In addition to making analysis more feasible, emulating advection or diffusion in the lab would provide a closer approximation to environments in which dolomite forms.

Appendix I: Primary Precipitation Geochemical Modeling

This appendix includes PHREEQC model outputs for primary precipitation batch experiments conducted at all three treatments for each of the three environments. Model results for primary precipitation experiments consider some heterogeneities in experimental set up (i.e. slightly different pH between runs) but also show that the resulting thermodynamic environment is not significantly impacted.

Input file: /Users/adamyoerg/Desktop/ActualBatchExperiments.txt
Output file: /Users/adamyoerg/Desktop/ActualBatchExperiments.txt.out
Database file: /Users/adamyoerg/Desktop/PHREEQ/database/pitzer.dat

Reading data base.

```
SOLUTION_MASTER_SPECIES
SOLUTION_SPECIES
PHASES
PITZER
EXCHANGE_MASTER_SPECIES
EXCHANGE_SPECIES
SURFACE_MASTER_SPECIES
SURFACE_SPECIES
END
```

Reading input data for simulation 1.

```
TITLE Actual Experimental Fluids
Solution 1 Dilute 5d 30C
  pH 7.2
  temp 30
  units mg/L
  Ca 340
  Mg 1900
  Na 5000
  Cl 13000
  Alkalinity 400 as CO3
SAVE Solution 1
```

Solution 2 Dilute 5d 40C

pH 7.1
temp 40
units mg/L
Ca 200
Mg 1200
Na 3400
Cl 8500
Alkalinity 300 as CO₃

SAVE Solution 2

Solution 3 Dilute 10d 40C

pH 7.3
temp 40
units mg/L
Ca 200
Mg 1300
Na 3600
Cl 9000
Alkalinity 600 as CO₃

SAVE Solution 3

Solution 4 Alkaline 5d 40C

pH 8.94
temp 40
units mg/L
Ca 200
Mg 1200
Na 22000
Cl 22000
Alkalinity 13000 as CO₃

SAVE Solution 4

Solution 5 Alkaline 10d 40C

pH 8.97
temp 40
units mg/L
Ca 200
Mg 1200
Na 18500
Cl 22000
Alkalinity 8700 as CO₃

SAVE Solution 5

Solution 6 Saline 5d 30C

pH 7.35
temp 30
units mg/L
Ca 200
Mg 1200

Na 200000
 Cl 310000
 Alkalinity 300 as CO3
 SAVE Solution 6
 Solution 7 Saline 5d 40C
 pH 7.08
 temp 40
 units mg/L
 Ca 200
 Mg 1200
 Na 60000
 Cl 95000
 Alkalinity 1150 as CO3
 SAVE Solution 7
 Solution 8 Saline 10d 40C
 pH 7.5
 temp 40
 units mg/L
 Ca 200
 Mg 1200
 Na 61000
 Cl 95000
 Alkalinity 2300 as CO3
 SAVE Solution 8

 TITLE

Actual Experimental Fluids

 Beginning of initial solution calculations.

Initial solution 1. Dilute 5d 30C

-----Solution composition-----

Elements	Molality	Moles
Alkalinity	6.806e-03	6.806e-03
Ca	8.662e-03	8.662e-03
Cl	3.744e-01	3.744e-01
Mg	7.982e-02	7.982e-02
Na	2.221e-01	2.221e-01

-----Description of solution-----

pH = 7.200
 pe = 4.000
 Specific Conductance ($\mu\text{S}/\text{cm}$, 30°C) = 40009
 Density (g/cm^3) = 1.01127
 Volume (L) = 1.00972
 Activity of water = 0.989
 Ionic strength = 4.784e-01
 Mass of water (kg) = 1.000e+00
 Total carbon (mol/kg) = 7.217e-03
 Total CO2 (mol/kg) = 7.217e-03
 Temperature (°C) = 30.00
 Electrical balance (eq) = 1.782e-02
 Percent error, $100 \cdot (\text{Cat} - |\text{An}|) / (\text{Cat} + |\text{An}|)$ = 2.28
 Iterations = 16
 Gamma iterations = 4
 Osmotic coefficient = 0.90155
 Density of water = 0.99564
 Total H = 1.110190e+02
 Total O = 5.552735e+01

-----Distribution of species-----

MacInnes	MacInnes						
Species	Log Molality	Log Activity	Log mole V Molality	Activity	Gamma	cm ³ /mol	
OH-	4.439e-07	2.301e-07	-6.353	-6.638	-0.285	-2.78	
H+	7.882e-08	6.310e-08	-7.103	-7.200	-0.097	0.00	
H2O	5.551e+01	9.888e-01	1.744	-0.005	0.000	18.09	
C(4)	7.217e-03						
HCO3-	6.598e-03	4.152e-03	-2.181	-2.382	-0.201	26.46	
CO2	5.153e-04	5.506e-04	-3.288	-3.259	0.029	34.68	
MgCO3	6.582e-05	6.582e-05	-4.182	-4.182	0.000	-17.09	
CO3-2	3.761e-05	3.311e-06	-4.425	-5.480	-1.055	-0.53	
Ca	8.662e-03						
Ca+2	8.662e-03	2.282e-03	-2.062	-2.642	-0.579	-16.77	
Cl	3.744e-01						
Cl-	3.744e-01	2.443e-01	-0.427	-0.612	-0.185	18.81	
Mg	7.982e-02						
Mg+2	7.975e-02	2.182e-02	-1.098	-1.661	-0.563	-20.72	
MgCO3	6.582e-05	6.582e-05	-4.182	-4.182	0.000	-17.09	
MgOH+	8.421e-07	8.155e-07	-6.075	-6.089	-0.014	(0)	
Na	2.221e-01						
Na+	2.221e-01	1.617e-01	-0.654	-0.791	-0.138	-0.43	

-----Saturation indices-----

Phase	SI**	log IAP	log K(303 K, 1 atm)	
Aragonite	0.13	-8.12	-8.25	CaCO ₃
Artinite	-3.41	15.87	19.28	Mg ₂ CO ₃ (OH) ₂ :3H ₂ O
Bischofite	-7.44	-2.91	4.53	MgCl ₂ :6H ₂ O
Brucite	-4.12	-14.94	-10.82	Mg(OH) ₂
Calcite	0.43	-8.12	-8.55	CaCO ₃
CO ₂ (g)	-1.73	-3.26	-1.52	CO ₂
Dolomite	1.93	-15.26	-17.20	CaMg(CO ₃) ₂
Gaylussite	-5.79	-15.21	-9.42	CaNa ₂ (CO ₃) ₂ :5H ₂ O
H ₂ O(g)	-1.38	-0.00	1.38	H ₂ O
Halite	-2.99	-1.40	1.59	NaCl
Huntite	1.94	11.65	9.71	CaMg ₃ (CO ₃) ₄
Magnesite	0.71	-7.14	-7.85	MgCO ₃
MgCl ₂ _2H ₂ O	-17.04	-2.89	14.15	MgCl ₂ :2H ₂ O
MgCl ₂ _4H ₂ O	-9.78	-2.90	6.88	MgCl ₂ :4H ₂ O
Nahcolite	-2.73	-13.47	-10.74	NaHCO ₃
Natron	-6.29	-7.11	-0.82	Na ₂ CO ₃ :10H ₂ O
Nesquehonite	-1.99	-7.16	-5.17	MgCO ₃ :3H ₂ O
Pirssonite	-5.96	-15.19	-9.23	Na ₂ Ca(CO ₃) ₂ :2H ₂ O
Portlandite	-10.73	-15.92	-5.19	Ca(OH) ₂
Trona	-9.16	-20.54	-11.38	Na ₃ H(CO ₃) ₂ :2H ₂ O

**For a gas, SI = log₁₀(fugacity). Fugacity = pressure * phi / 1 atm.
For ideal gases, phi = 1.

Initial solution 2. Dilute 5d 40C

-----Solution composition-----

Elements	Molality	Moles
Alkalinity	5.068e-03	5.068e-03
Ca	5.059e-03	5.059e-03
Cl	2.431e-01	2.431e-01
Mg	5.005e-02	5.005e-02
Na	1.499e-01	1.499e-01

-----Description of solution-----

pH = 7.100
pe = 4.000
Specific Conductance (μS/cm, 40°C) = 33529

Density (g/cm³) = 1.00239
 Volume (L) = 1.01140
 Activity of water = 0.993
 Ionic strength = 3.092e-01
 Mass of water (kg) = 1.000e+00
 Total carbon (mol/kg) = 5.507e-03
 Total CO2 (mol/kg) = 5.507e-03
 Temperature (°C) = 40.00
 Electrical balance (eq) = 1.203e-02
 Percent error, 100*(Cat-|An|)/(Cat+|An|) = 2.37
 Iterations = 14
 Gamma iterations = 3
 Osmotic coefficient = 0.89797
 Density of water = 0.99221
 Total H = 1.110174e+02
 Total O = 5.552224e+01

-----Distribution of species-----

Species	MacInnes Log Molality	MacInnes Log Activity	Log mole V Molality	Log mole V Activity	Gamma	cm ³ /mol
OH-	6.307e-07	3.659e-07	-6.200	-6.437	-0.236	-2.88
H+	1.025e-07	7.943e-08	-6.989	-7.100	-0.111	0.00
H2O	5.551e+01	9.927e-01	1.744	-0.003	0.000	18.16
C(4)	5.507e-03					
HCO3-	4.954e-03	3.349e-03	-2.305	-2.475	-0.170	26.52
CO2	4.970e-04	5.189e-04	-3.304	-3.285	0.019	35.16
MgCO3	3.700e-05	3.700e-05	-4.432	-4.432	0.000	-17.10
CO3-2	1.927e-05	2.471e-06	-4.715	-5.607	-0.892	-0.57
Ca	5.059e-03					
Ca+2	5.059e-03	1.385e-03	-2.296	-2.858	-0.563	-16.86
Cl	2.431e-01					
Cl-	2.431e-01	1.658e-01	-0.614	-0.780	-0.166	18.83
Mg	5.005e-02					
Mg+2	5.002e-02	1.418e-02	-1.301	-1.848	-0.547	-21.19
MgCO3	3.700e-05	3.700e-05	-4.432	-4.432	0.000	-17.10
MgOH+	1.039e-06	9.570e-07	-5.984	-6.019	-0.036	(0)
Na	1.499e-01					
Na+	1.499e-01	1.100e-01	-0.824	-0.959	-0.135	-0.21

-----Saturation indices-----

Phase SI** log IAP log K(313 K, 1 atm)

Aragonite	-0.14	-8.47	-8.33	CaCO ₃
Artinite	-3.46	15.11	18.57	Mg ₂ CO ₃ (OH) ₂ :3H ₂ O
Bischofite	-7.83	-3.43	4.41	MgCl ₂ :6H ₂ O
Brucite	-4.01	-14.72	-10.71	Mg(OH) ₂
Calcite	0.19	-8.47	-8.65	CaCO ₃
CO ₂ (g)	-1.66	-3.28	-1.63	CO ₂
Dolomite	1.49	-15.92	-17.41	CaMg(CO ₃) ₂
Gaylussite	-6.59	-16.01	-9.42	CaNa ₂ (CO ₃) ₂ :5H ₂ O
H ₂ O(g)	-1.14	-0.00	1.14	H ₂ O
Halite	-3.35	-1.74	1.61	NaCl
Huntite	1.41	10.10	8.69	CaMg ₃ (CO ₃) ₄
Magnesite	0.43	-7.46	-7.89	MgCO ₃
MgCl ₂ _2H ₂ O	-16.78	-3.42	13.37	MgCl ₂ :2H ₂ O
MgCl ₂ _4H ₂ O	-10.10	-3.42	6.68	MgCl ₂ :4H ₂ O
Nahcolite	-2.92	-13.67	-10.74	NaHCO ₃
Natron	-6.73	-7.56	-0.82	Na ₂ CO ₃ :10H ₂ O
Nesquehonite	-2.30	-7.46	-5.17	MgCO ₃ :3H ₂ O
Pirssonite	-6.76	-16.00	-9.23	Na ₂ Ca(CO ₃) ₂ :2H ₂ O
Portlandite	-10.54	-15.73	-5.19	Ca(OH) ₂
Trona	-9.81	-21.20	-11.38	Na ₃ H(CO ₃) ₂ :2H ₂ O

**For a gas, SI = log₁₀(fugacity). Fugacity = pressure * phi / 1 atm.
For ideal gases, phi = 1.

Initial solution 3. Dilute 10d 40C

-----Solution composition-----

Elements	Molality	Moles
Alkalinity	1.015e-02	1.015e-02
Ca	5.064e-03	5.064e-03
Cl	2.576e-01	2.576e-01
Mg	5.428e-02	5.428e-02
Na	1.589e-01	1.589e-01

-----Description of solution-----

pH = 7.300
pe = 4.000
Specific Conductance (μS/cm, 40°C) = 35674
Density (g/cm³) = 1.00318
Volume (L) = 1.01172
Activity of water = 0.992
Ionic strength = 3.318e-01
Mass of water (kg) = 1.000e+00

Total carbon (mol/kg) = 1.057e-02
 Total CO2 (mol/kg) = 1.057e-02
 Temperature (°C) = 40.00
 Electrical balance (eq) = 9.834e-03
 Percent error, 100*(Cat-|An|)/(Cat+|An|) = 1.80
 Iterations = 13
 Gamma iterations = 3
 Osmotic coefficient = 0.89751
 Density of water = 0.99221
 Total H = 1.110222e+02
 Total O = 5.553732e+01

-----Distribution of species-----

Species	MacInnes Molality	MacInnes Log Activity	Log Molality	Log Activity	mole V Activity	Gamma	cm ³ /mol
OH-	1.016e-06	5.796e-07	-5.993	-6.237	-0.244	-2.84	
H+	6.482e-08	5.012e-08	-7.188	-7.300	-0.112	0.00	
H2O	5.551e+01	9.922e-01	1.744	-0.003	0.000	18.16	
C(4)	1.057e-02						
HCO3-	9.776e-03	6.511e-03	-2.010	-2.186	-0.176	26.57	
CO2	6.082e-04	6.369e-04	-3.216	-3.196	0.020	35.16	
MgCO3	1.211e-04	1.211e-04	-3.917	-3.917	0.000	-17.10	
CO3-2	6.324e-05	7.613e-06	-4.199	-5.118	-0.919	-0.49	
Ca	5.064e-03						
Ca+2	5.064e-03	1.376e-03	-2.295	-2.861	-0.566	-16.83	
Cl	2.576e-01						
Cl-	2.576e-01	1.745e-01	-0.589	-0.758	-0.169	18.84	
Mg	5.428e-02						
Mg+2	5.416e-02	1.506e-02	-1.266	-1.822	-0.556	-21.16	
MgCO3	1.211e-04	1.211e-04	-3.917	-3.917	0.000	-17.10	
MgOH+	1.748e-06	1.610e-06	-5.757	-5.793	-0.036	(0)	
Na	1.589e-01						
Na+	1.589e-01	1.162e-01	-0.799	-0.935	-0.136	-0.19	

-----Saturation indices-----

Phase	SI**	log IAP	log K(313 K, 1 atm)
Aragonite	0.35	-7.98	-8.33 CaCO3
Artinite	-2.52	16.05	18.57 Mg2CO3(OH)2:3H2O
Bischofite	-7.77	-3.36	4.41 MgCl2:6H2O
Brucite	-3.59	-14.30	-10.71 Mg(OH)2
Calcite	0.67	-7.98	-8.65 CaCO3

CO2(g)	-1.57	-3.20	-1.63	CO2
Dolomite	2.49	-14.92	-17.41	CaMg(CO3)2
Gaylussite	-5.56	-14.98	-9.42	CaNa2(CO3)2:5H2O
H2O(g)	-1.14	-0.00	1.14	H2O
Halite	-3.30	-1.69	1.61	NaCl
Huntite	3.44	12.13	8.69	CaMg3(CO3)4
Magnesite	0.95	-6.94	-7.89	MgCO3
MgCl2_2H2O	-16.71	-3.35	13.37	MgCl2:2H2O
MgCl2_4H2O	-10.03	-3.35	6.68	MgCl2:4H2O
Nahcolite	-2.61	-13.35	-10.74	NaHCO3
Natron	-6.20	-7.02	-0.82	Na2CO3:10H2O
Nesquehonite	-1.78	-6.95	-5.17	MgCO3:3H2O
Pirssonite	-5.74	-14.97	-9.23	Na2Ca(CO3)2:2H2O
Portlandite	-10.15	-15.34	-5.19	Ca(OH)2
Trona	-8.96	-20.35	-11.38	Na3H(CO3)2:2H2O

**For a gas, SI = log10(fugacity). Fugacity = pressure * phi / 1 atm.
For ideal gases, phi = 1.

Initial solution 4. Alkaline 5d 40C

-----Solution composition-----

Elements	Molality	Moles
Alkalinity	2.301e-01	2.301e-01
Ca	5.300e-03	5.300e-03
Cl	6.590e-01	6.590e-01
Mg	5.243e-02	5.243e-02
Na	1.016e+00	1.016e+00

-----Description of solution-----

pH = 8.940
pe = 4.000
Specific Conductance (μS/cm, 40°C) = 95930
Density (g/cm³) = 1.03490
Volume (L) = 1.02290
Activity of water = 0.970
Ionic strength = 1.055e+00
Mass of water (kg) = 1.000e+00
Total carbon (mol/kg) = 1.711e-01
Total CO2 (mol/kg) = 1.711e-01
Temperature (°C) = 40.00
Electrical balance (eq) = 2.427e-01
Percent error, 100*(Cat-|An|)/(Cat+|An|) = 12.45

Iterations = 17
 Gamma iterations = 4
 Osmotic coefficient = 0.90483
 Density of water = 0.99221
 Total H = 1.111246e+02
 Total O = 5.601957e+01

-----Distribution of species-----

MacInnes Species	MacInnes		MacInnes		Gamma	cm ³ /mol
	Log Molality	Log Activity	Log Molality	Log Activity		
OH-	4.668e-05	2.473e-05	-4.331	-4.607	-0.276	-1.56
H+	1.455e-09	1.148e-09	-8.837	-8.940	-0.103	0.00
H2O	5.551e+01	9.697e-01	1.744	-0.013	0.000	18.16
C(4)	1.711e-01					
HCO3-	1.121e-01	5.725e-02	-0.951	-1.242	-0.292	28.05
CO3-2	4.107e-02	2.922e-03	-1.386	-2.534	-1.148	1.55
MgCO3	1.789e-02	1.789e-02	-1.747	-1.747	0.000	-17.10
CO2	1.095e-04	1.312e-04	-3.960	-3.882	0.078	35.16
Ca	5.300e-03					
Ca+2	5.300e-03	1.037e-03	-2.276	-2.984	-0.709	-16.16
Cl	6.590e-01					
Cl-	6.590e-01	3.979e-01	-0.181	-0.400	-0.219	19.27
Mg	5.243e-02					
Mg+2	3.451e-02	5.799e-03	-1.462	-2.237	-0.775	-20.53
MgCO3	1.789e-02	1.789e-02	-1.747	-1.747	0.000	-17.10
MgOH+	3.096e-05	2.645e-05	-4.509	-4.578	-0.068	(0)
Na	1.016e+00					
Na+	1.016e+00	7.008e-01	0.007	-0.154	-0.161	0.24

-----Saturation indices-----

Phase	SI**	log IAP	log K(313 K, 1 atm)	
Aragonite	2.81	-5.52	-8.33	CaCO3
Artinite	2.47	21.04	18.57	Mg2CO3(OH)2:3H2O
Bischofite	-7.52	-3.12	4.41	MgCl2:6H2O
Brucite	-0.74	-11.45	-10.71	Mg(OH)2
Calcite	3.13	-5.52	-8.65	CaCO3
CO2(g)	-2.26	-3.88	-1.63	CO2
Dolomite	7.12	-10.29	-17.41	CaMg(CO3)2
Gaylussite	0.99	-8.43	-9.42	CaNa2(CO3)2:5H2O
H2O(g)	-1.15	-0.01	1.14	H2O
Halite	-2.16	-0.55	1.61	NaCl

Huntite	12.41	21.10	8.69	CaMg ₃ (CO ₃) ₄
Magnesite	3.11	-4.77	-7.89	MgCO ₃
MgCl ₂ _2H ₂ O	-16.43	-3.06	13.37	MgCl ₂ :2H ₂ O
MgCl ₂ _4H ₂ O	-9.77	-3.09	6.68	MgCl ₂ :4H ₂ O
Nahcolite	-0.89	-11.63	-10.74	NaHCO ₃
Natron	-2.15	-2.98	-0.82	Na ₂ CO ₃ :10H ₂ O
Nesquehonite	0.36	-4.81	-5.17	MgCO ₃ :3H ₂ O
Pirssonite	0.85	-8.39	-9.23	Na ₂ Ca(CO ₃) ₂ :2H ₂ O
Portlandite	-7.01	-12.20	-5.19	Ca(OH) ₂
Trona	-3.11	-14.50	-11.38	Na ₃ H(CO ₃) ₂ :2H ₂ O

**For a gas, SI = log₁₀(fugacity). Fugacity = pressure * phi / 1 atm.
For ideal gases, phi = 1.

Initial solution 5. Alkaline 10d 40C

-----Solution composition-----

Elements	Molality	Moles
Alkalinity	1.527e-01	1.527e-01
Ca	5.256e-03	5.256e-03
Cl	6.536e-01	6.536e-01
Mg	5.200e-02	5.200e-02
Na	8.476e-01	8.476e-01

-----Description of solution-----

pH = 8.970
pe = 4.000
Specific Conductance (μS/cm, 40°C) = 89825
Density (g/cm³) = 1.02883
Volume (L) = 1.02140
Activity of water = 0.973
Ionic strength = 9.228e-01
Mass of water (kg) = 1.000e+00
Total carbon (mol/kg) = 1.108e-01
Total CO₂ (mol/kg) = 1.108e-01
Temperature (°C) = 40.00
Electrical balance (eq) = 1.558e-01
Percent error, 100*(Cat-|An|)/(Cat+|An|) = 9.12
Iterations = 17
Gamma iterations = 4
Osmotic coefficient = 0.91120
Density of water = 0.99221
Total H = 1.110814e+02

Total O = 5.583863e+01

-----Distribution of species-----

MacInnes	MacInnes	MacInnes	Log	Log	Log	mole V	
Species	Molality	Activity	Molality	Activity	Activity	Gamma	cm ³ /mol
OH-	5.007e-05	2.659e-05	-4.300	-4.575	-0.275	-1.77	
H+	1.336e-09	1.072e-09	-8.874	-8.970	-0.096	0.00	
H2O	5.551e+01	9.732e-01	1.744	-0.012	0.000	18.16	
C(4)	1.108e-01						
HCO3-	6.884e-02	3.713e-02	-1.162	-1.430	-0.268	27.80	
CO3-2	2.677e-02	2.030e-03	-1.572	-2.692	-1.120	1.24	
MgCO3	1.511e-02	1.511e-02	-1.821	-1.821	0.000	-17.10	
CO2	6.793e-05	7.915e-05	-4.168	-4.102	0.066	35.16	
Ca	5.256e-03						
Ca+2	5.256e-03	1.088e-03	-2.279	-2.964	-0.684	-16.26	
Cl	6.536e-01						
Cl-	6.536e-01	3.992e-01	-0.185	-0.399	-0.214	19.21	
Mg	5.200e-02						
Mg+2	3.686e-02	7.047e-03	-1.433	-2.152	-0.718	-20.62	
MgCO3	1.511e-02	1.511e-02	-1.821	-1.821	0.000	-17.10	
MgOH+	3.792e-05	3.456e-05	-4.421	-4.461	-0.040	(0)	
Na	8.476e-01						
Na+	8.476e-01	5.911e-01	-0.072	-0.228	-0.157	0.18	

-----Saturation indices-----

Phase	SI**	log IAP	log K(313 K, 1 atm)	
Aragonite	2.67	-5.66	-8.33	CaCO3
Artinite	2.55	21.12	18.57	Mg2CO3(OH)2:3H2O
Bischofite	-7.43	-3.02	4.41	MgCl2:6H2O
Brucite	-0.59	-11.30	-10.71	Mg(OH)2
Calcite	3.00	-5.66	-8.65	CaCO3
CO2(g)	-2.48	-4.10	-1.63	CO2
Dolomite	6.91	-10.50	-17.41	CaMg(CO3)2
Gaylussite	0.56	-8.86	-9.42	CaNa2(CO3)2:5H2O
H2O(g)	-1.15	-0.01	1.14	H2O
Halite	-2.23	-0.63	1.61	NaCl
Huntite	12.05	20.74	8.69	CaMg3(CO3)4
Magnesite	3.04	-4.84	-7.89	MgCO3
MgCl2_2H2O	-16.34	-2.97	13.37	MgCl2:2H2O
MgCl2_4H2O	-9.67	-3.00	6.68	MgCl2:4H2O
Nahcolite	-1.15	-11.89	-10.74	NaHCO3

Natron	-2.44	-3.27	-0.82	Na ₂ CO ₃ :10H ₂ O
Nesquehonite	0.29	-4.88	-5.17	MgCO ₃ :3H ₂ O
Pirssonite	0.41	-8.83	-9.23	Na ₂ Ca(CO ₃) ₂ :2H ₂ O
Portlandite	-6.92	-12.11	-5.19	Ca(OH) ₂
Trona	-3.68	-15.06	-11.38	Na ₃ H(CO ₃) ₂ :2H ₂ O

**For a gas, SI = log₁₀(fugacity). Fugacity = pressure * phi / 1 atm.
 For ideal gases, phi = 1.

Input file: /Users/adamyoerg/Desktop/Saline5d40C.txt
 Output file: /Users/adamyoerg/Desktop/Saline5d40C.txt.out
 Database file: /Users/adamyoerg/Desktop/PHREEQ/database/pitzer.dat

 Reading data base.

SOLUTION_MASTER_SPECIES
 SOLUTION_SPECIES
 PHASES
 PITZER
 EXCHANGE_MASTER_SPECIES
 EXCHANGE_SPECIES
 SURFACE_MASTER_SPECIES
 SURFACE_SPECIES
 END

 Reading input data for simulation 1.

Solution 1 Saline 5d 40C
 pH 7.08
 temp 40
 units mg/L
 Ca 200
 Mg 1200
 Na 60000
 Cl 95000
 Alkalinity 1150 as CO₃
 SAVE Solution 1

 Beginning of initial solution calculations.

Initial solution 1. Saline 5d 40C

-----Solution composition-----

Elements	Molality	Moles
Alkalinity	2.275e-02	2.275e-02
Ca	5.923e-03	5.923e-03
Cl	3.181e+00	3.181e+00
Mg	5.861e-02	5.861e-02
Na	3.098e+00	3.098e+00

-----Description of solution-----

pH = 7.080
 pe = 4.000
 Specific Conductance ($\mu\text{S}/\text{cm}$, 40°C) = 323067
 Density (g/cm^3) = 1.10573
 Volume (L) = 1.07354
 Activity of water = 0.884
 Ionic strength = 3.279e+00
 Mass of water (kg) = 1.000e+00
 Total carbon (mol/kg) = 2.307e-02
 Total CO2 (mol/kg) = 2.307e-02
 Temperature ($^\circ\text{C}$) = 40.00
 Electrical balance (eq) = 2.352e-02
 Percent error, $100 \cdot (\text{Cat} - |\text{An}|) / (\text{Cat} + |\text{An}|)$ = 0.37
 Iterations = 18
 Gamma iterations = 5
 Osmotic coefficient = 1.07510
 Density of water = 0.99221
 Total H = 1.110342e+02
 Total O = 5.557460e+01

-----Distribution of species-----

Species	MacInnes		MacInnes		mole V	Gamma	cm \geq /mol
	Molality	Activity	Log Molality	Log Activity			
OH-	7.893e-07	3.112e-07	-6.103	-6.507	-0.404	1.71	
H+	4.056e-08	8.318e-08	-7.392	-7.080	0.312	0.00	
H2O	5.551e+01	8.840e-01	1.744	-0.054	0.000	18.16	
C(4)	2.307e-02						
HCO3-	2.176e-02	7.521e-03	-1.662	-2.124	-0.461	31.93	
CO2	8.160e-04	1.370e-03	-3.088	-2.863	0.225	35.16	
CO3-2	2.683e-04	5.299e-06	-3.571	-5.276	-1.704	5.17	
MgCO3	2.247e-04	2.247e-04	-3.648	-3.648	0.000	-17.10	

Ca	5.923e-03						
Ca+2	5.923e-03	3.539e-03	-2.227	-2.451	-0.224	-14.94	
Cl	3.181e+00						
Cl-	3.181e+00	1.853e+00	0.503	0.268	-0.235	19.91	
Mg	5.861e-02						
Mg+2	5.838e-02	4.015e-02	-1.234	-1.396	-0.163	-19.36	
MgCO3	2.247e-04	2.247e-04	-3.648	-3.648	0.000	-17.10	
MgOH+	2.464e-06	2.304e-06	-5.608	-5.638	-0.029	(0)	
Na	3.098e+00						
Na+	3.098e+00	2.939e+00	0.491	0.468	-0.023	0.93	

-----Saturation indices-----

Phase	SI**	log IAP	log K(313 K, 1 atm)	
Aragonite	0.60	-7.73	-8.33	CaCO3
Artinite	-2.51	16.06	18.57	Mg2CO3(OH)2:3H2O
Bischofite	-5.59	-1.18	4.41	MgCl2:6H2O
Brucite	-3.70	-14.41	-10.71	Mg(OH)2
Calcite	0.92	-7.73	-8.65	CaCO3
CO2(g)	-1.24	-2.86	-1.63	CO2
Dolomite	3.02	-14.40	-17.41	CaMg(CO3)2
Gaylussite	-2.91	-12.33	-9.42	CaNa2(CO3)2:5H2O
H2O(g)	-1.19	-0.05	1.14	H2O
Halite	-0.87	0.74	1.61	NaCl
Huntite	4.50	13.18	8.69	CaMg3(CO3)4
Magnesite	1.21	-6.67	-7.89	MgCO3
MgCl2_2H2O	-14.34	-0.97	13.37	MgCl2:2H2O
MgCl2_4H2O	-7.75	-1.07	6.68	MgCl2:4H2O
Nahcolite	-1.15	-11.89	-10.74	NaHCO3
Natron	-4.05	-4.87	-0.82	Na2CO3:10H2O
Nesquehonite	-1.67	-6.83	-5.17	MgCO3:3H2O
Pirssonite	-2.94	-12.17	-9.23	Na2Ca(CO3)2:2H2O
Portlandite	-10.28	-15.47	-5.19	Ca(OH)2
Trona	-4.95	-16.33	-11.38	Na3H(CO3)2:2H2O

**For a gas, SI = log10(fugacity). Fugacity = pressure * phi / 1 atm.
For ideal gases, phi = 1.

Input file: /Users/adamyoerg/Desktop/Saline10d40C
Output file: /Users/adamyoerg/Desktop/Saline10d40C.out
Database file: /Users/adamyoerg/Desktop/PHREEQ/database/pitzer.dat

Reading data base.

SOLUTION_MASTER_SPECIES
 SOLUTION_SPECIES
 PHASES
 PITZER
 EXCHANGE_MASTER_SPECIES
 EXCHANGE_SPECIES
 SURFACE_MASTER_SPECIES
 SURFACE_SPECIES
 END

 Reading input data for simulation 1.

Solution 1 Saline 10d 40C
 pH 7.5
 temp 40
 units mg/L
 Ca 200
 Mg 1200
 Na 61000
 Cl 95000
 Alkalinity 2300 as CO3
 SAVE Solution 1

 Beginning of initial solution calculations.

Initial solution 1. Saline 10d 40C

-----Solution composition-----

Elements	Molality	Moles
Alkalinity	4.561e-02	4.561e-02
Ca	5.938e-03	5.938e-03
Cl	3.189e+00	3.189e+00
Mg	5.876e-02	5.876e-02
Na	3.158e+00	3.158e+00

-----Description of solution-----

pH = 7.500
 pe = 4.000
 Specific Conductance ($\mu\text{S}/\text{cm}$, 40°C) = 327670
 Density (g/cm^3) = 1.10754

Volume (L) = 1.07443
 Activity of water = 0.882
 Ionic strength = 3.324e+00
 Mass of water (kg) = 1.000e+00
 Total carbon (mol/kg) = 4.377e-02
 Total CO2 (mol/kg) = 4.377e-02
 Temperature (∞C) = 40.00
 Electrical balance (eq) = 5.254e-02
 Percent error, 100*(Cat-|An|)/(Cat+|An|) = 0.81
 Iterations = 17
 Gamma iterations = 5
 Osmotic coefficient = 1.07609
 Density of water = 0.99221
 Total H = 1.110532e+02
 Total O = 5.563695e+01

-----Distribution of species-----

Species	MacInnes		MacInnes		Log	mole V	Gamma	cm ³ /mol
	Molality	Activity	Log Molality	Log Activity				
OH-	2.071e-06	8.170e-07	-5.684	-6.088	-0.404	1.78		
H+	1.530e-08	3.162e-08	-7.815	-7.500	0.315	0.00		
H2O	5.551e+01	8.824e-01	1.744	-0.054	0.000	18.16		
C(4)	4.377e-02							
HCO3-	4.079e-02	1.393e-02	-1.389	-1.856	-0.467	32.00		
CO3-2	1.323e-03	2.581e-05	-2.878	-4.588	-1.710	5.24		
MgCO3	1.082e-03	1.082e-03	-2.966	-2.966	0.000	-17.10		
CO2	5.698e-04	9.663e-04	-3.244	-3.015	0.229	35.16		
Ca	5.938e-03							
Ca+2	5.938e-03	3.632e-03	-2.226	-2.440	-0.213	-14.92		
Cl	3.189e+00							
Cl-	3.189e+00	1.859e+00	0.504	0.269	-0.234	19.92		
Mg	5.876e-02							
Mg+2	5.767e-02	3.972e-02	-1.239	-1.401	-0.162	-19.34		
MgCO3	1.082e-03	1.082e-03	-2.966	-2.966	0.000	-17.10		
MgOH+	6.463e-06	5.984e-06	-5.190	-5.223	-0.033	(0)		
Na	3.158e+00							
Na+	3.158e+00	3.006e+00	0.499	0.478	-0.021	0.94		

-----Saturation indices-----

Phase	SI**	log IAP	log K(313 K, 1 atm)
Aragonite	1.30	-7.03	-8.33 CaCO3

Artinite	-1.00	17.57	18.57	Mg ₂ CO ₃ (OH) ₂ :3H ₂ O
Bischofite	-5.60	-1.19	4.41	MgCl ₂ :6H ₂ O
Brucite	-2.87	-13.58	-10.71	Mg(OH) ₂
Calcite	1.62	-7.03	-8.65	CaCO ₃
CO ₂ (g)	-1.39	-3.01	-1.63	CO ₂
Dolomite	4.40	-13.02	-17.41	CaMg(CO ₃) ₂
Gaylussite	-1.51	-10.93	-9.42	CaNa ₂ (CO ₃) ₂ :5H ₂ O
H ₂ O(g)	-1.19	-0.05	1.14	H ₂ O
Halite	-0.86	0.75	1.61	NaCl
Huntite	7.25	15.93	8.69	CaMg ₃ (CO ₃) ₄
Magnesite	1.90	-5.99	-7.89	MgCO ₃
MgCl ₂ _2H ₂ O	-14.34	-0.97	13.37	MgCl ₂ :2H ₂ O
MgCl ₂ _4H ₂ O	-7.76	-1.08	6.68	MgCl ₂ :4H ₂ O
Nahcolite	-0.87	-11.61	-10.74	NaHCO ₃
Natron	-3.35	-4.18	-0.82	Na ₂ CO ₃ :10H ₂ O
Nesquehonite	-0.99	-6.15	-5.17	MgCO ₃ :3H ₂ O
Pirssonite	-1.54	-10.77	-9.23	Na ₂ Ca(CO ₃) ₂ :2H ₂ O
Portlandite	-9.43	-14.62	-5.19	Ca(OH) ₂
Trona	-3.97	-15.35	-11.38	Na ₃ H(CO ₃) ₂ :2H ₂ O

**For a gas, SI = log₁₀(fugacity). Fugacity = pressure * phi / 1 atm.
For ideal gases, phi = 1.

Appendix II: Dolomitization Geochemical Modeling

This appendix includes PHREEQC model outputs for dolomitization batch experiments conducted for each of the three environments. Models assume the ooids are pure aragonite. Different models also account for varying water/rock ratios.

Input file: /Users/adamyoerg/Desktop/Sabkha_Dissolution_dolomitization.txt
Output file: /Users/adamyoerg/Desktop/Sabkha_Dissolution_dolomitization.txt.out
Database file: /Users/adamyoerg/Desktop/PHREEQC/database/pitzer.dat

Reading data base.

SOLUTION_MASTER_SPECIES
SOLUTION_SPECIES
PHASES
PITZER
EXCHANGE_MASTER_SPECIES
EXCHANGE_SPECIES
SURFACE_MASTER_SPECIES
SURFACE_SPECIES
END

Reading input data for simulation 1.

TITLE Sabkha
Solution 1 Sabkha
pH 7.5
temp 40
units mg/L
Ca 200
Mg 1200
Na 59000
Cl 95000
EQUILIBRIUM PHASES
Aragonite 0.0 0.1
END

TITLE

Sabkha

Beginning of initial solution calculations.

Initial solution 1. Sabkha

-----Solution composition-----

Elements	Molality	Moles
Ca	5.908e-03	5.908e-03
Cl	3.173e+00	3.173e+00
Mg	5.846e-02	5.846e-02
Na	3.039e+00	3.039e+00

-----Description of solution-----

pH = 7.500
pe = 4.000
Specific Conductance ($\mu\text{S}/\text{cm}$, 40°C) = 318376
Density (g/cm^3) = 1.10391
Volume (L) = 1.07254
Activity of water = 0.886
Ionic strength = 3.234e+00
Mass of water (kg) = 1.000e+00
Total alkalinity (eq/kg) = 8.477e-06
Total carbon (mol/kg) = 0.000e+00
Total CO2 (mol/kg) = 0.000e+00
Temperature ($^\circ\text{C}$) = 40.00
Electrical balance (eq) = -5.364e-03
Percent error, $100 * (\text{Cat} - |\text{An}|) / (\text{Cat} + |\text{An}|)$ = -0.08
Iterations = 7
Gamma iterations = 4
Osmotic coefficient = 1.07393
Density of water = 0.99221
Total H = 1.110124e+02
Total O = 5.550623e+01

-----Distribution of species-----

MacInnes MacInnes

MacInnes	Log	Log	Log	mole V		
Species	Molality	Activity	Molality	Activity	Gamma	cm^3/mol

OH-	2.079e-06	8.200e-07	-5.682	-6.086	-0.404	1.66
H+	1.555e-08	3.162e-08	-7.808	-7.500	0.308	0.00
H2O	5.551e+01	8.857e-01	1.744	-0.053	0.000	18.16
Ca	5.908e-03					
Ca+2	5.908e-03	3.430e-03	-2.229	-2.465	-0.236	-14.96
Cl	3.173e+00					
Cl-	3.173e+00	1.847e+00	0.501	0.267	-0.235	19.90
Mg	5.846e-02					
Mg+2	5.845e-02	4.005e-02	-1.233	-1.397	-0.164	-19.38
MgOH+	6.413e-06	6.057e-06	-5.193	-5.218	-0.025	(0)
Na	3.039e+00					
Na+	3.039e+00	2.871e+00	0.483	0.458	-0.025	0.92

-----Saturation indices-----

Phase	SI**	log IAP	log K(313 K, 1 atm)
Bischofite	-5.59	-1.18	4.41 MgCl2:6H2O
Brucite	-2.86	-13.57	-10.71 Mg(OH)2
H2O(g)	-1.19	-0.05	1.14 H2O
Halite	-0.88	0.72	1.61 NaCl
MgCl2_2H2O	-14.34	-0.97	13.37 MgCl2:2H2O
MgCl2_4H2O	-7.75	-1.08	6.68 MgCl2:4H2O
Portlandite	-9.45	-14.64	-5.19 Ca(OH)2

**For a gas, SI = log10(fugacity). Fugacity = pressure * phi / 1 atm.
For ideal gases, phi = 1.

Beginning of batch-reaction calculations.

Reaction step 1.

Using solution 1. Sabkha
Using pure phase assemblage 1. PHASES

-----Phase assemblage-----

Phase	SI	log IAP	log K(T, P)	Moles in assemblage		
				Initial	Final	Delta
Aragonite	0.00	-8.33	-8.33	1.000e-01	9.975e-02	-2.473e-04

-----Solution composition-----

Elements	Molality	Moles
C	2.473e-04	2.473e-04
Ca	6.155e-03	6.155e-03
Cl	3.173e+00	3.173e+00
Mg	5.846e-02	5.846e-02
Na	3.039e+00	3.039e+00

-----Description of solution-----

pH = 8.703 Charge balance
 pe = 4.000 Adjusted to redox equilibrium
 Specific Conductance ($\mu\text{S}/\text{cm}$, 40°C) = 318370
 Density (g/cm^3) = 1.10394
 Volume (L) = 1.07254
 Activity of water = 0.886
 Ionic strength = 3.235e+00
 Mass of water (kg) = 1.000e+00
 Total alkalinity (eq/kg) = 5.031e-04
 Total CO2 (mol/kg) = 2.473e-04
 Temperature ($^\circ\text{C}$) = 40.00
 Electrical balance (eq) = -5.364e-03
 Percent error, $100 * (\text{Cat} - |\text{An}|) / (\text{Cat} + |\text{An}|)$ = -0.08
 Iterations = 16
 Gamma iterations = 4
 Osmotic coefficient = 1.07391
 Density of water = 0.99221
 Total H = 1.110124e+02
 Total O = 5.550697e+01

-----Distribution of species-----

MacInnes	MacInnes						
Species	Log Molality	Log Activity	Log mole V	Activity	Gamma	cm ³ /mol	
OH-	3.319e-05	1.309e-05	-4.479	-4.883	-0.404	1.65	
H+	9.743e-10	1.982e-09	-9.011	-8.703	0.308	0.00	
H2O	5.551e+01	8.857e-01	1.744	-0.053	0.000	18.16	
C(4)	2.473e-04						
HCO3-	1.265e-04	4.432e-05	-3.898	-4.353	-0.456	31.86	
CO3-2	6.538e-05	1.311e-06	-4.185	-5.883	-1.698	5.12	
MgCO3	5.527e-05	5.527e-05	-4.257	-4.257	0.000	-17.10	
CO2	1.155e-07	1.920e-07	-6.937	-6.717	0.221	35.16	
Ca	6.155e-03						
Ca+2	6.155e-03	3.573e-03	-2.211	-2.447	-0.236	-14.96	

Cl	3.173e+00					
Cl-	3.173e+00	1.847e+00	0.501	0.267	-0.235	19.90
Mg	5.846e-02					
Mg+2	5.830e-02	3.994e-02	-1.234	-1.399	-0.164	-19.38
MgOH+	1.021e-04	9.638e-05	-3.991	-4.016	-0.025	(0)
MgCO3	5.527e-05	5.527e-05	-4.257	-4.257	0.000	-17.10
Na	3.039e+00					
Na+	3.039e+00	2.871e+00	0.483	0.458	-0.025	0.92

-----Saturation indices-----

Phase	SI**	log IAP	log K(313 K, 1 atm)	
Aragonite	0.00	-8.33	-8.33	CaCO3
Artinite	0.13	18.69	18.57	Mg2CO3(OH)2:3H2O
Bischofite	-5.59	-1.18	4.41	MgCl2:6H2O
Brucite	-0.46	-11.17	-10.71	Mg(OH)2
Calcite	0.32	-8.33	-8.65	CaCO3
CO2(g)	-5.09	-6.72	-1.63	CO2
Dolomite	1.80	-15.61	-17.41	CaMg(CO3)2
Gaylussite	-4.14	-13.56	-9.42	CaNa2(CO3)2:5H2O
H2O(g)	-1.19	-0.05	1.14	H2O
Halite	-0.88	0.72	1.61	NaCl
Huntite	2.07	10.76	8.69	CaMg3(CO3)4
Magnesite	0.60	-7.28	-7.89	MgCO3
MgCl2_2H2O	-14.34	-0.97	13.37	MgCl2:2H2O
MgCl2_4H2O	-7.75	-1.08	6.68	MgCl2:4H2O
Nahcolite	-3.39	-14.13	-10.74	NaHCO3
Natron	-4.67	-5.49	-0.82	Na2CO3:10H2O
Nesquehonite	-2.27	-7.44	-5.17	MgCO3:3H2O
Pirssonite	-4.17	-13.40	-9.23	Na2Ca(CO3)2:2H2O
Portlandite	-7.02	-12.21	-5.19	Ca(OH)2
Trona	-7.82	-19.20	-11.38	Na3H(CO3)2:2H2O

**For a gas, SI = log10(fugacity). Fugacity = pressure * phi / 1 atm.
For ideal gases, phi = 1.

End of simulation.

Reading input data for simulation 2.

End of Run after 0.023904 Seconds.

Input file: /Users/adamyoerg/Desktop/Dolomitization_Experiments.txt
Output file: /Users/adamyoerg/Desktop/Dolomitization_Experiments.txtLOOK.out
Database file: /Users/adamyoerg/Desktop/PHREEQ/database/pitzer.dat

Reading data base.

SOLUTION_MASTER_SPECIES
SOLUTION_SPECIES
PHASES
PITZER
EXCHANGE_MASTER_SPECIES
EXCHANGE_SPECIES
SURFACE_MASTER_SPECIES
SURFACE_SPECIES
END

Reading input data for simulation 1.

TITLE Dolomitization Experiments
Solution 1 Initial Mixing Zone
pH 7.5
temp 40
units mg/L
Ca 200
Mg 1200
Na 3400
Cl 8800
Alkalinity 280 as CO3
EQUILIBRIUM PHASES
Aragonite 0.0 1.0
SAVE Solution 1
END

TITLE

Dolomitization Experiments

Beginning of initial solution calculations.

Initial solution 1. Initial Mixing Zone

-----Solution composition-----

Elements	Molality	Moles
Alkalinity	4.731e-03	4.731e-03
Ca	5.060e-03	5.060e-03
Cl	2.517e-01	2.517e-01
Mg	5.007e-02	5.007e-02
Na	1.500e-01	1.500e-01

-----Description of solution-----

pH = 7.500
 pe = 4.000
 Specific Conductance ($\mu\text{S}/\text{cm}$, 40 ∞C) = 34207
 Density (g/cm^3) = 1.00251
 Volume (L) = 1.01154
 Activity of water = 0.993
 Ionic strength = 3.132e-01
 Mass of water (kg) = 1.000e+00
 Total carbon (mol/kg) = 4.778e-03
 Total CO2 (mol/kg) = 4.778e-03
 Temperature (∞C) = 40.00
 Electrical balance (eq) = 3.788e-03
 Percent error, $100 \cdot (\text{Cat} - |\text{An}|) / (\text{Cat} + |\text{An}|) = 0.73$
 Iterations = 14
 Gamma iterations = 3
 Osmotic coefficient = 0.89905
 Density of water = 0.99221
 Total H = 1.110169e+02
 Total O = 5.552038e+01

-----Distribution of species-----

Species	MacInnes		MacInnes		mole V Gamma	cm \geq /mol
	MacInnes Molality	Log Activity	Log Molality	Log Activity		
OH-	1.587e-06	9.190e-07	-5.800	-6.037	-0.237	-2.87
H+	4.077e-08	3.162e-08	-7.390	-7.500	-0.110	0.00
H2O	5.551e+01	9.926e-01	1.744	-0.003	0.000	18.16
C(4)	4.778e-03					
HCO3-	4.471e-03	3.017e-03	-2.350	-2.520	-0.171	26.53

CO2	1.783e-04	1.862e-04	-3.749	-3.730	0.019	35.16
MgCO3	8.402e-05	8.402e-05	-4.076	-4.076	0.000	-17.10
CO3-2	4.411e-05	5.592e-06	-4.356	-5.252	-0.897	-0.56
Ca	5.060e-03					
Ca+2	5.060e-03	1.387e-03	-2.296	-2.858	-0.562	-16.86
Cl	2.517e-01					
Cl-	2.517e-01	1.715e-01	-0.599	-0.766	-0.167	18.83
Mg	5.007e-02					
Mg+2	4.998e-02	1.423e-02	-1.301	-1.847	-0.546	-21.18
MgCO3	8.402e-05	8.402e-05	-4.076	-4.076	0.000	-17.10
MgOH+	2.601e-06	2.411e-06	-5.585	-5.618	-0.033	(0)
Na	1.500e-01					
Na+	1.500e-01	1.099e-01	-0.824	-0.959	-0.135	-0.21

-----Saturation indices-----

Phase	SI**	log IAP	log K(313 K, 1 atm)	
Aragonite	0.22	-8.11	-8.33	CaCO3
Artinite	-2.30	16.27	18.57	Mg2CO3(OH)2:3H2O
Bischofite	-7.80	-3.40	4.41	MgCl2:6H2O
Brucite	-3.21	-13.92	-10.71	Mg(OH)2
Calcite	0.54	-8.11	-8.65	CaCO3
CO2(g)	-2.11	-3.73	-1.63	CO2
Dolomite	2.20	-15.21	-17.41	CaMg(CO3)2
Gaylussite	-5.88	-15.30	-9.42	CaNa2(CO3)2:5H2O
H2O(g)	-1.14	-0.00	1.14	H2O
Halite	-3.33	-1.72	1.61	NaCl
Huntite	2.83	11.52	8.69	CaMg3(CO3)4
Magnesite	0.79	-7.10	-7.89	MgCO3
MgCl2_2H2O	-16.75	-3.38	13.37	MgCl2:2H2O
MgCl2_4H2O	-10.07	-3.39	6.68	MgCl2:4H2O
Nahcolite	-2.97	-13.71	-10.74	NaHCO3
Natron	-6.38	-7.20	-0.82	Na2CO3:10H2O
Nesquehonite	-1.94	-7.11	-5.17	MgCO3:3H2O
Pirssonite	-6.05	-15.29	-9.23	Na2Ca(CO3)2:2H2O
Portlandite	-9.74	-14.93	-5.19	Ca(OH)2
Trona	-9.50	-20.89	-11.38	Na3H(CO3)2:2H2O

**For a gas, SI = log10(fugacity). Fugacity = pressure * phi / 1 atm.
For ideal gases, phi = 1.

Beginning of batch-reaction calculations.

Reaction step 1.

Using solution 1. Initial Mixing Zone
Using pure phase assemblage 1. PHASES

-----Phase assemblage-----

Phase	Moles in assemblage					
	SI	log IAP	log K(T, P)	Initial	Final	Delta
Aragonite	0.00	-8.33	-8.33	1.000e+00	1.000e+00	1.371e-04

-----Solution composition-----

Elements	Molality	Moles
C	4.640e-03	4.640e-03
Ca	4.923e-03	4.923e-03
Cl	2.517e-01	2.517e-01
Mg	5.007e-02	5.007e-02
Na	1.500e-01	1.500e-01

-----Description of solution-----

pH = 7.310 Charge balance
pe = 4.000 Adjusted to redox equilibrium
Specific Conductance ($\mu\text{S}/\text{cm}$, 40°C) = 34190
Density (g/cm^3) = 1.00250
Volume (L) = 1.01154
Activity of water = 0.993
Ionic strength = 3.129e-01
Mass of water (kg) = 1.000e+00
Total alkalinity (eq/kg) = 4.457e-03
Total CO2 (mol/kg) = 4.640e-03
Temperature (°C) = 40.00
Electrical balance (eq) = 3.788e-03
Percent error, $100 \cdot (\text{Cat} - |\text{An}|) / (\text{Cat} + |\text{An}|)$ = 0.73
Iterations = 10
Gamma iterations = 2
Osmotic coefficient = 0.89915
Density of water = 0.99221
Total H = 1.110169e+02
Total O = 5.551996e+01

-----Distribution of species-----

MacInnes MacInnes						
Species	MacInnes Molality	Log Activity	Log Molality	Log Activity	mole V Gamma	cm ³ /mol
OH-	1.024e-06	5.934e-07	-5.990	-6.227	-0.237	-2.87
H+	6.313e-08	4.898e-08	-7.200	-7.310	-0.110	0.00
H2O	5.551e+01	9.926e-01	1.744	-0.003	0.000	18.16
C(4)	4.640e-03					
HCO3-	4.296e-03	2.899e-03	-2.367	-2.538	-0.171	26.53
CO2	2.653e-04	2.770e-04	-3.576	-3.558	0.019	35.16
MgCO3	5.218e-05	5.218e-05	-4.282	-4.282	0.000	-17.10
CO3-2	2.733e-05	3.468e-06	-4.563	-5.460	-0.896	-0.56
Ca	4.923e-03					
Ca+2	4.923e-03	1.350e-03	-2.308	-2.870	-0.562	-16.86
Cl	2.517e-01					
Cl-	2.517e-01	1.715e-01	-0.599	-0.766	-0.167	18.83
Mg	5.007e-02					
Mg+2	5.001e-02	1.425e-02	-1.301	-1.846	-0.545	-21.18
MgCO3	5.218e-05	5.218e-05	-4.282	-4.282	0.000	-17.10
MgOH+	1.681e-06	1.559e-06	-5.774	-5.807	-0.033	(0)
Na	1.500e-01					
Na+	1.500e-01	1.099e-01	-0.824	-0.959	-0.135	-0.21

-----Saturation indices-----

Phase	SI**	log IAP	log K(313 K, 1 atm)	
Aragonite	0.00	-8.33	-8.33	CaCO3
Artinite	-2.89	15.68	18.57	Mg2CO3(OH)2:3H2O
Bischofite	-7.80	-3.40	4.41	MgCl2:6H2O
Brucite	-3.59	-14.30	-10.71	Mg(OH)2
Calcite	0.32	-8.33	-8.65	CaCO3
CO2(g)	-1.93	-3.56	-1.63	CO2
Dolomite	1.78	-15.64	-17.41	CaMg(CO3)2
Gaylussite	-6.30	-15.72	-9.42	CaNa2(CO3)2:5H2O
H2O(g)	-1.14	-0.00	1.14	H2O
Halite	-3.33	-1.72	1.61	NaCl
Huntite	2.00	10.68	8.69	CaMg3(CO3)4
Magnesite	0.58	-7.31	-7.89	MgCO3
MgCl2_2H2O	-16.75	-3.38	13.37	MgCl2:2H2O
MgCl2_4H2O	-10.07	-3.39	6.68	MgCl2:4H2O
Nahcolite	-2.99	-13.73	-10.74	NaHCO3
Natron	-6.59	-7.41	-0.82	Na2CO3:10H2O
Nesquehonite	-2.15	-7.32	-5.17	MgCO3:3H2O
Pirssonite	-6.48	-15.71	-9.23	Na2Ca(CO3)2:2H2O
Portlandite	-10.13	-15.32	-5.19	Ca(OH)2

Trona -9.73 -21.11 -11.38 Na₃H(CO₃)₂·2H₂O

**For a gas, SI = log₁₀(fugacity). Fugacity = pressure * phi / 1 atm.
For ideal gases, phi = 1.

End of simulation.

Reading input data for simulation 2.

Solution 2 Mixing Zone - Water:Rock Increased

pH 7.5

temp 40

units mg/L

Ca 200

Mg 1200

Na 3400

Cl 8800

Alkalinity 280 as CO₃

EQUILIBRIUM PHASES

Aragonite 0.0 0.1

END

Beginning of initial solution calculations.

Initial solution 2. Mixing Zone - Water:Rock Increased

-----Solution composition-----

Elements	Molality	Moles
Alkalinity	4.731e-03	4.731e-03
Ca	5.060e-03	5.060e-03
Cl	2.517e-01	2.517e-01
Mg	5.007e-02	5.007e-02
Na	1.500e-01	1.500e-01

-----Description of solution-----

pH = 7.500

pe = 4.000

Specific Conductance (μS/cm, 40°C) = 34207

Density (g/cm³) = 1.00251
 Volume (L) = 1.01154
 Activity of water = 0.993
 Ionic strength = 3.132e-01
 Mass of water (kg) = 1.000e+00
 Total carbon (mol/kg) = 4.778e-03
 Total CO2 (mol/kg) = 4.778e-03
 Temperature (°C) = 40.00
 Electrical balance (eq) = 3.788e-03
 Percent error, 100*(Cat-|An|)/(Cat+|An|) = 0.73
 Iterations = 14
 Gamma iterations = 3
 Osmotic coefficient = 0.89905
 Density of water = 0.99221
 Total H = 1.110169e+02
 Total O = 5.552038e+01

-----Distribution of species-----

Species	MacInnes		MacInnes		Log	mole V	Gamma	cm ³ /mol
	Molality	Activity	Molality	Activity				
OH-	1.587e-06	9.190e-07	-5.800	-6.037	-0.237	-2.87		
H+	4.077e-08	3.162e-08	-7.390	-7.500	-0.110	0.00		
H2O	5.551e+01	9.926e-01	1.744	-0.003	0.000	18.16		
C(4)	4.778e-03							
HCO3-	4.471e-03	3.017e-03	-2.350	-2.520	-0.171	26.53		
CO2	1.783e-04	1.862e-04	-3.749	-3.730	0.019	35.16		
MgCO3	8.402e-05	8.402e-05	-4.076	-4.076	0.000	-17.10		
CO3-2	4.411e-05	5.592e-06	-4.356	-5.252	-0.897	-0.56		
Ca	5.060e-03							
Ca+2	5.060e-03	1.387e-03	-2.296	-2.858	-0.562	-16.86		
Cl	2.517e-01							
Cl-	2.517e-01	1.715e-01	-0.599	-0.766	-0.167	18.83		
Mg	5.007e-02							
Mg+2	4.998e-02	1.423e-02	-1.301	-1.847	-0.546	-21.18		
MgCO3	8.402e-05	8.402e-05	-4.076	-4.076	0.000	-17.10		
MgOH+	2.601e-06	2.411e-06	-5.585	-5.618	-0.033	(0)		
Na	1.500e-01							
Na+	1.500e-01	1.099e-01	-0.824	-0.959	-0.135	-0.21		

-----Saturation indices-----

Phase SI** log IAP log K(313 K, 1 atm)

Aragonite	0.22	-8.11	-8.33	CaCO3
Artinite	-2.30	16.27	18.57	Mg2CO3(OH)2:3H2O
Bischofite	-7.80	-3.40	4.41	MgCl2:6H2O
Brucite	-3.21	-13.92	-10.71	Mg(OH)2
Calcite	0.54	-8.11	-8.65	CaCO3
CO2(g)	-2.11	-3.73	-1.63	CO2
Dolomite	2.20	-15.21	-17.41	CaMg(CO3)2
Gaylussite	-5.88	-15.30	-9.42	CaNa2(CO3)2:5H2O
H2O(g)	-1.14	-0.00	1.14	H2O
Halite	-3.33	-1.72	1.61	NaCl
Huntite	2.83	11.52	8.69	CaMg3(CO3)4
Magnesite	0.79	-7.10	-7.89	MgCO3
MgCl2_2H2O	-16.75	-3.38	13.37	MgCl2:2H2O
MgCl2_4H2O	-10.07	-3.39	6.68	MgCl2:4H2O
Nahcolite	-2.97	-13.71	-10.74	NaHCO3
Natron	-6.38	-7.20	-0.82	Na2CO3:10H2O
Nesquehonite	-1.94	-7.11	-5.17	MgCO3:3H2O
Pirssonite	-6.05	-15.29	-9.23	Na2Ca(CO3)2:2H2O
Portlandite	-9.74	-14.93	-5.19	Ca(OH)2
Trona	-9.50	-20.89	-11.38	Na3H(CO3)2:2H2O

**For a gas, SI = log10(fugacity). Fugacity = pressure * phi / 1 atm.
For ideal gases, phi = 1.

Beginning of batch-reaction calculations.

Reaction step 1.

Using solution 2. Mixing Zone - Water:Rock Increased
Using pure phase assemblage 1. PHASES

-----Phase assemblage-----

Phase	SI	log IAP	log K(T, P)	Moles in assemblage		
				Initial	Final	Delta
Aragonite	0.00	-8.33	-8.33	1.000e-01	1.001e-01	1.371e-04

-----Solution composition-----

Elements	Molality	Moles
C	4.640e-03	4.640e-03
Ca	4.923e-03	4.923e-03

Cl	2.517e-01	2.517e-01
Mg	5.007e-02	5.007e-02
Na	1.500e-01	1.500e-01

-----Description of solution-----

pH = 7.310 Charge balance
 pe = 4.000 Adjusted to redox equilibrium
 Specific Conductance ($\mu\text{S}/\text{cm}$, 40°C) = 34190
 Density (g/cm^3) = 1.00250
 Volume (L) = 1.01154
 Activity of water = 0.993
 Ionic strength = 3.129e-01
 Mass of water (kg) = 1.000e+00
 Total alkalinity (eq/kg) = 4.457e-03
 Total CO2 (mol/kg) = 4.640e-03
 Temperature (°C) = 40.00
 Electrical balance (eq) = 3.788e-03
 Percent error, $100 \cdot (\text{Cat} - |\text{An}|) / (\text{Cat} + |\text{An}|)$ = 0.73
 Iterations = 10
 Gamma iterations = 2
 Osmotic coefficient = 0.89915
 Density of water = 0.99221
 Total H = 1.110169e+02
 Total O = 5.551996e+01

-----Distribution of species-----

Species	MacInnes		MacInnes		mole V Gamma	cm \geq /mol
	Molality	Activity	Log Molality	Log Activity		
OH-	1.024e-06	5.934e-07	-5.990	-6.227	-0.237	-2.87
H+	6.313e-08	4.898e-08	-7.200	-7.310	-0.110	0.00
H2O	5.551e+01	9.926e-01	1.744	-0.003	0.000	18.16
C(4)	4.640e-03					
HCO3-	4.296e-03	2.899e-03	-2.367	-2.538	-0.171	26.53
CO2	2.653e-04	2.770e-04	-3.576	-3.558	0.019	35.16
MgCO3	5.218e-05	5.218e-05	-4.282	-4.282	0.000	-17.10
CO3-2	2.733e-05	3.468e-06	-4.563	-5.460	-0.896	-0.56
Ca	4.923e-03					
Ca+2	4.923e-03	1.350e-03	-2.308	-2.870	-0.562	-16.86
Cl	2.517e-01					
Cl-	2.517e-01	1.715e-01	-0.599	-0.766	-0.167	18.83
Mg	5.007e-02					
Mg+2	5.001e-02	1.425e-02	-1.301	-1.846	-0.545	-21.18

MgCO3	5.218e-05	5.218e-05	-4.282	-4.282	0.000	-17.10
MgOH+	1.681e-06	1.559e-06	-5.774	-5.807	-0.033	(0)
Na	1.500e-01					
Na+	1.500e-01	1.099e-01	-0.824	-0.959	-0.135	-0.21

-----Saturation indices-----

Phase	SI**	log IAP	log K(313 K, 1 atm)	
Aragonite	0.00	-8.33	-8.33	CaCO3
Artinite	-2.89	15.68	18.57	Mg2CO3(OH)2:3H2O
Bischofite	-7.80	-3.40	4.41	MgCl2:6H2O
Brucite	-3.59	-14.30	-10.71	Mg(OH)2
Calcite	0.32	-8.33	-8.65	CaCO3
CO2(g)	-1.93	-3.56	-1.63	CO2
Dolomite	1.78	-15.64	-17.41	CaMg(CO3)2
Gaylussite	-6.30	-15.72	-9.42	CaNa2(CO3)2:5H2O
H2O(g)	-1.14	-0.00	1.14	H2O
Halite	-3.33	-1.72	1.61	NaCl
Huntite	2.00	10.68	8.69	CaMg3(CO3)4
Magnesite	0.58	-7.31	-7.89	MgCO3
MgCl2_2H2O	-16.75	-3.38	13.37	MgCl2:2H2O
MgCl2_4H2O	-10.07	-3.39	6.68	MgCl2:4H2O
Nahcolite	-2.99	-13.73	-10.74	NaHCO3
Natron	-6.59	-7.41	-0.82	Na2CO3:10H2O
Nesquehonite	-2.15	-7.32	-5.17	MgCO3:3H2O
Pirssonite	-6.48	-15.71	-9.23	Na2Ca(CO3)2:2H2O
Portlandite	-10.13	-15.32	-5.19	Ca(OH)2
Trona	-9.73	-21.11	-11.38	Na3H(CO3)2:2H2O

**For a gas, SI = log10(fugacity). Fugacity = pressure * phi / 1 atm.
For ideal gases, phi = 1.

End of simulation.

Reading input data for simulation 3.

Solution 3 Ca/Mg Solution
temp 40
units mol/L
Ca 0.1
Mg 0.3

Cl 0.8
 EQUILIBRIUM PHASES
 Aragonite 0.0 0.1
 END

 Beginning of initial solution calculations.

Initial solution 3. Ca/Mg Solution

-----Solution composition-----

Elements	Molality	Moles
Ca	1.041e-01	1.041e-01
Cl	8.330e-01	8.330e-01
Mg	3.124e-01	3.124e-01

-----Description of solution-----

pH = 7.000
 pe = 4.000
 Specific Conductance ($\mu\text{S}/\text{cm}$, 40°C) = 77436
 Density (g/cm^3) = 1.02498
 Volume (L) = 1.01592
 Activity of water = 0.980
 Ionic strength = 1.250e+00
 Mass of water (kg) = 1.000e+00
 Total alkalinity (eq/kg) = 5.472e-06
 Total carbon (mol/kg) = 0.000e+00
 Total CO2 (mol/kg) = 0.000e+00
 Temperature ($^\circ\text{C}$) = 40.00
 Electrical balance (eq) = -5.472e-06
 Percent error, $100 \cdot (\text{Cat} - |\text{An}|) / (\text{Cat} + |\text{An}|)$ = -0.00
 Iterations = 5
 Gamma iterations = 3
 Osmotic coefficient = 0.90527
 Density of water = 0.99221
 Total H = 1.110124e+02
 Total O = 5.550622e+01

-----Distribution of species-----

Species	MacInnes		MacInnes		mole V Gamma	cm \geq /mol
	MacInnes Molality	Log Activity	Log Molality	Log Activity		

OH-	1.070e-06	2.869e-07	-5.970	-6.542	-0.572	-1.25
H+	1.122e-07	1.000e-07	-6.950	-7.000	-0.050	0.00
H2O	5.551e+01	9.798e-01	1.744	-0.009	0.000	18.16
Ca	1.041e-01					
Ca+2	1.041e-01	2.483e-02	-0.982	-1.605	-0.623	-16.03
Cl	8.330e-01					
Cl-	8.330e-01	4.963e-01	-0.079	-0.304	-0.225	19.35
Mg	3.124e-01					
Mg+2	3.124e-01	8.135e-02	-0.505	-1.090	-0.584	-20.41
MgOH+	4.514e-06	4.304e-06	-5.345	-5.366	-0.021	(0)

-----Saturation indices-----

Phase	SI**	log IAP	log K(313 K, 1 atm)	
Bischofite	-6.16	-1.75	4.41	MgCl2:6H2O
Brucite	-3.46	-14.17	-10.71	Mg(OH)2
H2O(g)	-1.15	-0.01	1.14	H2O
MgCl2_2H2O	-15.08	-1.72	13.37	MgCl2:2H2O
MgCl2_4H2O	-8.41	-1.73	6.68	MgCl2:4H2O
Portlandite	-9.50	-14.69	-5.19	Ca(OH)2

**For a gas, SI = log10(fugacity). Fugacity = pressure * phi / 1 atm.
For ideal gases, phi = 1.

Beginning of batch-reaction calculations.

Reaction step 1.

Using solution 3. Ca/Mg Solution
Using pure phase assemblage 1. PHASES

-----Phase assemblage-----

				Moles in assemblage		
Phase	SI	log IAP	log K(T, P)	Initial	Final	Delta
Aragonite	0.00	-8.33	-8.33	1.000e-01	9.992e-02	-8.392e-05

-----Solution composition-----

Elements	Molality	Moles
----------	----------	-------

C	8.392e-05	8.392e-05
Ca	1.042e-01	1.042e-01
Cl	8.330e-01	8.330e-01
Mg	3.124e-01	3.124e-01

-----Description of solution-----

pH = 8.034 Charge balance
 pe = 4.000 Adjusted to redox equilibrium
 Specific Conductance ($\mu\text{S}/\text{cm}$, 40 ∞C) = 77436
 Density (g/cm^3) = 1.02499
 Volume (L) = 1.01592
 Activity of water = 0.980
 Ionic strength = 1.250e+00
 Mass of water (kg) = 1.000e+00
 Total alkalinity (eq/kg) = 1.733e-04
 Total CO2 (mol/kg) = 8.392e-05
 Temperature (∞C) = 40.00
 Electrical balance (eq) = -5.472e-06
 Percent error, $100 \cdot (\text{Cat} - |\text{An}|) / (\text{Cat} + |\text{An}|)$ = -0.00
 Iterations = 15
 Gamma iterations = 4
 Osmotic coefficient = 0.90525
 Density of water = 0.99221
 Total H = 1.110124e+02
 Total O = 5.550647e+01

-----Distribution of species-----

Species	MacInnes		MacInnes		mole V Gamma	cm \geq /mol
	MacInnes Molality	Log Activity	Log Molality	Log Activity		
OH-	1.156e-05	3.099e-06	-4.937	-5.509	-0.572	-1.25
H+	1.039e-08	9.258e-09	-7.983	-8.034	-0.050	0.00
H2O	5.551e+01	9.798e-01	1.744	-0.009	0.000	18.16
C(4)	8.392e-05					
HCO3-	5.388e-05	2.976e-05	-4.269	-4.526	-0.258	28.41
MgCO3	1.618e-05	1.618e-05	-4.791	-4.791	0.000	-17.10
CO3-2	1.338e-05	1.884e-07	-4.873	-6.725	-1.851	1.96
CO2	4.715e-07	5.446e-07	-6.327	-6.264	0.063	35.16
Ca	1.042e-01					
Ca+2	1.042e-01	2.485e-02	-0.982	-1.605	-0.623	-16.03
Cl	8.330e-01					
Cl-	8.330e-01	4.963e-01	-0.079	-0.304	-0.225	19.35
Mg	3.124e-01					

Mg+2	3.123e-01	8.133e-02	-0.505	-1.090	-0.584	-20.41
MgOH+	4.875e-05	4.648e-05	-4.312	-4.333	-0.021	(0)
MgCO3	1.618e-05	1.618e-05	-4.791	-4.791	0.000	-17.10

-----Saturation indices-----

Phase	SI**	log IAP	log K(313 K, 1 atm)	
Aragonite	0.00	-8.33	-8.33	CaCO3
Artinite	-1.22	17.35	18.57	Mg2CO3(OH)2:3H2O
Bischofite	-6.16	-1.75	4.41	MgCl2:6H2O
Brucite	-1.40	-12.11	-10.71	Mg(OH)2
Calcite	0.32	-8.33	-8.65	CaCO3
CO2(g)	-4.64	-6.26	-1.63	CO2
Dolomite	1.27	-16.14	-17.41	CaMg(CO3)2
H2O(g)	-1.15	-0.01	1.14	H2O
Huntite	0.47	9.15	8.69	CaMg3(CO3)4
Magnesite	0.07	-7.81	-7.89	MgCO3
MgCl2_2H2O	-15.08	-1.72	13.37	MgCl2:2H2O
MgCl2_4H2O	-8.41	-1.73	6.68	MgCl2:4H2O
Nesquehonite	-2.67	-7.84	-5.17	MgCO3:3H2O
Portlandite	-7.43	-12.62	-5.19	Ca(OH)2

**For a gas, SI = log10(fugacity). Fugacity = pressure * phi / 1 atm.
For ideal gases, phi = 1.

End of simulation.

Reading input data for simulation 4.

```

Solution 4 Initial Ca/Mg Solution
  pH 5.2
  temp 25
  units mol/L
  Ca 0.1
  Mg 0.3
  Cl 0.8
EQUILIBRIUM PHASES
  Aragonite 0.0 0.1
END

```

Beginning of initial solution calculations.

 Initial solution 4. Initial Ca/Mg Solution

-----Solution composition-----

Elements	Molality	Moles
Ca	1.041e-01	1.041e-01
Cl	8.330e-01	8.330e-01
Mg	3.124e-01	3.124e-01

-----Description of solution-----

pH = 5.200
 pe = 4.000
 Specific Conductance ($\mu\text{S}/\text{cm}$, 25°C) = 57916
 Density (g/cm^3) = 1.03010
 Volume (L) = 1.01088
 Activity of water = 0.980
 Ionic strength = 1.250e+00
 Mass of water (kg) = 1.000e+00
 Total alkalinity (eq/kg) = -6.690e-06
 Total carbon (mol/kg) = 0.000e+00
 Total CO2 (mol/kg) = 0.000e+00
 Temperature ($^\circ\text{C}$) = 25.00
 Electrical balance (eq) = 6.690e-06
 Percent error, $100 \cdot (\text{Cat} - |\text{An}|) / (\text{Cat} + |\text{An}|)$ = 0.00
 Iterations = 5
 Gamma iterations = 3
 Osmotic coefficient = 0.91517
 Density of water = 0.99704
 Total H = 1.110124e+02
 Total O = 5.550622e+01

-----Distribution of species-----

Species	MacInnes		MacInnes		mole V Gamma	cm \geq /mol
	MacInnes Molality	Log Activity	Log Molality	Log Activity		
H+	6.718e-06	6.310e-06	-5.173	-5.200	-0.027	0.00
OH-	5.838e-09	1.571e-09	-8.234	-8.804	-0.570	-1.72
H2O	5.551e+01	9.796e-01	1.744	-0.009	0.000	18.07
Ca	1.041e-01					
Ca+2	1.041e-01	2.762e-02	-0.982	-1.559	-0.576	-16.32

Cl	8.330e-01						
Cl-	8.330e-01	4.934e-01	-0.079	-0.307	-0.227	19.05	
Mg	3.124e-01						
Mg+2	3.124e-01	9.133e-02	-0.505	-1.039	-0.534	-20.03	
MgOH+	2.204e-08	2.201e-08	-7.657	-7.657	-0.001	(0)	

-----Saturation indices-----

Phase	SI**	log IAP	log K(298 K, 1 atm)	
Bischofite	-6.30	-1.71	4.59	MgCl2:6H2O
Brucite	-7.77	-18.65	-10.88	Mg(OH)2
H2O(g)	-1.51	-0.01	1.50	H2O
MgCl2_2H2O	-16.23	-1.67	14.56	MgCl2:2H2O
MgCl2_4H2O	-8.67	-1.69	6.98	MgCl2:4H2O
Portlandite	-13.98	-19.17	-5.19	Ca(OH)2

**For a gas, SI = log10(fugacity). Fugacity = pressure * phi / 1 atm.
For ideal gases, phi = 1.

Beginning of batch-reaction calculations.

Reaction step 1.

Using solution 4. Initial Ca/Mg Solution
Using pure phase assemblage 1. PHASES

-----Phase assemblage-----

Phase	SI	log IAP	log K(T, P)	Moles in assemblage		
				Initial	Final	Delta
Aragonite	0.00	-8.22	-8.22	1.000e-01	9.993e-02	-7.382e-05

-----Solution composition-----

Elements	Molality	Moles
C	7.382e-05	7.382e-05
Ca	1.042e-01	1.042e-01
Cl	8.330e-01	8.330e-01
Mg	3.124e-01	3.124e-01

-----Description of solution-----

pH = 8.310 Charge balance
 pe = 4.000 Adjusted to redox equilibrium
 Specific Conductance ($\mu\text{S}/\text{cm}$, 25°C) = 57914
 Density (g/cm^3) = 1.03010
 Volume (L) = 1.01088
 Activity of water = 0.980
 Ionic strength = 1.250e+00
 Mass of water (kg) = 1.000e+00
 Total alkalinity (eq/kg) = 1.410e-04
 Total CO2 (mol/kg) = 7.382e-05
 Temperature (°C) = 25.00
 Electrical balance (eq) = 6.690e-06
 Percent error, $100 \cdot (\text{Cat} - |\text{An}|) / (\text{Cat} + |\text{An}|)$ = 0.00
 Iterations = 17
 Gamma iterations = 4
 Osmotic coefficient = 0.91515
 Density of water = 0.99704
 Total H = 1.110124e+02
 Total O = 5.550644e+01

-----Distribution of species-----

Species	MacInnes		MacInnes		mole V Gamma	cm ³ /mol
	Molality	Activity	Log Molality	Log Activity		
OH-	7.517e-06	2.023e-06	-5.124	-5.694	-0.570	-1.72
H+	5.219e-09	4.901e-09	-8.282	-8.310	-0.027	0.00
H2O	5.551e+01	9.796e-01	1.744	-0.009	0.000	18.07
C(4)	7.382e-05					
HCO3-	4.213e-05	2.337e-05	-4.375	-4.631	-0.256	27.84
MgCO3	1.689e-05	1.689e-05	-4.772	-4.772	0.000	-17.09
CO3-2	1.458e-05	2.183e-07	-4.836	-6.661	-1.825	1.05
CO2	2.222e-07	2.566e-07	-6.653	-6.591	0.063	34.43
Ca	1.042e-01					
Ca+2	1.042e-01	2.764e-02	-0.982	-1.558	-0.576	-16.32
Cl	8.330e-01					
Cl-	8.330e-01	4.934e-01	-0.079	-0.307	-0.227	19.05
Mg	3.124e-01					
Mg+2	3.123e-01	9.131e-02	-0.505	-1.039	-0.534	-20.03
MgOH+	2.837e-05	2.833e-05	-4.547	-4.548	-0.001	(0)
MgCO3	1.689e-05	1.689e-05	-4.772	-4.772	0.000	-17.09

-----Saturation indices-----

Phase	SI**	log IAP	log K(298 K, 1 atm)	
Aragonite	0.00	-8.22	-8.22	CaCO3
Artinite	-1.49	18.17	19.66	Mg2CO3(OH)2:3H2O
Bischofite	-6.30	-1.71	4.59	MgCl2:6H2O
Brucite	-1.55	-12.43	-10.88	Mg(OH)2
Calcite	0.28	-8.22	-8.50	CaCO3
CO2(g)	-5.12	-6.59	-1.47	CO2
Dolomite	1.16	-15.92	-17.08	CaMg(CO3)2
H2O(g)	-1.51	-0.01	1.50	H2O
Huntite	-0.21	10.04	10.24	CaMg3(CO3)4
Magnesite	0.13	-7.70	-7.83	MgCO3
MgCl2_2H2O	-16.23	-1.67	14.56	MgCl2:2H2O
MgCl2_4H2O	-8.67	-1.69	6.98	MgCl2:4H2O
Nesquehonite	-2.56	-7.73	-5.17	MgCO3:3H2O
Portlandite	-7.76	-12.95	-5.19	Ca(OH)2

**For a gas, SI = log10(fugacity). Fugacity = pressure * phi / 1 atm.
For ideal gases, phi = 1.

End of simulation.

Reading input data for simulation 5.

End of Run after 0.039338 Seconds.

Appendix III: Primary Precipitation Aqueous Geochemistry

This appendix contains the raw geochemical data (pH, cations, alkalinity) for primary precipitation experiments. Empty cells represent data that is not currently available but will be collected.

Environment	Sample	pH	[Ca] mmol	[Mg] mmol	Mg:Ca	Total Alkalinity (mmol)	[Na] mmol	[Cl] mmol
Evaporative Lake Samples	ELS 40C 5d Start	8.94	1.54	37.09	24.04	371.01	947	626
	ELS 40C 5d	8.8	0.20	12.56	62.18	322.11	947	626
	ELNS 40C 5d	8.76	0.22	13.00	58.29	331.01	947	626
	ELS 40C 10d Start	8.97	4.27	41.26	9.66	267.01	805	630
	ELS1 40C 10d	8.56	0.04	10.13	276.01	178.81	805	630
	ELNS 40C 10d	8.64	0.02	9.84	484.28	178.41	805	630
	EL 30C 5d S Start	8.99		22.42	#DIV/0!	220.01	941	634
	EL 30C 5d NS Start	8.99		21.76	#DIV/0!	214.49	941	634
	ELS 30C 5d	8.89		22.63	#DIV/0!	188.61	941	634
ELNS 30C 5d	8.96		21.87	#DIV/0!	191.01	941	634	
Mixing Zone Samples	MZ 40C 5d Start	7.1	4.61	51.82	10.64	8.6	146	249
	MZS 40C 5d	7.23	4.87	54.68	12.07	8.1	146	249
	MZNS 40C 5d	7.22	4.53	50.61	11.18	8.5	146	249
	MZ 30C 5d Start	7.25	4.85	57.56	11.88	8.6	146	249
	MZS 30C 5d	7.16	4.76	53.10	11.16	8.2	146	249
	MZNS 30C 5d	7.15	4.72	51.32	10.86	8.4	146	249
	MZ 40C 10d Start	7.3	4.54	45.42	10.00	17.29	156	251
	MZS1 40C 10d	7.43	3.53	40.58	11.49	14.98	156	251
	MZS2 40C 10d	7.37	3.43	42.22	12.31	14.85	156	251
MZNS 40C 10d	7.16	2.42	43.34	17.94	12.52	156	251	
Sabkha Samples	Sab S 30C Start				#DIV/0!			
	Sab S 30C 5d				#DIV/0!			
	Sab S2 30C 5d				#DIV/0!			
	Sab NS 30C 5d				#DIV/0!			
	Sab 40C 10d Start	7.53	3.57	45.91	12.87	64.96	2642	2679
	Sab S 40C 10d	7.13	0.30	45.89	154.46	58	2642	2679
	Sab NS 40C 10d	7.12	0.23	45.43	198.37	55.72	2642	2679
	Sab 40C 5d Start	7.08	3.91	45.71	11.70	34.16	2604	2679
Sab S1 40C 5d	7.3	2.11	52.37	24.79	29.3	2604	2679	
Sab NS 40C 5d	7.13	1.10	45.28	41.08	27.92	2604	2679	

Appendix IV: Dolomitization Aqueous Geochemistry

This appendix contains the raw geochemical data (pH, cations, alkalinity) for dolomitization experiments.

Notes	Sample	pH	[Ca] mmol	[Mg] mmol	Mg:Ca	CO ₃ [mmol]	HCO ₃ [mmol]	[Na] mmol	[Cl] mmol
MZ Dolomitization Start	MZD start	6.9	4.64	49.40	10.65	8.75	8.75	156	259
sph 6wk	AA	7.35	4.37	46.07	10.55	8.32	8.32	156	259
sph 1 wk	AB	7.4	4.26	45.16	10.59	8.64	8.64	156	259
sph 6wk	AC	7.35	4.43	47.10	10.63	8.32	8.32	156	259
control 1wk	AD	7.29	4.34	45.67	10.52	8.64	8.64	156	259
sph 2wk	AE	7.26	4.43	47.22	10.66	8.64	8.64	156	259
control 6wk	AF	7.25	4.39	46.78	10.67	8.44	8.44	156	259
control 2wk	AG	7.34	4.54	47.08	10.36	8.72	8.72	156	259
sph 2wk	AH	7.31	4.27	46.69	10.92	8.68	8.68	156	259
sph 1wk	AI	7.29	4.40	49.09	11.17	8.64	8.64	156	259
Start	SD t0	3	3.96	38.15	9.63	0	0	2567	2680
control 2wk	SD1	8.12	4.35	56.32	12.93	0.6	0.6	2567	2680
sph 2wk	SD2	7.8	4.24	52.11	12.28	0.56	0.56	2567	2680
sph 2wk	SD3	8.09	4.29	42.04	9.80	0.66	0.66	2567	2680
control 4wk	SD4	8.19	4.32	43.42	10.05	0.78	0.78	2567	2680
sph 4wk	SD5	8.07	4.83	45.43	9.40	0.7	0.7	2567	2680
sph 4wk	SD6	8.11	4.26	44.47	10.43	0.71	0.71	2567	2680
control 6wk	SD7	8.21	4.36	53.73	12.32	0.75	0.75	2567	2680
sph 6wk	SD8	8.18	4.24	44.90	10.58	0.67	0.67	2567	2680
sph 6wk	SD9	8.15	4.38	51.27	11.71	0.71	0.71	2567	2680
F4 Start	F4 Start	5	98.87	284.79	2.88	0.05	0.05	0	767
control 1wk	A	7.86	97.51	282.27	2.89	0.26	0.26	0	767
sph 1wk	B	7.64	93.82	268.98	2.87	0.32	0.32	0	767
sph 1wk	C	7.51	97.65	280.23	2.87	0.32	0.32	0	767
sph 2wk	D	7.76	94.65	275.35	2.91	0.28	0.28	0	767
sph 2wk	E	7.84	98.80	283.73	2.87	0.32	0.32	0	767
control 2wk	F	7.75	98.31	281.64	2.86	0.34	0.34	0	767
sph 6wk	G	7.7	98.78	288.92	2.92	0.29	0.29	0	767
control 6wk	H	7.66	96.92	283.50	2.93	0.41	0.41	0	767
sph 6wk	I	7.6	99.11	290.66	2.93	0.29	0.29	0	767

Appendix V: Early Phase Experiments

Methodology

Early phase experiments were conducted following the methodology of Pimentel & Pina (2014) to attempt to determine a crystallization route for precipitates produced here. The fluid used was identical to the alkaline lake solution but pH was not adjusted to 9, and instead was left very high (~11). Polystyrene microspheres were added at the same concentration used in other batch experiments. Experiments were shaken at 40°C and at 70 rpm. At each time step, (0, 4, 20, 24 and each 24 hours after that), serum bottles were uncapped, pH was measured, and the precipitate was filtered out and stored in a Falcon tube. Precipitate was analyzed by XRD following the methodology described in Chapters 1 and 2.

Results

Results of these experiments show that immediately upon solution creation, an amorphous precipitate form (0 hours). In the laboratory, this was observed as a white gel-like substance in solution. Within the next few hours, crystallinity begins to develop. Calcite, huntite, and hydromagnesite are all observed at each time step (Figure 1). Figure 2 shows the development of calcite and huntite peaks within the first four days of experimentation, and the development of a broad, diffuse peak at the 2Θ value of dolomite and hydromagnesite.

Discussion

These experiments were run far from equilibrium and most of the precipitation reflects thermodynamic drivers and not the presence of the microspheres. Additionally, without detailed microscopy, the role of the microspheres in producing these changes in crystallinity and mineralogy is unclear.

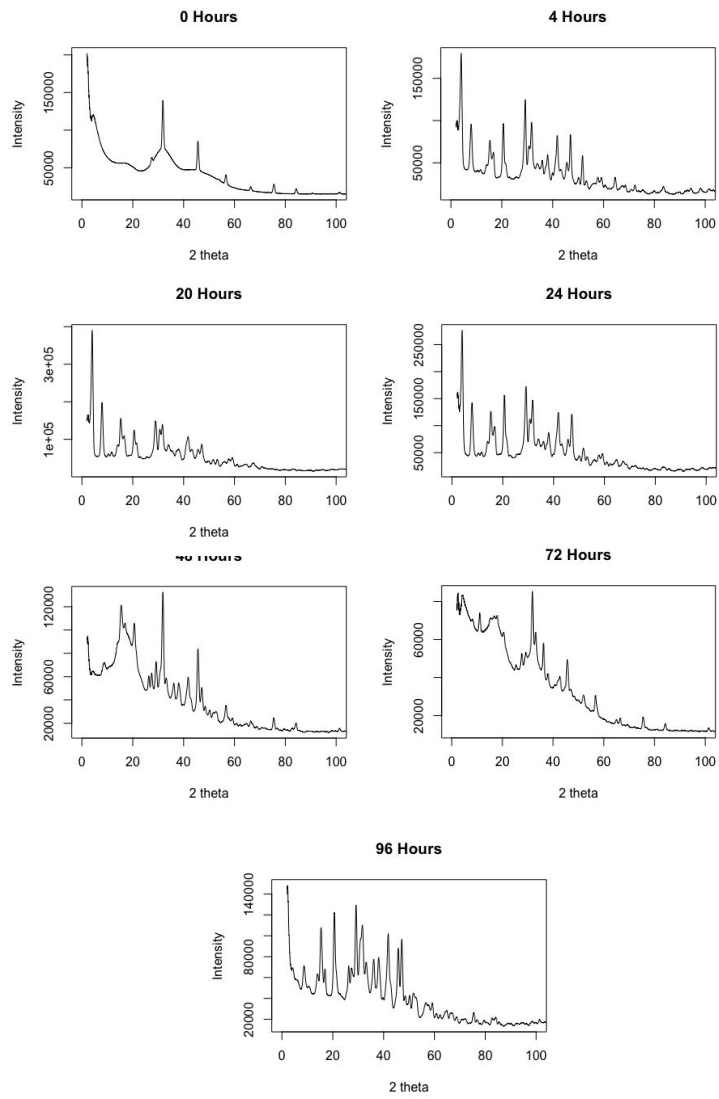


Figure 1: Diffractograms of experimental precipitates at the first seven time steps.

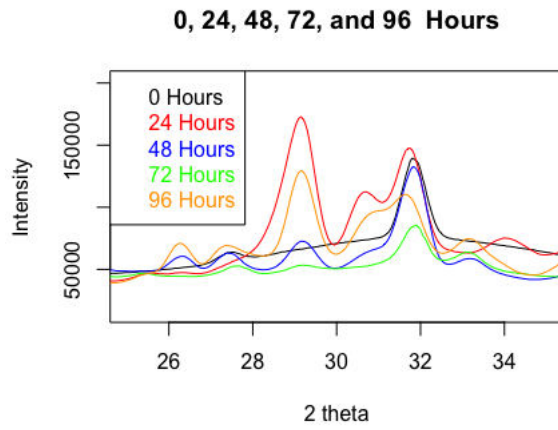


Figure 2: 24 hour time steps focusing on the 2 theta region where the Ca-Mg carbonates occur.

Appendix VI: Compiled SEM Images

Mixing Zone

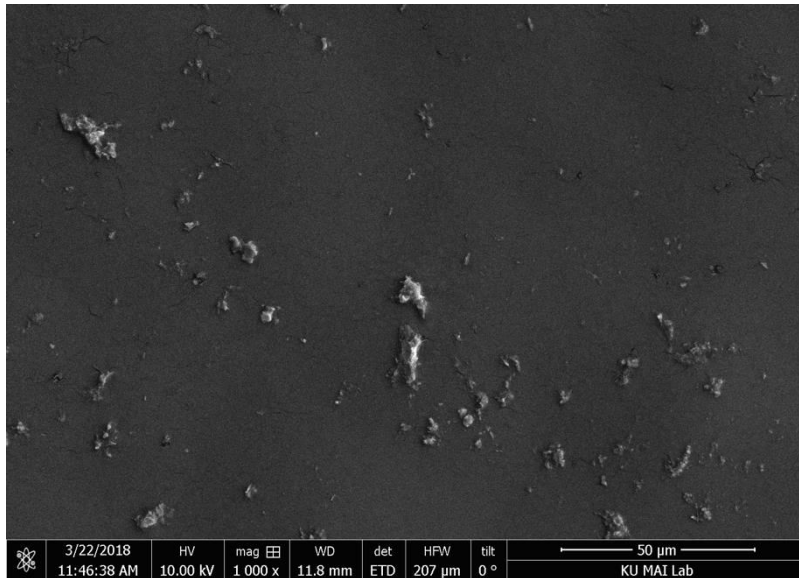


Figure 7: Mixing Zone, No Spheres, 5d, 30C.

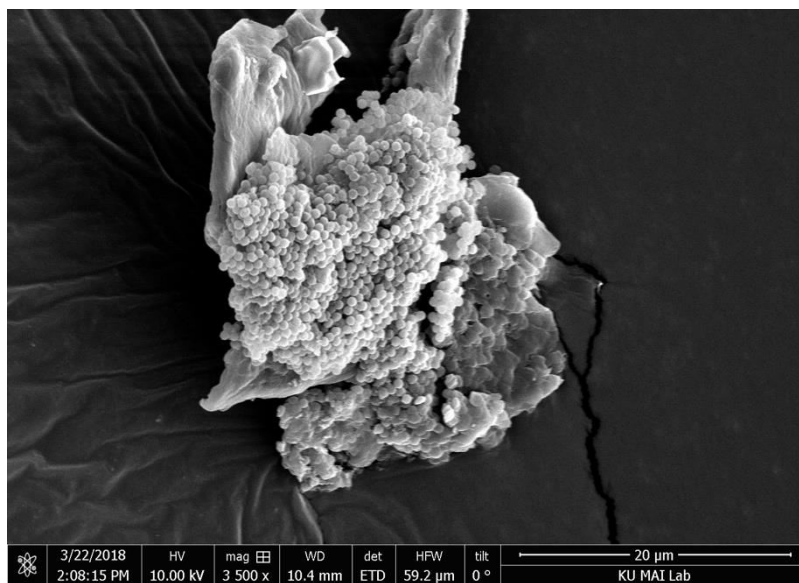


Figure 8: Mixing Zone, Spheres, 40C, 5d.

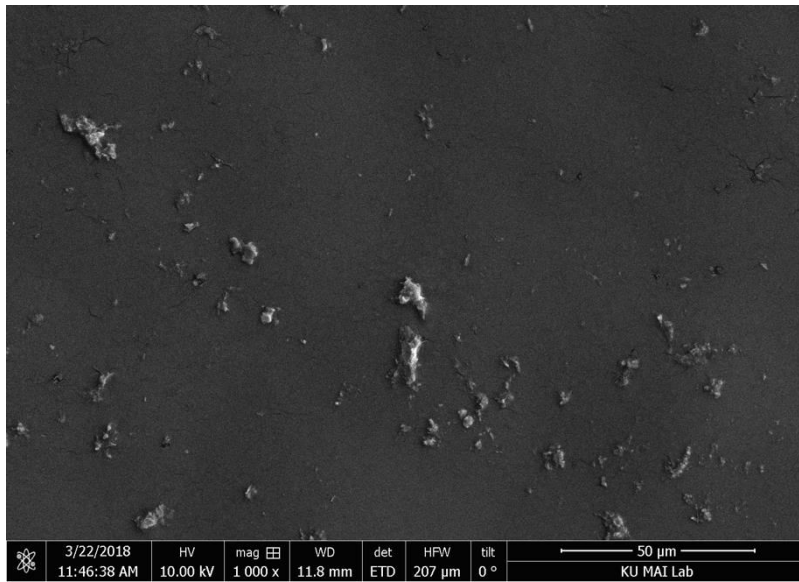


Figure 3: Mixing Zone, No Spheres, 5 days, 30°C.

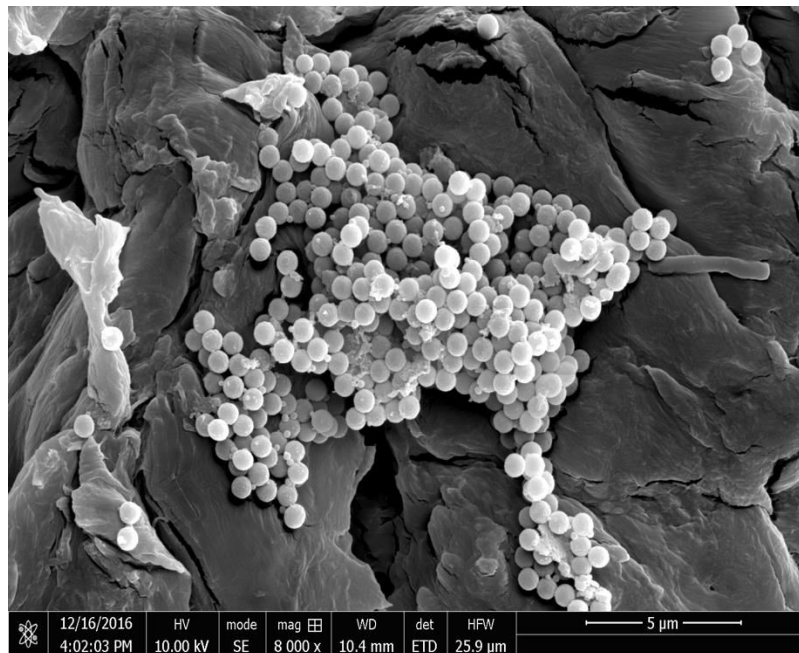


Figure 4: Mixing Zone, Spheres, 5 days, 30 °C.

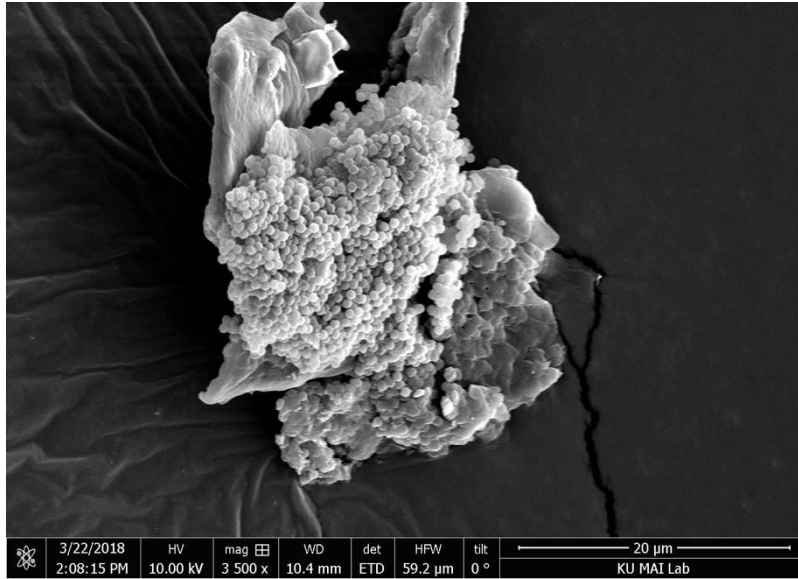


Figure 5: Mixing Zone, Spheres, 5 days, 40 °C.

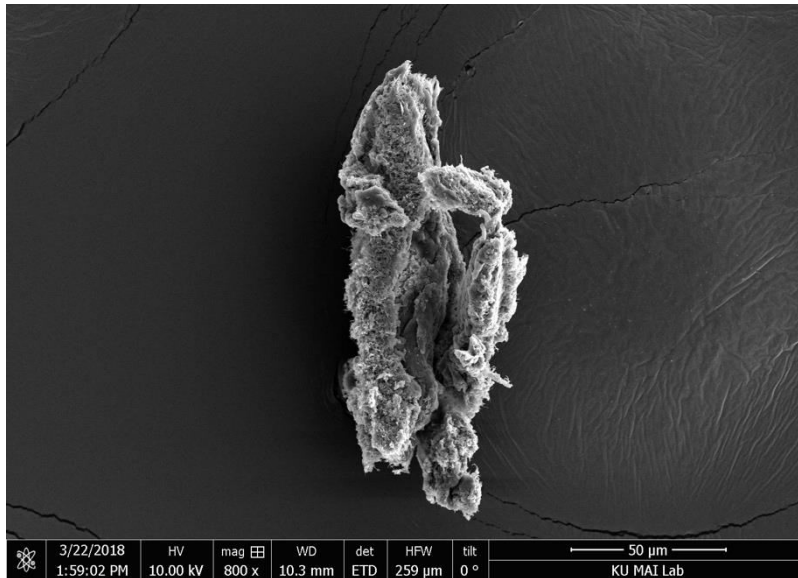


Figure 6: Mixing Zone, No spheres, 5 days, 40 °C.

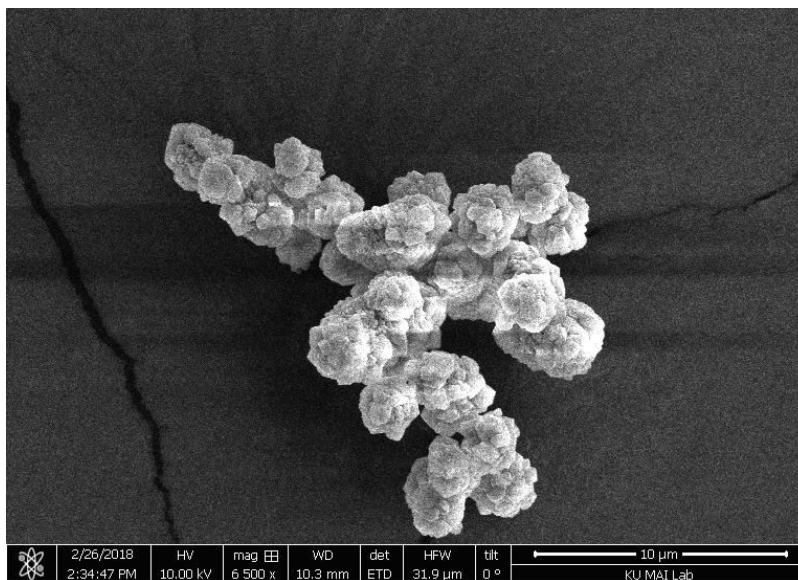


Figure 7: Mixing Zone, No Spheres, 5 days, 40 °C.

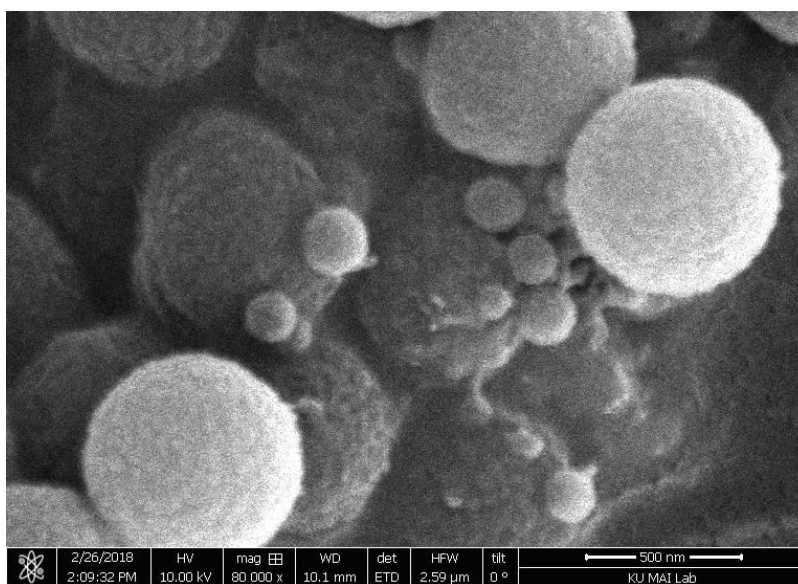


Figure 8: Mixing Zone, Spheres, 10 days, 40 °C.

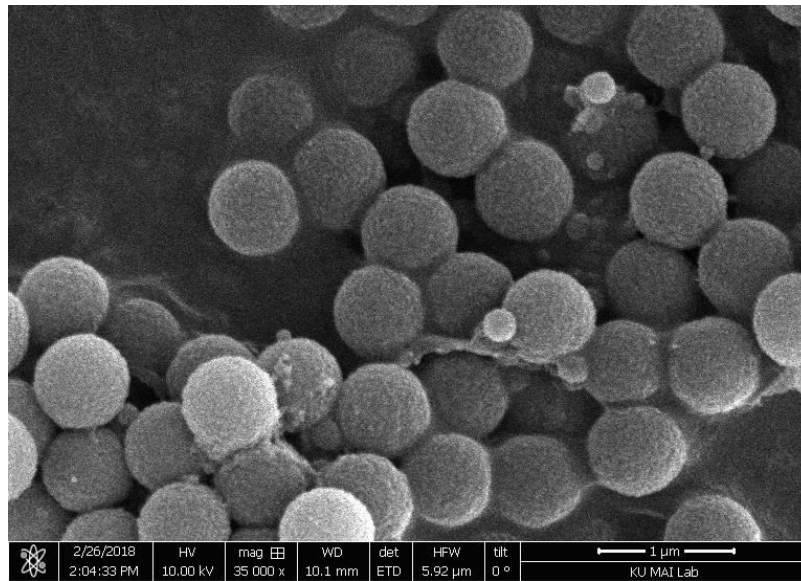


Figure 9: Mixing Zone, Spheres, 10 days, 40 °C.

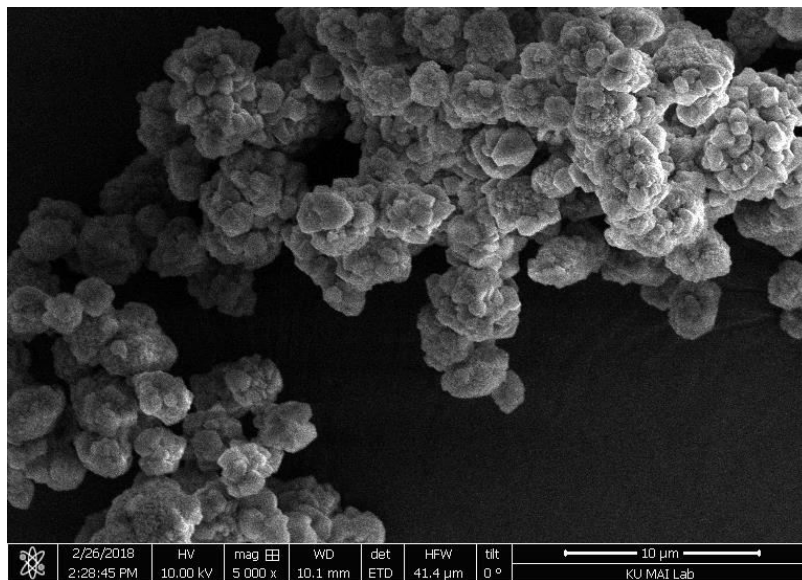


Figure 10: Mixing Zone, Spheres, 10 days, 40 °C.

Sabkha

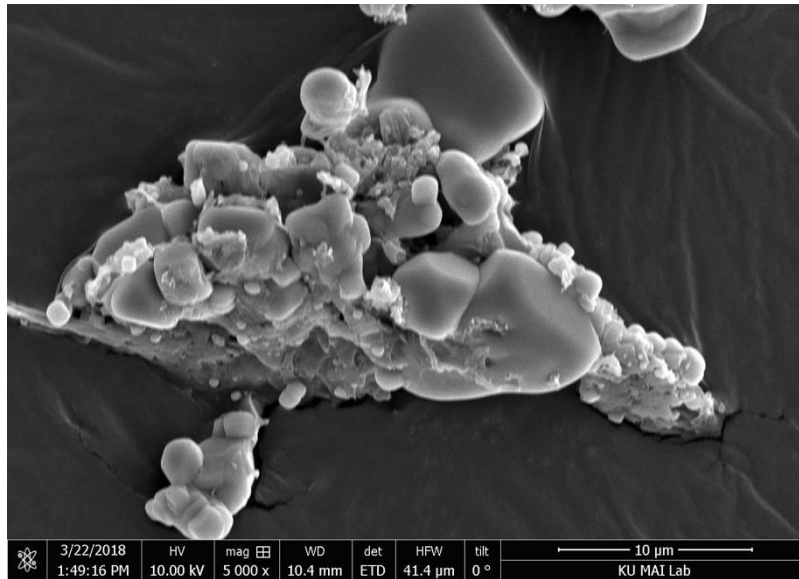


Figure 11: Sabkha, No Spheres, 5 days, 30 °C.

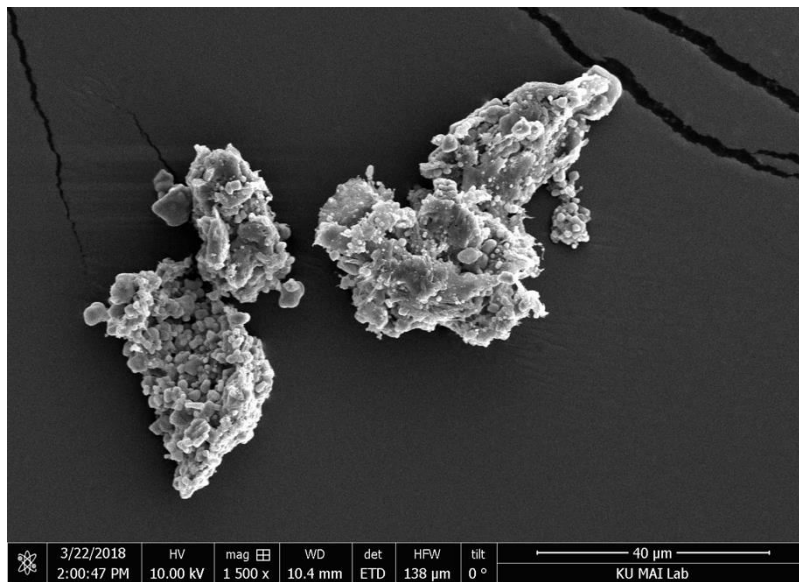


Figure 12: Sabkha, No spheres, 5 days, 30 °C.

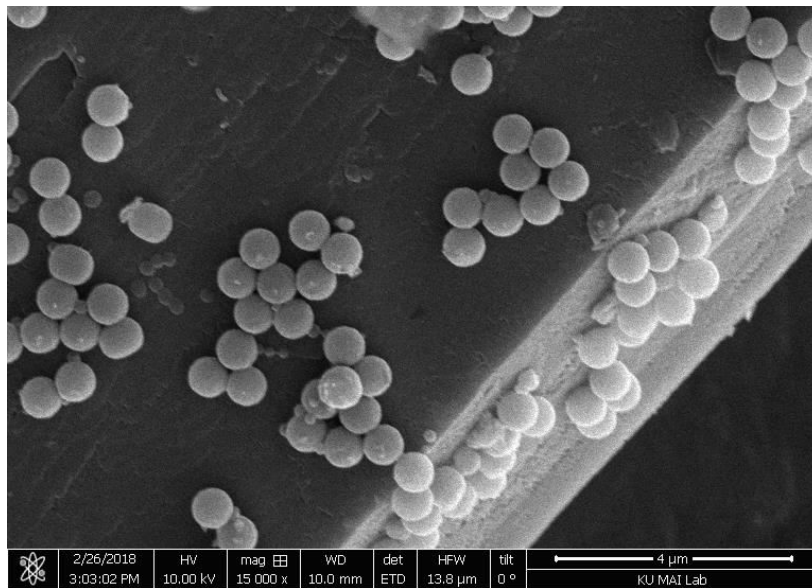


Figure 13: Sabkha, Spheres, 5 days, 30 °C.

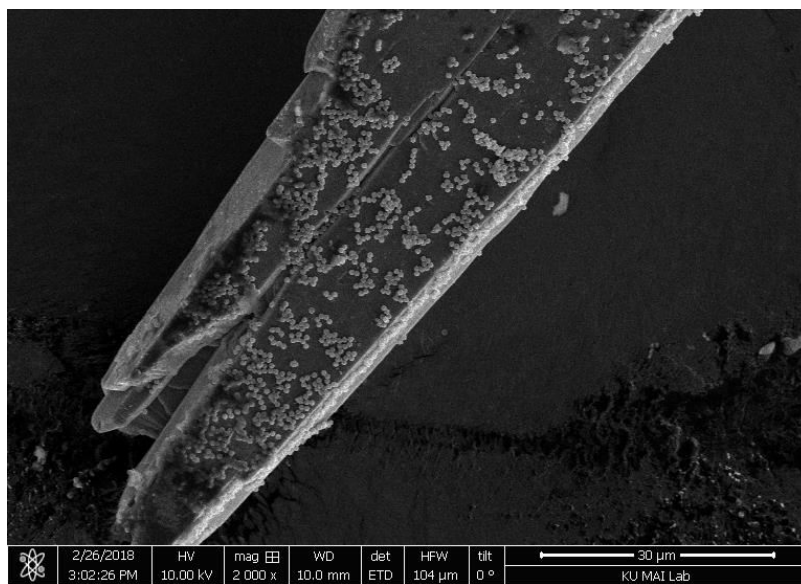


Figure 14: Sabkha, Spheres, 5 days, 30 °C.

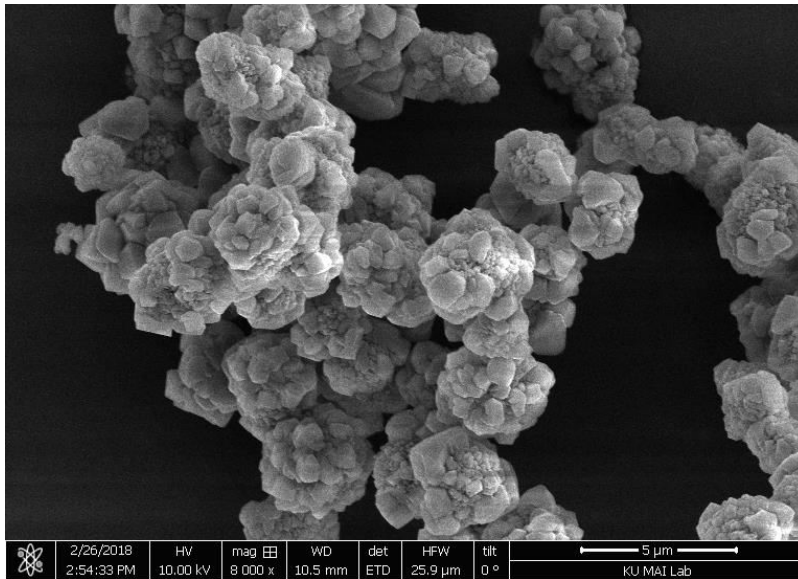


Figure 15: Sabkha, No Spheres, 10 days, 40 °C.

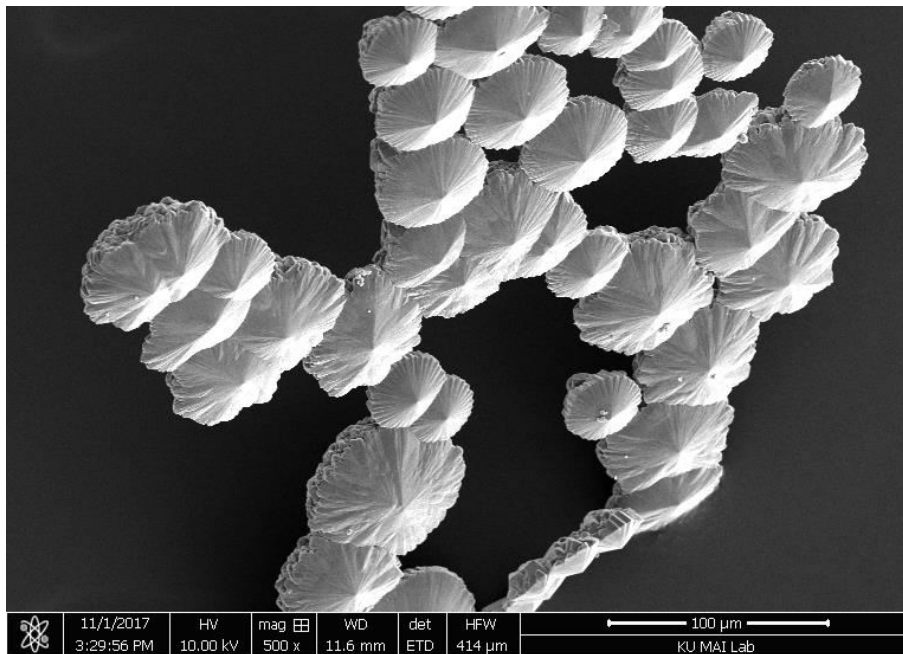


Figure 16: Sabkha, Spheres, 5 days, 40 °C.

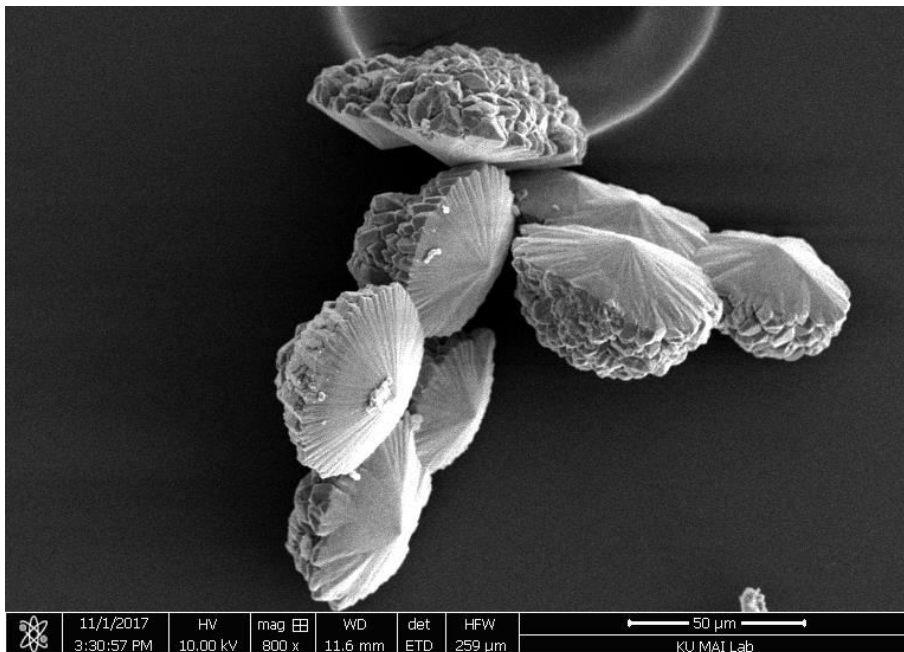


Figure 17: Sabkha, No Spheres, 5 days, 40 °C.

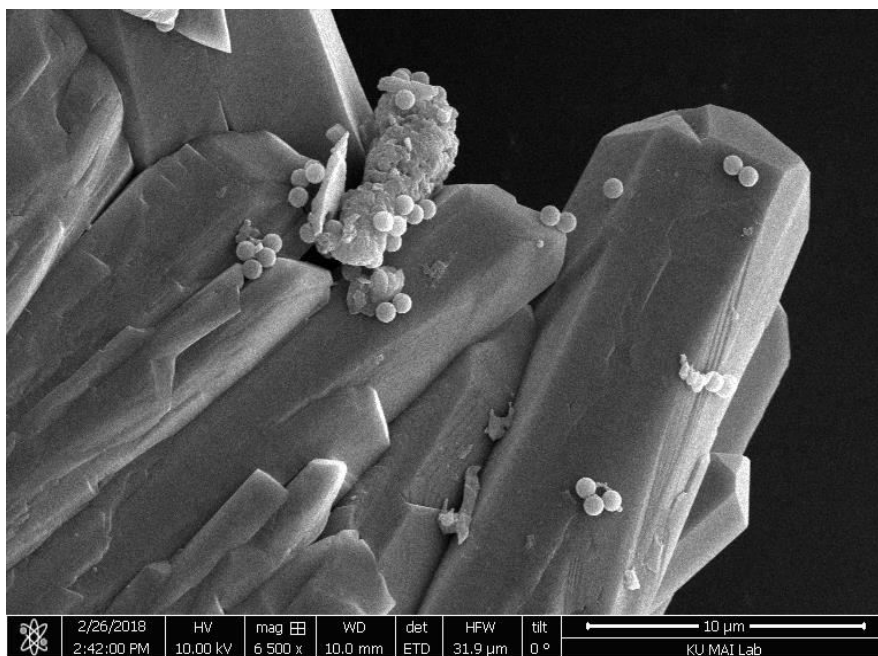


Figure 18: Sabkha, Spheres, 10 days, 40 °C.

Alkaline Lake

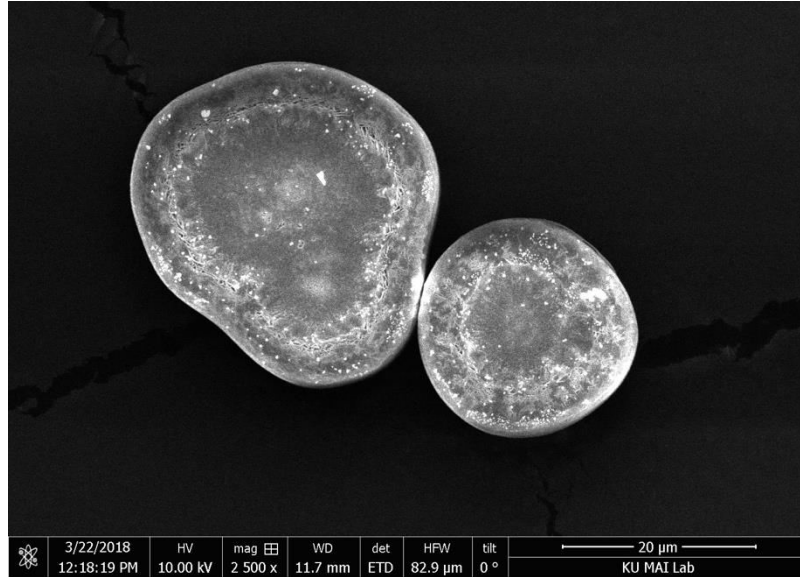


Figure 19: Alkaline Lake, No Spheres, 5 days, 30 °C.

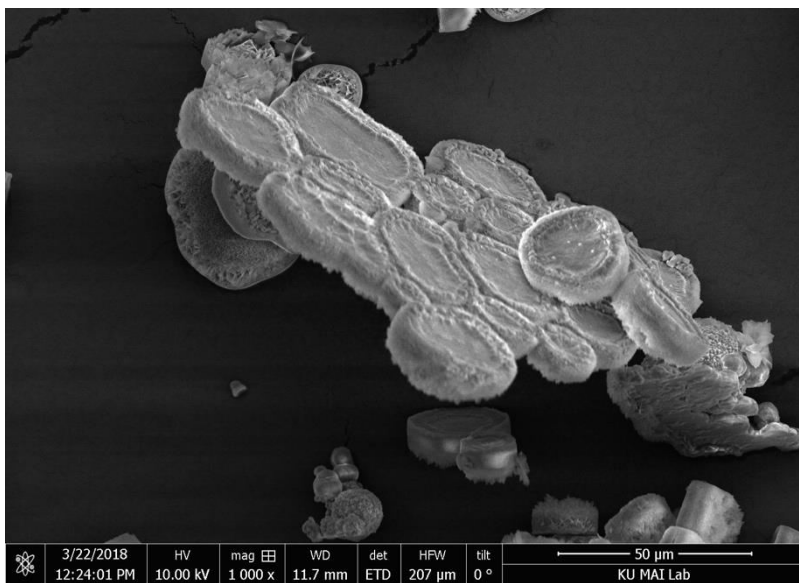


Figure 20: Alkaline Lake, No Spheres, 5 days, 30 °C.

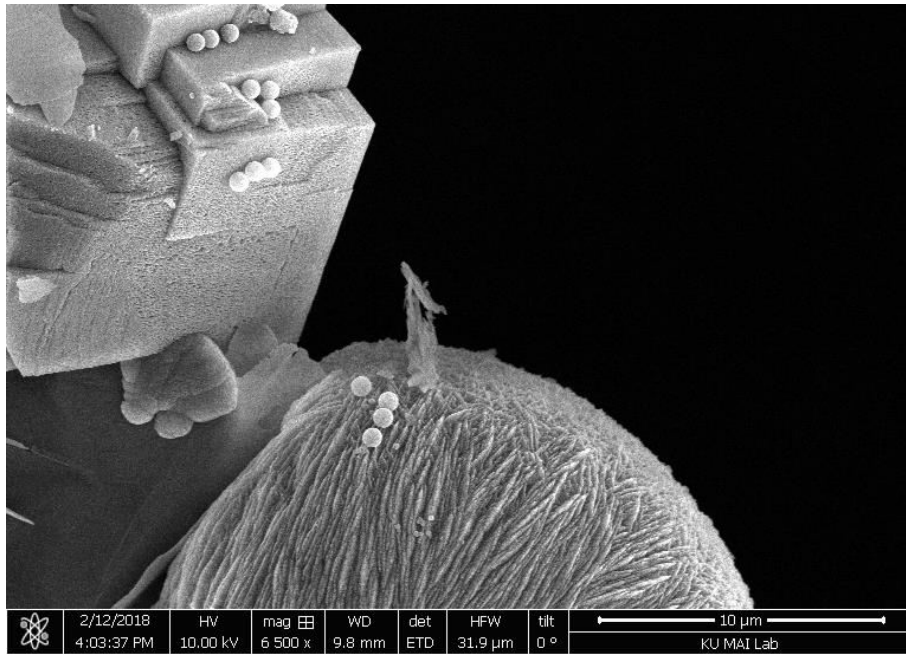


Figure 21: Alkaline Lake, Spheres, 5 days, 40 °C.



Figure 22: Alkaline Lake, No Spheres, 5 days, 40 °C.

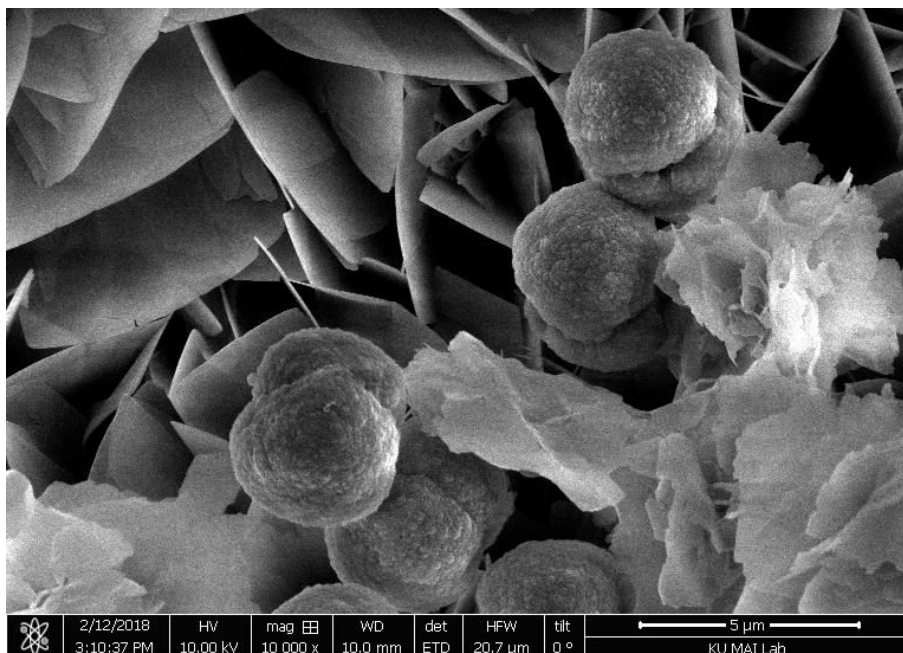


Figure 23: Alkaline Lake, Spheres, 5 days, 40 °C.

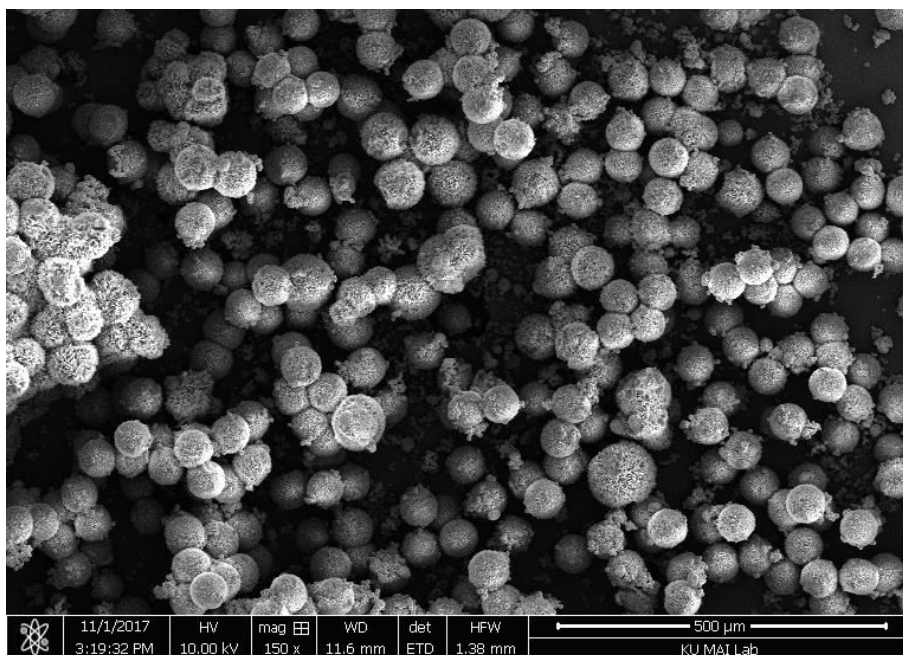


Figure 24: Alkaline Lake, No Spheres, 10 days, 40 °C.

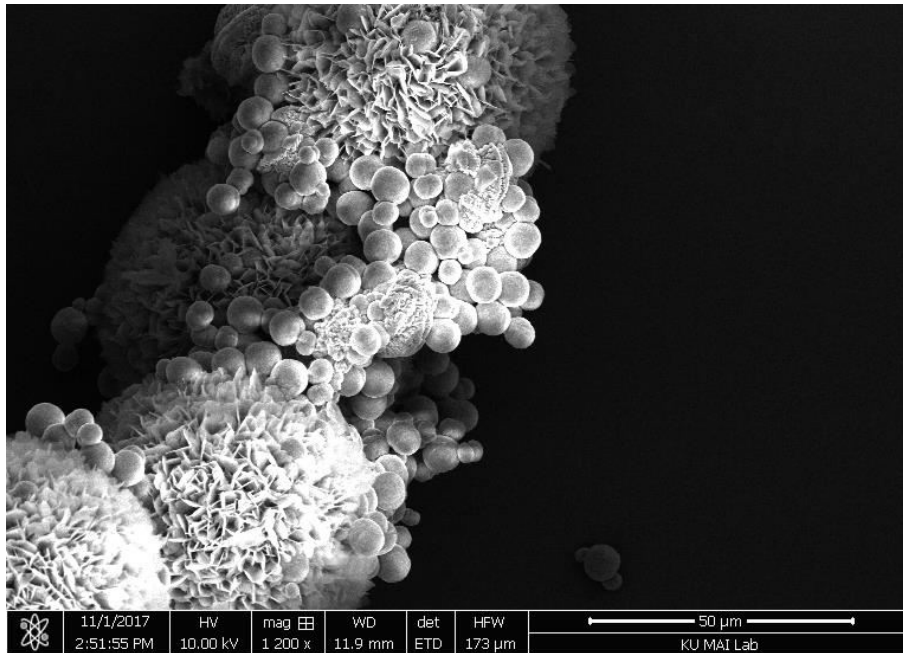


Figure 25: Alkaline Lake, Spheres, 10 days, 40 °C.